Modelling the effects of climate change on soil heterotrophic respiration in forest ecosystems. Empirical versus Mechanistic approach.

Thesis · July 2020

CITATIONS
0

READS
2

3 authors, including:

Corrado Biondo
Centro Euro-Mediterraneo sui Cambiamenti Climatici
13 PUBLICATIONS **17** CITATIONS
SEE PROFILE

Alessio Collalti
Italian National Research Council
92 PUBLICATIONS **326** CITATIONS
SEE PROFILE

Università degli Studi della Tuscia di Viterbo

Dipartimento per la Innovazione nei sistemi Biologici, Agroalimentari e Forestali

Corso di Dottorato di Ricerca in

Scienze, Tecnologie e Biotecnologie per la Sostenibilità - **XXXII ciclo**

Modelling the effects of climate change on soil heterotrophic respiration in forest ecosystems. Empirical versus Mechanistic approach

(s.s.d. AGR/05)

Tesi di dottorato di:
Dr. Corrado BIONDO

Coordinatore del corso
Prof. Andrea VANNINI

Tutore
Prof. Dario PAPALE

Co-tutore
Dr. Alessio COLLALTI

INDEX

Main acronyms

AIC	Akaike Information Criterion
GHG	Green House Gas
IPCC	Intergovernmental Panel on Climate Change
MAP	Mean Annual Precipitation
MAT	Mean Annual Temperature
MCMC	Monte Carlo Markov Chain
MMRT	MacroMolecular Rate Theory
NRMSE	Normalized Root Mean Square Error
OAT	One-At-Time
ODE	Ordinary Differential Equation
PET	Potential Evapotranspiration
PPT	Total Precipitation
RCP	Representative Concentration Pathway
SOM	Soil Organic Matter
TST	Transition State Theory

Abstract

The soil stores more carbon than the whole atmosphere and vegetation together, about 1950 Pg, as well as an amount of nitrogen 20 times higher than the quantity stored in the standing vegetation of either forests or cultivations. Furthermore, soil exchanges several greenhouse gases which entrap the long-wavelength radiation, causing an increase of the global mean air temperature. Hence, soil plays a key role in the mitigation of climate change by terrestrial ecosystems, especially forests, which cover about 4 million hectares on the planet, equal to 30.6% of the lands.

The carbon and nitrogen compounds stored into the soil and exchanged with the atmosphere are regulated by the soil biogeochemical processes. Some of them are expected to be more affected by climate change – in particular the processes under the temperature control – such as the soil organic matter decomposition and heterotrophic respiration. However, studying the temperature effect on these key processes is complex, both under present-day and even more on the long-term (up to 100 years), because of many other physical, chemical and biological factors involved. To manage this complexity, models are fundamental, even if they are based on different approaches, reflecting different assumptions. For example, most models simulate an exponential decomposition rate-soil temperature relationship that never reaches an optimum, even if the laboratory and field experiments show an acclimation of the process, that is, a decrease of the decay rate after an optimum temperature, always explained as the enzyme denaturation.

A recently developed theory – the *Macromolecular Rate Theory* (MMRT) – explains through a thermodynamic point of view the reason why the acclimation occurs at definitely lower temperatures than those of enzyme denaturation, which can be registered under the expected climate change, but also under current climate.

In the present work, two different approaches to simulate the temperature effect on the heterotrophic respiration (R_{het}) have been compared: the classical empirical Exponential Function (EF) and the MMRT. Both approaches have been implemented in the conventional scheme introduced by the CENTURY model.

The work aimed to understand if, and to what extent, simulating the acclimation of the process at high, or increasing, temperatures implies some relevant differences in the R_{het} estimates, especially on the long-term projections.

The model has been ran on two contrasting forest ecosystems and with different climate conditions, a temperate European beech forest located in Germany (Hainich) and a tropical forest located in Central Africa (Ankasa, Ghana), at different modeling time scales (from daily to monthly), both under current and climate change scenarios (2006-2099). Moreover, sensitivity and uncertainty analyses have been

carried out to detect the parameters to which the model is more sensitive and to quantify the uncertainty in the R_{het} estimates. Thus, the work aimed also to understand if the implementation of the MMRT can reduce the uncertainty, compared to the EF, in the model estimates.

The results show that the incorporation of the acclimation in a conventional scheme of the soil biogeochemical cycles – despite the application of a more complex mechanistic approach than the classical empirical EF – conversely to the initial hypothesis, does not imply relevant differences in the R_{het} simulation by the two approaches. Indeed, the MMRT does not improve the simulation of the monthly R_{het} fluxes under current climate scenario, with a difference of the correlation coefficient (*rPea*) between EF and MMRT equal to just 0.004 at Hainich and 0.0013 at Ankasa. Under climate change scenario, the relevant differences are detected only for the warmest Representative Concentration Pathway (RCP8.5) and only if the result is scaled on the entire surface of the analyzed forests, with a difference in the R_{het} simulated by the two approaches on the whole period 2006-2099 equal to $95 \cdot 10^3$ tons C at Hainich and $307 \cdot 10^3$ tons C at Ankasa. Furthermore, the MMRT is more uncertain than EF both under present-day and climate change scenarios.

The results achieved in the present work put in doubt the possibility to simulate the R_{het} acclimation at increasing soil temperature by a mechanistic approach – the MMRT – using the 'conventional' scheme of soil C and N cycles. This point is crucial to have reliable model predictions of the CO_2 fluxes from the soil under changing climate and to better understand the contribution of the forest soils in the mitigation of climate change.

Keywords: *soil biogeochemical cycles, carbon, nitrogen, forests, models, CENTURY, macromolecular rate theory, climate change, uncertainty analysis*.

1. Introduction

The soil is the largest sink of carbon (C) in the terrestrial biosphere (Bradford et al., 2016). The amount of C stored in a thickness of just one meter of soil (1950 Pg) is definitely higher than the C stored in the whole atmosphere (589 Pg) and vegetation (550 Pg) together (Ciais et al., 2013) (*Fig.1*). Soil also stores most of the nitrogen (N) that can be found in terrestrial ecosystems. The amount of N stocked in the soil is up to 20 times higher than the quantity stored in the standing vegetation of either forests or cultivations (Weil & Brady, 2017).

Moreover, soil exchanges greenhouse gases (GHGs), as carbon dioxide (CO_2), methane (CH_4), nitrous oxide (N_2O) and dinitrogen (N_2), with the atmosphere. These gases exert a heat-trapping effect, hindering that the long-wavelength radiation can leave the atmosphere, with a consequent increase of the global mean air temperature. The estimated annual CO_2 emitted to the atmosphere due to the soil respiration (being the amount due to microbial and the one due to plants' fine and coarse root respiration) is estimated to be 107.2 Pg C y^{-1}, while the N_2O flux can reach about 0.066 Pg y^{-1} (Ciais et al., 2013).

Hence, soil plays a key role in the issue of climate change, storing C and N and exchanging GHGs with the atmosphere, in particular regarding the atmospheric CO_2 concentration, which enhanced from 280 ppm (parts per million) during the pre-industrial level to the current 400 ppm (0.5% per year) (Kuzyakov et al., 2018). The atmospheric CO_2 increment generates an increase of global mean air temperature, which currently is between 0.8°C and 1.2°C higher than the pre-industrial level (IPCC, 2018).

The role of the soil in the climate change issue is also important in the forests, which cover about 4 million hectares on the planet equal to 30.6% of the lands and 90% of the global carbon biomass (FAO, 2015).

The soil processes involved in the C and N cycles are fundamental to define the contribution given by the soil in the mitigation of climate change. A central role in the soil biogeochemical cycles is played by the organic matter (SOM) decomposition, that is the transformation of the organic C in progressively more recalcitrant compounds, and the heterotrophic respiration, the production of CO_2 due to the activity of microbial decomposers (Schulze et al., 2000). Other processes, as the N pathways (i.e. mineralization and immobilization) – strongly linked to SOM decomposition – are crucial for regulating the conversion of organic N compounds in more stable or inorganic forms, the latter taken up by plants for their growth. Processes like N deposition, denitrification and biological fixation are crucial in the regulation of N exchange between soil and atmosphere.

Some of these processes are expected to be more affected by climate change, in particular the processes under the temperature control, such as the soil organic matter decomposition and heterotrophic respiration. Enhancing temperatures is expected to accelerate decomposition, to increase the amount of organic carbon that can be converted into CO_2 (Bond-Lamberty & Thomson, 2010), as well as the organic N that can be transformed into mineral inorganic compounds available for the plants (Weil & Brady, 2017). Ultimately, all these processes are expected to have a strong feedback with the atmosphere and to climate change. However, studying the temperature effect on these key processes is not straightforward because of many other physical (e.g. moisture, texture), chemical (e.g. pH) and biological (e.g. C:N ratio) factors involved (Blagodatskaya & Kuzyakov, 2008).

To manage this complexity, models are fundamental, even if they simulate the processes basing on different approaches, which are based on different assumptions and suitable for different spatial and time scales. For this reason, the model estimates can be affected by uncertainty, which can be defined as '*the quantitative measure of systematic and random variation from the "true" value of a simulated entity*' (Aubinet et al., 2012; Collalti et al., 2019). In the projections of atmospheric CO_2 concentration of the Earth System Models (ESMs) over 100 years, the land processes have been recognized as the main source of potential uncertainty (Friedlingstein et al., 2013).

Most models, through empirical or to some extent semi-empirical relationships, simulate historically an exponential increase of microbial decomposition at increasing soil temperature. Some main approaches are constituted by the exponential function, the Arrhenius equation and the Q_{10} model, the latter based on the Q_{10} factor, that is, the decay rate increment corresponding to a temperature increase of 10°C (Chen & Tian, 2005). However, both in the laboratory and field experiments – after an initial exponential increase of decomposition rate up to an optimum temperature – an acclimation of the microbial activity is usually observed, with a consequent decline of the process rate (Schipper et al., 2014). The theory usually used to explain this acclimation is the enzyme denaturation, that is the lost of enzymes produced by soil decomposers to degrade the soil organic matter at high temperatures, in some cases higher than 45 or 50 °C (Fields, 2001). However, the acclimation observed in the experiments occurs at definitely lower temperatures than those of enzyme denaturation (Schipper et al., 2014) (i.e. about 30°C), which can be easily reached in the Mediterranean and tropical forests and questioning on its capability to be predictive under the expected climate change.

A recently developed theory – the *MacroMolecular Rate Theory* (MMRT) (Hobbs et al., 2013; Schipper et al., 2014) – provides a thermodynamic explanation of the phenomenon, without invoking the enzyme denaturation. To reproduce the temperature-decomposition relationship, the

MMRT introduces a more mechanistic approach than the empirical ones classically used by models. This approach – derived by the Arrhenius formulation – is based on the concept of the activation energy, that is, the energy barrier that the reactants of a reaction must to overcome to be converted into products. In the MMRT the activation energy is a function of the changes in enthalpy, entropy and the heat capacity of the process.
Whether the acclimation of the soil organic matter decomposition occurs at temperatures easily reached in some forest ecosystems even under current climate conditions, reproducing this phenomenon in the models could affect their estimates of the soil C and N fluxes. Moreover, the effect could be more pronounced on the long-term, under climate change scenario. However, even if a mechanistic approach with a more complex structure, as the MMRT, is able to reproduce more aspects of the process, it introduces a higher number of parameters, increasing the uncertainty in the simulation and, ultimately, questioning on its usability in models.

In the present work, two inherently different approaches to simulate the temperature effect on SOM decomposition have been compared. The first *empirical* approach reproduces an exponential increase of SOM decomposition with increasing temperature and it is represented by a (relatively simple) empirical exponential function (EF). The second approach – a *mechanistic* one – describes the mechanisms behind the SOM decomposition and takes into account the acclimation of decomposition rate after an optimum temperature and it is constituted by the *MacroMolecular Rate Theory* (MMRT) formulation. Both approaches have been embedded and included in the "conventional" scheme introduced by CENTURY (Parton et al., 1987), a process-based model developed in the '80s to simulate the cycle of carbon and some plant macronutrients (nitrogen, phosphorous and sulfur) in several plant-soil systems. During the last 30 years, the CENTURY approach has constituted the basis to develop and implement several models of soil biogeochemical cycles and it has also been widely used as the soil biogeochemistry model component in most-used coupled global climate and vegetation models. The main examples are: BIOME-BGC (Thornton et al, 2002), CENW (Kirschbaum & Paul, 2002), 3D-CMCC-FEM (Collalti et al., 2014; Marconi et al., 2017), CASA (Wang et al., 2010), CLM (Yang et al., 2014) and ORCHIDEE (Krinner et al., 2005).
The CENTURY model simulates the key processes of the carbon and nitrogen cycles: SOM decomposition, heterotrophic respiration, the nitrogen pathways (mineralization and immobilization) and plant uptake.
The aim is to understand if the simulation of the acclimation of SOM decomposition to soil temperature increment affects – and the degree to which it affects – the model estimates of soil carbon and nitrogen fluxes simulated by both approaches, especially the carbon dioxide emitted from the soil due to the heterotrophic respiration (i.e. soil microbial respiration). A further aim is to

evaluate if the introduction of a more complex approach to simulate the acclimation can increase the uncertainty on model estimates. In particular, the present work tries to give answer to the following four questions:

1. Is it possible to improve the simulation of the heterotrophic respiration fluxes taking into account the acclimation process at higher temperatures?
2. By comparing the MMRT approach to the classical empirical EF, is there any difference, and to what extent, in the simulated heterotrophic respiration fluxes under different climate conditions and different time scales?
3. How large is the uncertainty in the simulation of the heterotrophic respiration due to the implementation of the MMRT and how large is by using the EF one? And which generates the largest uncertainty in the model estimates at different temporal scale?
4. Which are the most relevant scientific implications of the results of this study?

The acclimation at increasing soil temperature of soil respiration (autotrophic and heterotrophic components) has been widely observed in forest (Eliasson et al, 2005; Bradford et al., 2008; Crowther & Bradford, 2013; Noh et al., 2015), for several other ecosystems (Oechel et al., 2000; Luo et al., 2001), in laboratory experiments (Bradford et al., 2010; Wei et al., 2014) and simulated by models (Kirschbaum, 2004; Allison et al., 2010). Hence, basing on the scientific evidences regarding the acclimation of the process to soil temperature enhancement, significant different results are expected from the simulation of the heterotrophic respiration applying MMRT and EF at different temporal scales. The differences are expected under present-day climate and – even more – under warming climate change scenario, when the soil temperature increases up to 5°C. Furthermore, an approach like the MMRT – which tends to have a more mechanistic imprint, reproducing the process on the base of its thermodynamic properties – is expected to simulate the heterotrophic respiration fluxes with a lower uncertainty than the simpler empirical EF.

To give answer to the asked questions and to verify the initial hypotheses, the model has been ran on two contrasting forest ecosystems, a temperate European beech forest (Hainich, Germany) and a tropical forest located in Africa (Ankasa, Ghana), at different time scales model runs (from daily to monthly) and under different climate scenarios (current climate and climate change).

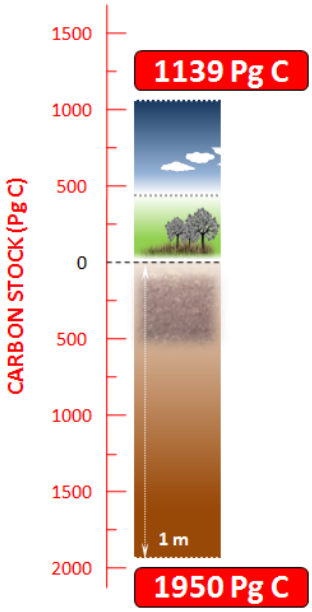

Figure 1. *Carbon stored in soil, vegetation and atmosphere on Earth.*

2. State-of-the-art

2.1 The soil carbon and nitrogen cycles

Carbon is the base of life. This fundamental element is comprised in the compounds of living tissues, fixed in chains or rings and associated with other elements. Nitrogen represents a fundamental component of many important plant compounds. It is contained in the amino acids (which regulate the biological processes), nucleic acids and chlorophyll (important for the hereditary control and photosynthesis, respectively) and carbohydrates.

The soil carbon and nitrogen cycles involve all the transformation processes of these two elements among different organic, inorganic and gaseous forms (*Fig.2*).

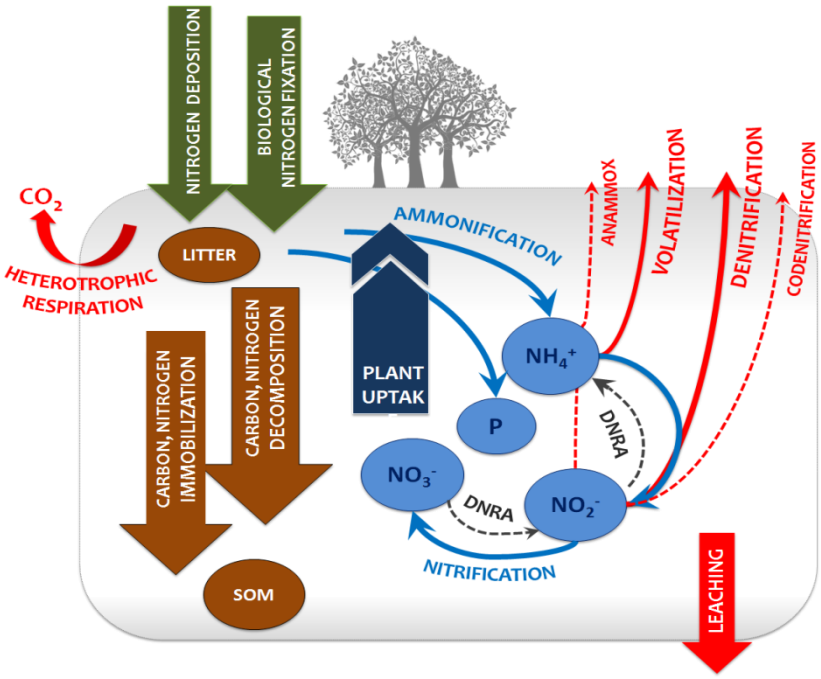

Figure 2. *Soil carbon and nitrogen processes*

Carbon (C) and nitrogen (N) are contained in the litter and soil organic matter (SOM) under different chemically structured compounds (Gessner et al., 2010) which can be decomposed by soil microorganisms. The more complex constituents, such as lignin, cellulose, hemicelluloses, fat, wax and polyphenol (Weil & Brady, 2017), are degraded through the energetically expensive production of extracellular enzymes (Burns, 2010) and reduced into simpler molecules (sugar and simple proteins) which microbes are able to metabolize. The chemical composition is the main determinant of the rate at which the microorganisms degrade organic substances. However, thought recent evidences suggest that several environmental factors are responsible of the persistence of organic compounds in the soil, as the physical disconnection between organic matter and the microbial

decomposers, the belowground origin of organic carbon, soil depth, and microbial diversity (Schmidt et al., 2011; Kleber, 2010).

Litter and SOM decomposition can be influenced by several physical (e.g. soil temperature, moisture, texture), chemical (e.g. soil pH) and biological (e.g. C:N ratio) factors (Weil & Brady, 2017). Microbial activity is accelerated by temperature enhancement and restrained by high level of soil moisture. Indeed, a saturated soil prevents microbes from accessing oxygen to carry out their vital functions (Weil & Brady, 2017). Microbial activity is also reduced by low pH values, although only a pH lower than 2 has been recognized to strongly inhibit the process (Schulze et al., 2000). The increase of the soil clay fraction and C:N ratio delay decomposition. Clay particles form ultra-micropores which entrap the organic substances and prevent the attack by the living decomposers, whereas the C:N ratio enhancement causes a need of higher nitrogen amount by microbes to perform their metabolic and physiological activities (Weil & Brady, 2017).

The decomposed C and N may follow different fates. C may be transferred in more stable organic forms (humus) or emitted as carbon dioxide (CO_2) to the atmosphere through the process of heterotrophic respiration.

Also nitrogen can be transferred in more recalcitrant organic compounds or converted into inorganic forms through the mineralization process. During this process, the amino compounds, produced by the activity of microbial decomposers, are hydrolyzed and converted in ammonium (NH_4^+), which can eventually further oxidized to nitrites (NO_2^-) and nitrates (NO_3^-):

$$R-NH_2 \xrightarrow{+2H_2O} OH^- + R-OH + {NH_4}^+ \xrightarrow{+O_2} 4H^+ + energy + {NO_2}^- \xrightarrow{+\frac{1}{2}O_2} energy + {NO_3}^- \qquad \textit{(Eq. 2.1)}$$

When the amount of organic nitrogen stored into the soil is insufficient to satisfy the demand of the microbial decomposers, they take the inorganic nitrogen from the soil solution and incorporate it as protein in their cells:

$$R-NH_2 \xleftarrow[-2H_2O]{} OH^- + R-OH + {NH_4}^+ \xleftarrow[-O_2]{} 4H^+ + energy + {NO_2}^- \xleftarrow[-\frac{1}{2}O_2]{} energy + {NO_3}^- \qquad \textit{(Eq. 2.2)}$$

The N cycle also involves a series of processes which cause the transformation of inorganic nitrogen into gaseous compounds with the consequent emission of them to the atmosphere. In forest ecosystems, the denitrification process assumes particular relevance. The soil bacteria convert the nitrate ions into nitrous oxide (N_2O) and dinitrogen (N_2), which are emitted to the atmosphere (Weil & Brady, 2017).

The inert atmospheric N_2 can be fixed by soil bacteria and transformed into reactive N through the process of biological N fixation (*Eq.2.3*). Some bacteria species, such as actinomycetes and

cyanobacteria, by the production of enzyme nitrogenase, reduce N_2 to ammonia (NH_3). The ammonia is combined further with organic acids to form amino acids and proteins. Biological N fixation is one of the most important biochemical reactions for life on Earth, next to plant photosynthesis (Weil & Brady, 2017).

$$N_2 + 8H^+ + 6e^- \xrightarrow[(Fe,Mo)]{(Nitrogenase\ )} 2NH_3 + H_2$$
$$NH_3 + organic\ acids \rightarrow amino\ acids \rightarrow proteins \qquad \textit{(Eq. 2.3)}$$

2.2 Simulation of the temperature effect on SOM decomposition

Temperature, soil moisture and substrate availability and the demand for microbial respiratory products are considered to control SOM decomposition rate. Substrate availability has been shown to vary because of increased litterfall production due to CO_2 fertilization effects (Collalti et al., 2020). Changes in soil moisture are also expected but varying locally based on site specific conditions while soil temperature variations, connected to climate change, have already been registered in several parts of the world (Fang et al., 2019), with an increase of the minimum and maximum daily soil temperature of about 0.055 and 0.031 °C year^{-1} respectively in the last 50 years (Zhang et al., 2019). Moreover, basing on the projections of the *Intergovernmental Panel on Climate Change* (IPCC), the soil temperature trend will follow the increasing air temperature, which could be 6 °C higher at the end of the century (Oni et al., 2017).

Considering that soil temperature represents one of the most relevant factor affecting the soil organic matter decomposition, understanding their relationship under climate change is crucial to predict the effects of a changing climate on the carbon stored in the soil and emitted to the atmosphere (Fang et al., 2005).

Over the past, several empirical or semi-empirical formulations have been developed to simulate the temperature effect on SOM decomposition rate (all described in *Fig.3*).

One of the most used relationship is constituted by the Exponential Function (hereafter EF) between the decay rate (R_s) and soil temperature (T_s). One of the earliest versions of CENTURY (v.4) assumes the following form:

$$R_s = a \cdot e^{b \cdot T_s} \qquad \textit{(Eq. 2.4)}$$

where *a* is the rate measured at the reference temperature (*time*$^{-1}$) and *b* is a shape parameter of the curve that encapsulates the concept of the 'temperature sensitivity' of decomposition (Rey & Jarvis, 2006). This function simulates a decay rate that continuously increases with temperature enhancement, without ever reaching a threshold maximum.

Over the time, several and further improved versions of the exponential function have been implemented in models. For example, the CENW model reproduces the soil temperature – decay rate relationship by a more sophisticated exponential equation, calibrated on laboratory and field experiments of soil data (Kirschbaum 1995, 2000a). This equation takes into account the variation of decomposition response to the temperature range:

$$R_s = exp^{3.36 \cdot \left(\frac{T_S - 40}{T_S + 31.79}\right)} \qquad \textit{(Eq. 2.5)}$$

Another widely used formulation is the Q_{10} model – implemented in many models as JSBACH (Goll et al., 2012), CLM (Yang et al., 2014), CASA (Wang et al., 2010) and ORCHIDEE (Krinner et al., 2005) – derived from the Van't Hoff model (1898). The relationship assumes the following form:

$$R_s = R_{ref} \cdot Q_{10}^{\frac{\left(T_S - T_{ref}\right)}{10}} \qquad \textit{(Eq. 2.6)}$$

where R_{ref} ($time^{-1}$) is the rate at the reference temperature T_{ref} (commonly 25 °C). The factor Q_{10}, an indicator of 'temperature sensitivity', expresses the decay rate increment corresponding to a temperature increase of 10°C.

Even though Q_{10} varies with soil temperature, as well as in space and time (Janssen & Pilegaard, 2003), models usually opt for constant Q_{10} values (Li et al., 2019), generally comprised between 1.5 and 3.

The exponential increase of SOM decomposition with temperature increment is also reproduced by the Arrhenius equation:

$$R_s = A \cdot e^{\left(\frac{-E_a}{RT}\right)} \qquad \textit{(Eq. 2.7)}$$

based on the concept of the Activation Energy (E_a, kJ mol^{-1}), the energy needed by reaction to proceed (Davidson & Janssens, 2006). In the Arrhenius equation, the activation energy is independent on the temperature and assumes a constant value derived from the experimental data.

Some models like BIOME-BGC (Thornton et al., 2002) and LPJ (Sitch et al., 2003) incorporate a modified Arrhenius equation based on Lloyd and Taylor (1994). The equation has been derived by measurements, described in several different works (e.g. Nakane, Tsubota & Yamamoto, 1984; Nakane, 1978; Yoneda & Karita, 1980; Anderson, 1973; Chapman, 1979; Peterson & Billings, 1975; Kucera & Kirkham, 1971; Monteith, Szeicz & Yabuki, 1974; Dörr & Munnich, 1987; Bridge, Mott & Hartigan, 1983; Richards, 1981; Sivola, Valijokki & Aaltonen, 1985; Svensson, 1980;

Reinke, Adriano & McLeod, 1981; Hersterberg & Siegenthaler, 1991) of soil respiration rates involving several ecosystems (forest, tundra, grassland and savannah) and referred to the CO_2 produced by plant roots, soil organisms and chemical oxidation of carbon compounds.

The first implemented versions of CENTURY (Parton et al., 1987, 1988) and the PNET-N-DNDC (Li et al., 2000) models shape the soil temperature influence on the organic matter decay rate by a Generalized Poisson Density Function (GPDF, Parton & Innis, 1972):

$$R_s = \left(\frac{T_{max} - T_s}{T_{max} - T_{opt}}\right)^c \cdot e^{\left[\left(\frac{c}{d}\right)\cdot\left(1-\left(\frac{T_{max} - T_s}{T_{max} - T_{opt}}\right)^d\right)\right]} \qquad \textit{(Eq. 2.8)}$$

Equation (2.8) depends on four parameters, among them the optimum temperature (T_{opt}, 35 °C) at which the decomposition rate is equal to 1 (it means no temperature effect on decomposition) and the maximum temperature (T_{max}, 45°C) at which R_s reaches zero. The parameters *c* and *d* are the shape of the curve to the right and to the left of T_{opt}, respectively.

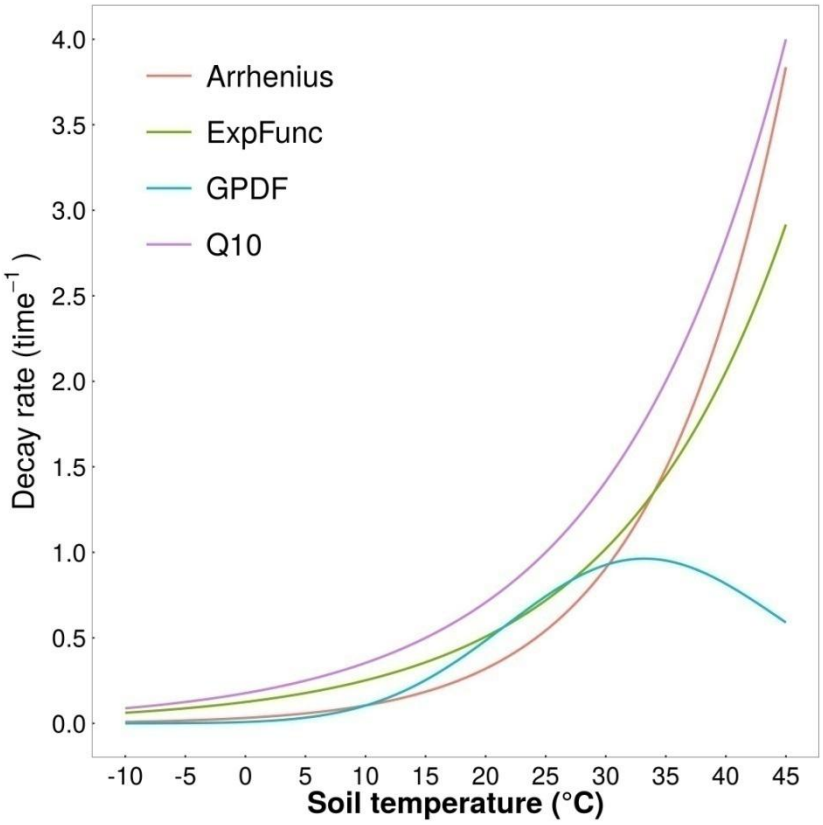

Figure 3. *Soil temperature-SOM decomposition rate relationship simulated by the Exponential Function (EF), Generalized Poisson Density Function (GPDF), Arrhenius equation and the Q_{10} model. No temperature influence on the decay rate when R_s is equal to 1. In the GPDF, T_{opt} = 35°C and T_{max} = 45°C. In the Q_{10} model, Q_{10} = 2.*

2.3 The MacroMolecular Rate Theory (MMRT)

The *Macromolecular Rate Theory* (*MMRT*) describes the relationship between the temperature and several soil biological processes (Liang et al., 2018), such as SOM decomposition, nitrification, denitrification, methane production and oxidation, amidase, myrosinase, cellulose activity, soil respiration. This formulation is an extension of the *Transition State Theory (TST)* developed by Eyring, Evans and Polanyi (Evans & Polanyi, 1935) from the *Arrhenius equation*, which assumes the following form:

$$k = A \cdot e^{\frac{-E_a}{RT}} \qquad \textit{(Eq. 2.9)}$$

where T is the temperature (°K), A is the pre-exponential term, R the universal gas constant ($0.00831\ kJ\ \mathrm{K}^{-1}\ \mathrm{mol}^{-1}$) and E_a is the activation energy. E_a plays a key role in the simulation of the temperature effect on the biological processes, representing an ideal barrier of energy that the reactants must overcome to be converted in the products of the reaction (Schipper et al., 2014). The rate of the process strongly depends on the activation energy and it is higher or slower if the energy barrier is lower or higher, respectively. In the Arrhenius equation, the activation energy is constant on the entire temperature range.

Starting from the Arrhenius equation, the TST explains the activation energy E_a(kJ mol^{-1}) (substituted by the Gibbs free energy, ΔG, kJ mol^{-1}) as function of the changes in Enthalpy (ΔH, kJ mol^{-1}) and Entropy (ΔS, kJ mol^{-1} K^{-1}) of the reaction:

$$\Delta G = \Delta H - T \cdot \Delta S \qquad \textit{(Eq. 2.10)}$$

Also the pre-exponential term A is expressed as function of temperature through some constants:

$$A = \frac{k_B \cdot T}{h} \qquad \textit{(Eq. 2.11)}$$

where k_B is the Boltzmann constant ($1.381 \cdot 10^{-23}$ J K^{-1}) and h is the Planck constant ($6.62 \cdot 10^{-34}$ J s^{-1}). The Δ in the equation 2.10 is referred to the difference between the ground state and the transition state.

The *Macromolecular Rate Theory* introduces a further concept in the relationship temperature-process rate, the *heat capacity* (C_p, kJ mol^{-1} K^{-1}), which can be defined as the dependence of the enthalpy and entropy, hence of the Gibbs free energy on the temperature (Schipper et al., 2014):

$$\Delta G = \left[\Delta H_{T0} + \Delta C_p \cdot (T - T_0)\right] - T \cdot \left[\Delta S_{T0} + \Delta C_p \cdot \left(\ln(T) - \ln(T_0)\right)\right] \qquad \textit{(Eq. 2.12)}$$

Thus, the MMRT assumes the following form:

$$k = \frac{k_B \cdot T}{h} \cdot exp\left(\frac{-[\Delta H_{T0} + \Delta C_p \cdot (T - T_0)] + [\Delta S_{T0} + \Delta C_p \cdot (\ln(T) - \ln(T_0))]}{R}\right) \quad \textit{(Eq. 2.13)}$$

where ΔH_{T0} (kJ mol^{-1}) and ΔS_{T0} (kJ mol^{-1} K^{-1}) are the changes in enthalpy and entropy, respectively, at the reference temperature T_0 (°K). The parameter ΔC_p (kJ mol^{-1} K^{-1}) is the changes in heat capacity. The introduction of the heat capacity becomes fundamental in the case of the biological processes. Indeed, they are mediated by the enzymes, which are characterized by high C_p values. For the soil processes, there are marked differences in the heat capacity changes (ΔC_p) between the enzymes linked to the substrate and the ones in the transition state. It means that, for marked differences in the heat capacity, the Gibbs free energy dependence on the temperature is high. This concept is well explained by the comparison between the classical exponential equation and the *Macromolecular Rate Theory* for different values of ΔC_p (*Fig.4*). For the processes in which ΔC_p is equal to zero, the Gibbs Free Energy is independent on the temperature and the MMRT curve describes an exponential relationship between the temperature and decomposition rate also at high temperatures. When ΔC_p is different from zero, the acclimation of the process occurs depending on significant changes between the heat capacity of enzymes in the reaction substrate and the one of enzymes in the transition state (Schipper et al., 2014). With the progressively decrease of ΔC_p, the acclimation occurs at progressively lower optimum temperatures. For example, with a ΔC_p equal to -10, the optimum temperature is reached at 28°C.

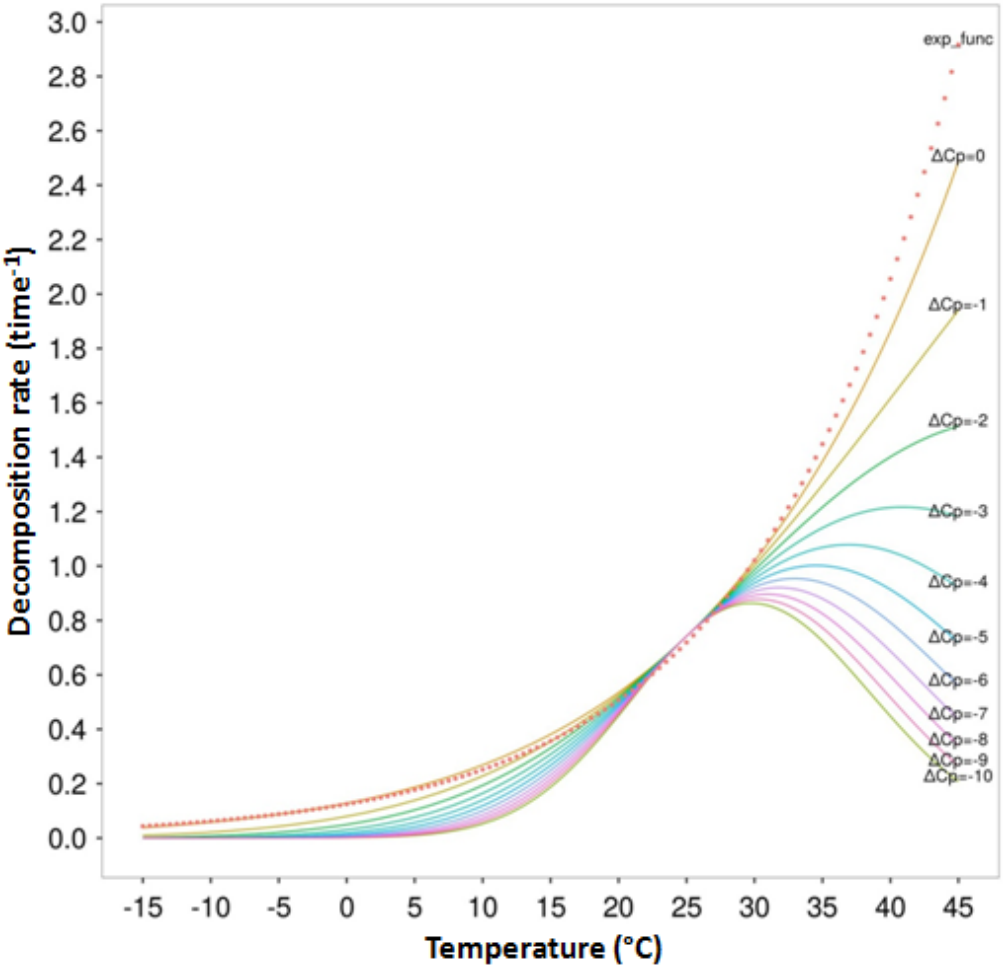

Figure 4. *Comparison between the exponential function (Eq.2.1) implemented in CENTURY v.4 (dotted line) and the MMRT. For the MMRT, the parameter* ΔC_p *varies between 0 and -10 kJ* $mol^{-1}\ K^{-1}$.

3. Materials and methods

3.1 The CENTURY model

The CENTURY model (version 4.0) (https://www.nrel.colostate.edu/projects/century/century-obtain.php, Colorado State University) is a process-based model of terrestrial biogeochemistry that simulates the cycles of Carbon and some fundamental plant macro-nutrients (Nitrogen, Phosphorous and Sulfur) in several plant-soil systems (Parton et al., 1988). The model has been implemented in 1987 to simulate the processes occurring in grassland ecosystems (Parton et al., 1987) and successively developed for cropland, savanna and forest. Three main sub-models, interacting with each other, constitute the skeleton of the model: plant, soil and water-budget. The plant sub-model, which simulates the plant growth, dry matter production, yields and nutrient allocation to shoots and roots, is connected to the soil sub-model that simulates the dynamics of soil organic matter (SOM), such as production and decomposition. The water sub-model reproduces the water dynamics in the plant-soil system.

3.1.1 The soil sub-model

The soil sub-model is focused on the simulation of SOM production and decomposition, basing on the central role that the soil organic matter plays on the plant nutrient cycles, as well as on the influences exerted on the water dynamics and soil structure (Parton et al., 1987).

In CENTURY, the SOM is partitioned into several pools, basing on the degree of decomposability of soil C and N components. In this structure, three main parts are sharply distinguishable: fresh litter, woody litter and soil organic matter (*Fig.5*). The C and N compounds of dead leaves and fine roots constitute the (above- and below-ground, respectively) fresh litter. The readily decomposable compounds of dead material (starch, sugar and proteins) converge to the metabolic pool, in which the turnover time ranges from 2 months to 1 year (*Tab.S3.1, Supplementary Material*). The resistant components, such as cellulose, hemicellulose and lignin, constitute the structural pool, with a turnover time between 1 and 5 years. The woody litter, further subdivided into fine, aboveground coarse and belowground coarse wood, represents the dead branches, stems and coarse roots of the plants. Litter C and N compounds decompose into the SOM, which is structured in three pools: microbes, slow and passive. The microbial pool, further partitioned in surface and soil layer, comprises the active fraction of carbon and nitrogen of live microbes. The slow pool involves the physically protected compounds, particularly resistant to biological decomposition (turnover time from 20 and 40 years), while the passive pool represents the chemically recalcitrant fraction of SOM, which needs between 200 and 1500 years to be decomposed.

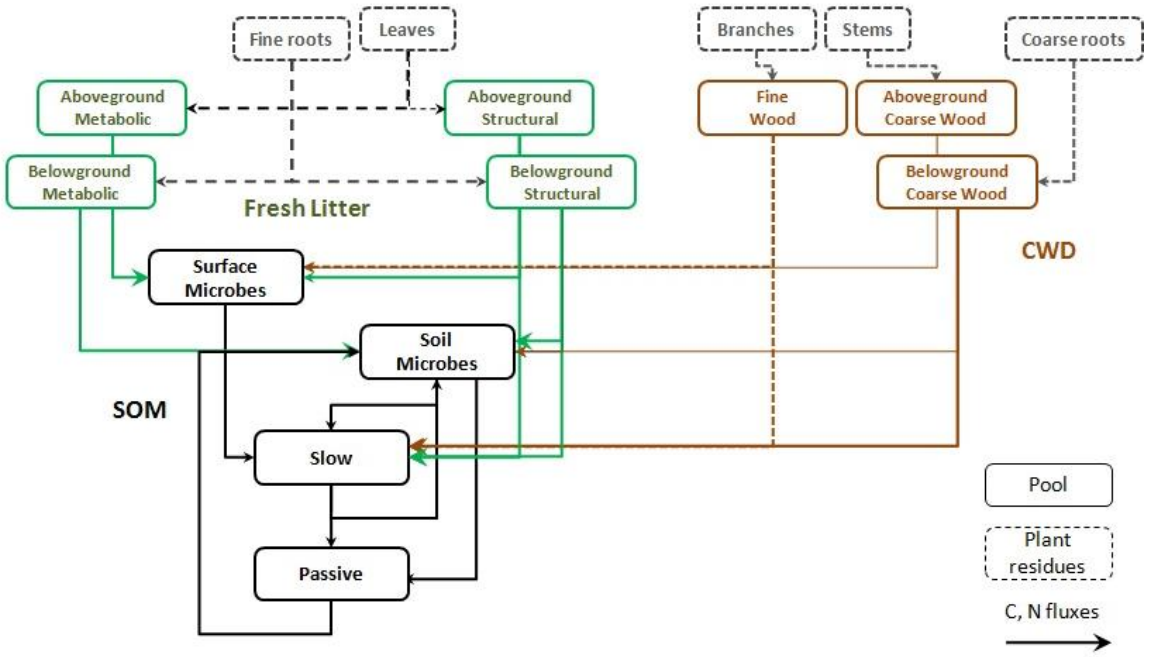

Figure 5. *The soil sub-model flowchart in CENTURY: pools (boxes) and fluxes (arrows) (based on Parton et al., 1987).*

Soil microbes need a balance between C and other nutrients to carry out their vital functions. The carbon metabolized and used as source of energy for the processes is balanced by microbes with N to synthesize amino acids and enzymes, as well as to build the DNA (Weill & Brady, 2016). In CENTURY, the C:N ratio of litter pools is allowed to vary depending on the quality of the plant residues. Instead, the C:N ratios of the SOM pools are constrained in specific ranges, between 10-16 for surface microbes, 3-15 for soil microbes, 12-40 for slow pool and 8-20 for the passive SOM. The choice of a varying C:N ratio for the soil organic matter pools is particular important in forest ecosystems, where the C:N ratios of plant residues can assume values between 20 and 50 (Kirschbaum & Paul, 2002). Moreover, the C:N ratios of SOM pools are computed as function of the available inorganic N in the soil (*Fig.6*). Indeed, the high litter C:N ratios imply an increased N demand by microorganisms, which are stimulated to immobilize inorganic N from the mineral pool (Kirschbaum & Paul, 2002).

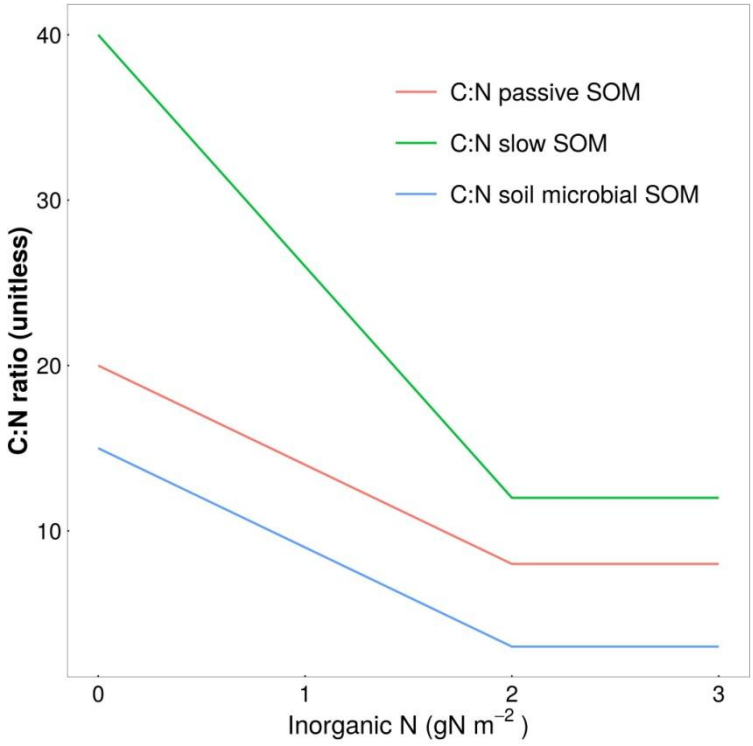

Figure 6. *Relationship between the C:N ratios of soil organic matter pools and the available inorganic nitrogen in CENTURY.*

3.1.2 The decomposition and heterotrophic respiration

In CENTURY, the litter and SOM decomposition is simulated by a system of ordinary differential equations (ODE), which allows reproducing the SOM dynamics, in continuous time (Manzoni & Porportato, 2009). For a generic pool *i*, the variation of the carbon amount *C* at the time *t* (i.e. the net balance) can be written as:

$$\underbrace{\frac{dC_i(t)}{dt}}_{\text{Relative change}} = \underbrace{I(t)_{i,ext}}_{\text{Incoming C Flux}} + \underbrace{I(t)_{i,int}}_{\text{Internal C Flux}} - \underbrace{decC(t)_i}_{\text{Outgoing C Flux}} \qquad \textit{(Eq. 3.1)}$$

where $I(t)_{i,ext}$ is the external input entering the pool (the litterfall), $I(t)_{i,int}$ represents the sum of the carbon fluxes coming from the other pools of the system and reaching the pool *i*, while $decC(t)_i$ is the decomposed carbon of the pool.

Equation 3.1 is none other than a mass balance writable in the following form:

$$\frac{dC_i(t)}{dt} = I_i - O_i \qquad \textit{(Eq. 3.2)}$$

In the generic pool *i*, the variation of the carbon amount over time is expressed by the difference between the input and the output into and from the pool.

The last term in the equation 3.1 ($decC(t)_i$), is crucial in the reproduction of SOM dynamics because embodies the effects of abiotic factors, mainly soil temperature and moisture, on carbon decomposition (Manzoni & Porporato, 2009).

In CENTURY, the decomposition of organic carbon from the litter and SOM pools is simulated by a simplified Michaelis-Menten equation, which, for the generic pool *i*, is a first-order rate:

$$decC(t)_i = K_i \cdot C_i(t) \qquad \textit{(Eq. 3.3)}$$

where $C_i(t)$ is the amount of carbon stored in the pool (g C m^{-2}) at the time *t*, K_i is the decay rate (time^{-1}).

The Michaelis-Menten model is based on the assumption that the decomposed C from the organic substrate depends on the availability of the substrate and also on the concentration of enzymes produced by soil microorganisms to degrade the SOM (Manzoni & Porporato, 2009). The simplified version of the model is based on some assumptions referred to microbial growth and activity. The changes in microbial concentration over time are extremely lower than the substrate modifications. It means that the decomposition rate is independent on microbial carbon concentration and only depends on the substrate $C(t)$. Furthermore, the enzyme production by the living decomposers is neglected, implying an implicit representation of microbes (Zhang et al., 2018), which are treated like a "*passive*" substrate rather than real decomposer organisms. Moreover, in a first order rate model, the microbial concentration never limits decomposition (Manzoni & Porporato, 2009).

The decay rate K_i is computed as:

$$K_i = k_i \cdot T_{mod} \cdot M_{mod} \qquad \textit{(Eq. 3.4)}$$

It is the product of the decay base rate k_i, which is intrinsic to each litter or SOM pool and computed without the influence of external factors, and the abiotic modifiers (related to the effects of soil temperature, T_{mod}, and moisture, M_{mod}, on decomposition) which can increase or decrease the rate at which the process occurs.

In the version 4 of CENTURY, the temperature modifier T_{mod}, at the generic temperature *T*, is computed by an exponential equation:

$$T_{mod} = a \cdot e^{b \cdot T} \qquad \textit{(Eq. 3.5)}$$

based on two parameters. The parameter *a* is the rate measured at the reference temperature, while *b* is the shape of the curve that encapsulates the concept of the temperature sensitivity of decomposition (Rey & Jarvis, 2006). This function reproduces an exponential increase of the

decomposition rate with the temperature increment, never reaching a threshold plateau (see *Par.2.2*).

In the present work, the MMRT approach (*Fig.7*) has been implemented (in parallel to the original version) to simulate the acclimation effect on SOM decomposition:

$$T_{mod} = \frac{k_B \cdot T}{h} \cdot exp\left(\frac{-[\Delta H_{T0} + \Delta C_p \cdot (T - T_0)] + [\Delta S_{T0} + \Delta C_p \cdot (\ln(T) - \ln(T_0))]}{R}\right) \quad \textit{(Eq. 3.6)}$$

where ΔH_{T0} and ΔS_{T0} are the changes in enthalpy and entropy of the process, respectively, at the reference temperature T_0. The term ΔC_p is the changes in heat capacity (see *Par.2.3*).

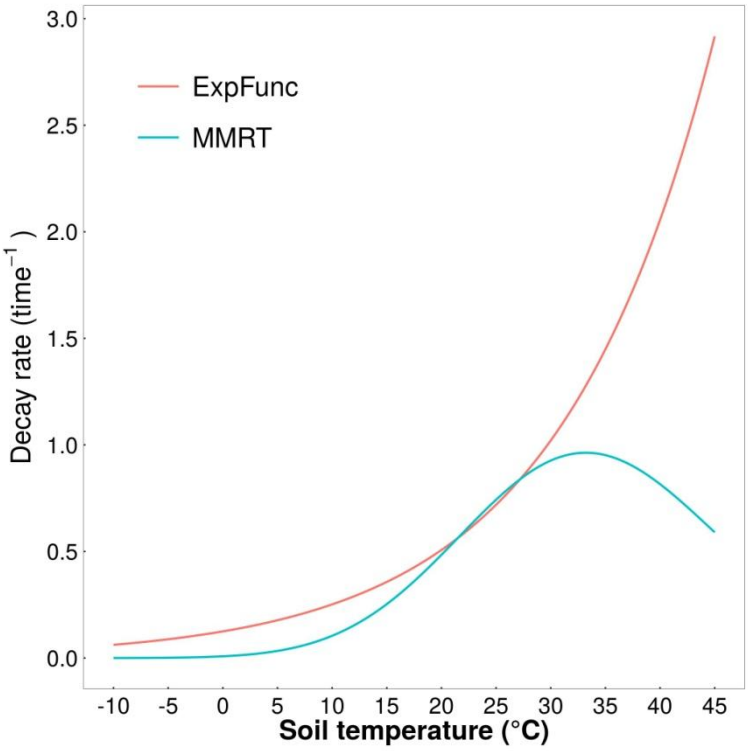

Figure 7. *Decay rate – Soil temperature relationship simulated by the exponential function (EF) and the MMRT approach.*

The soil moisture modifier (M_{mod}) is computed by the following equation (*Fig.8*):

$$\text{if } PPT/PET \leq 1 \qquad M_{mod} = \frac{1}{1+30e^{-8.5(PPT/PET)}} \quad \textit{(Eq. 3.7a)}$$

$$\text{if } PPT/PET > 1 \qquad M_{mod} = -0.35\left(\frac{PPT}{PET}\right) + 1.35 \quad \textit{(Eq. 3.7b)}$$

where PPT is the total precipitation (mm m^{-2} year^{-1}) and PET is the potential evapotranspiration (mm m^{-2} year^{-1}). The modifier increases with the increase of the PPT/PET ratio up to 1. With ratios higher than 1, the modifier decreases:

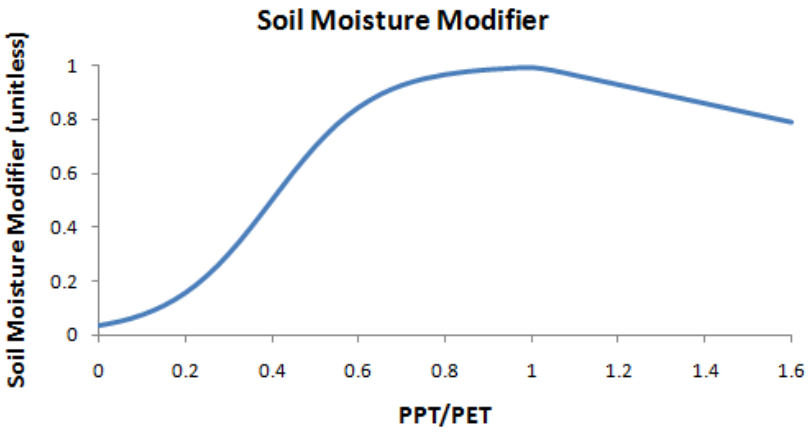

Figure 8. *Soil moisture modifier of decomposition in CENTURY (v.4)*

In the equation 3.4, for the structural and woody litter pools, a further modifier has to be added, which takes into account the lignin effect on decomposition. CENTURY assumes that microbes start to degrade the lignin contained in the plant residues after the more labile components, such as cellulose and hemicellulose (Parton et al., 1987). For the structural and woody litter pools the decay rate assumes the following form:

$$K = k_i \cdot T_{mod} \cdot M_{mod} \cdot Lig_{mod} \qquad \textit{(Eq. 3.8)}$$

where Lig_{mod} embodies the lignin effect on decomposition through a parameter (*pligst*, unitless):

$$Lig_{mod} = e^{(-pligst \cdot lignin_{fraction})} \qquad \textit{(Eq. 3.9)}$$

For the soil microbial pool the equation 3.4 assumes a further different form:

$$K = k_i \cdot T_{mod} \cdot M_{mod} \cdot TX_{mod} \qquad \textit{(Eq. 3.10)}$$

where TX_{mod} (unitless) allows to simulate the effect of soil texture on decomposition of microbial SOM:

$$TX_{mod} = peftxa + peftxb \cdot sand_{frac} \qquad \textit{(Eq. 3.11)}$$

with $peftxa$ and $peftxb$ representing two parameters, while $sand_{frac}$ is the fraction (in %) of sand in the soil.

The effect of soil texture is not only related to the decomposition of microbial SOM, but also to the stabilization efficiency of the microbial SOM into the slow pool, as well as of the slow SOM into the passive pool. Also in this case, the fractions of carbon transferred from one pool to another are expressed by empirical equations:

$$stabil\_effic_{soil\ mic \rightarrow slow} = 1 - \left(0.17 + 0.68 \cdot sand_{frac}\right) - (0.003 + 0.032 \cdot clay_{frac}) \quad \textit{(Eq. 3.12)}$$

$$stabil\_effic_{soil\ mic \rightarrow passive} = 0.003 + 0.032 \cdot clay_{frac} \quad \textit{(Eq. 3.13)}$$

In general, the carbon lost by a litter or SOM pool can follow two different fates. It can be transferred to another pool or released to the atmosphere as carbon dioxide (CO_2) due to the activity of microbial decomposers (heterotrophic respiration, R_{het}).
In CENTURY v.4 the heterotrophic respiration is strongly linked to the decomposition and simulated as a fixed fraction of $decC$ (*Tab.S3.2, Supplementary Material*). The fractions of respired C vary between 0.30-0.55 for the fluxes from the fresh and woody litter pools, between 0.55-0.60 for the C fluxes from the SOM pools. An exception is the respired C from the soil microbial pool which is simulated as function of the soil sand fraction.

In the model, in each litter and SOM pool the C and N amounts are balanced through the stoichiometric ratios. As for C, referring to a generic pool *i*, equation 3.1 can be also written as similarly for C also for N:

$$\underbrace{\frac{dN_i(t)}{dt}}_{\textit{Relative change}} = \underbrace{I(t)_{i,ext}}_{\textit{Incoming N Flux}} + \underbrace{I(t)_{i,int}}_{\textit{Internal N Flux}} - \underbrace{decN(t)_i}_{\textit{Outgoing N Flux}} \quad \textit{(Eq. 3.14)}$$

The variation of soil nitrogen stock ($N_i(t)$) in the pool *i* over time is given by the difference between the external ($I(t)_{i,ext}$) and internal ($I(t)_{i,int}$) input of N with the N lost by the pool due to decomposition ($decN(t)_i$). The last term is bonded to the decomposed carbon by the stoichiometric ratio of the pool:

$$decN(t)_i = \frac{decC\,(t)_i}{C{:}N_i} \quad \textit{(Eq. 3.15)}$$

In this way the model ensures that, at each time step, the amounts of C and N lost by the pools are always balanced to each other.
It is possible to write the equations 3.1 and 3.14 for all litter and SOM pools contained in CENTURY, obtaining the complete system of ordinary differential equations (ODE) for C and N. The system of equations can be written in a more compact form using vectors and matrices (Sierra et al., 2012):

$$\dot{X} = \begin{pmatrix} X_C \\ X_N \end{pmatrix} = \begin{pmatrix} I_C \\ I_N \end{pmatrix} + \xi(t) \cdot \begin{pmatrix} A_C & A_0 \\ A_0 & A_N \end{pmatrix} \cdot \begin{pmatrix} C \\ N \end{pmatrix} \quad \textit{(Eq. 3.16)}$$

The terms X_C and X_N express the variation of soil C and N content over the time:

$$X_C = \frac{dC_i(t)}{dt} \quad \textit{(Eq. 3.17)}$$

$$X_N = \frac{dN_i(t)}{dt} \quad \textit{(Eq. 3.18)}$$

The external inputs to the system are split for C and N (I_C and I_N), while the term $\xi(t)$ is a scalar changing over the time equal to the product of the abiotic modifiers (soil temperature and moisture). The matrices A_C and A_N contain the fractions of C and N, respectively, transferred among the pools. These two matrices represent the interactions among the litter and SOM pools. It is important to highlight that in the matrix containing A_C and A_N there are two matrices A_0 in which all terms are equal to zero, because the C pools do not interact with the N pools. The last term of equation 3.16 is expressed by the state variables C (g C m^{-2}) and N (g N m^{-2}).

3.1.3 The nitrogen pathways: mineralization and immobilization

The nitrogen fluxes can follow different fates. The decomposed organic N can move from one pool to another or can be converted into inorganic form (mineralization process). When the organic N lacks, microbes immobilize nitrogen from the mineral pool (immobilization process) to carry out their activities (Weil & Brady, 2017).

In CENTURY, the fluxes of organic nitrogen exchanged among the pools or converted in mineral form, as well as the nitrogen immobilized by microbes to satisfy their demand are regulated through the stoichiometric ratios (Parton et al., 1993). The carbon and nitrogen fluxes can leave a litter pool and reach a SOM pool, also can be transferred from a starting SOM pool to an ending SOM pool. To ensure that the C:N ratios of the SOM pools remain constrained in the prescribed range, the C:N ratio of the flux ($C:N_{flux}$) from a starting pool is compared to the C:N ratio of the ending pool ($C:N_{crit}$). If $C:N_{flux}$ is lower than $C:N_{crit}$, an excessive amount of N should reach the ending pool, unbalancing the C:N ratio of the pool beyond the maximum value. It means that the excess N has to be mineralized, hence converted into its inorganic form. Otherwise, if $C:N_{flux}$ is higher than $C:N_{crit}$, the amount of nitrogen reaching the SOM pool is insufficient to satisfy the microbial demand. In this case, the microorganisms compensate the lack immobilizing N from the mineral pool (*Fig.9*).

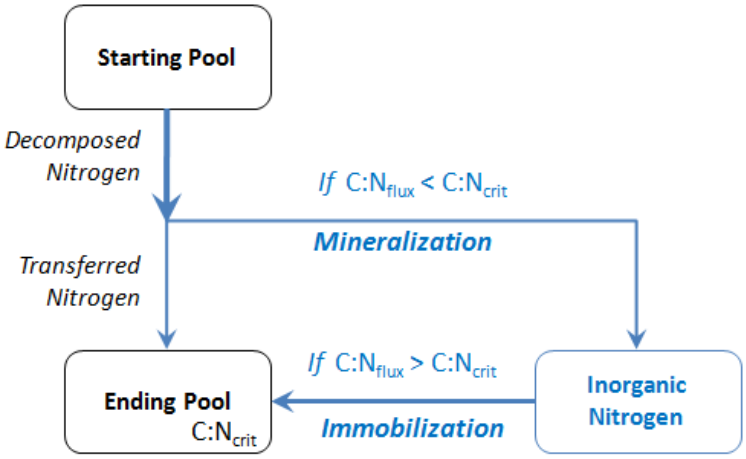

Figure 9. *Nitrogen pathways (mineralization and immobilization) in CENTURY (v.4)(derived by model code)*

The scheme implemented in CENTURY v.4 to simulate the N pathways can be defined a '*Parallel Scheme'* (Manzoni & Porporato, 2009). The model assumes that the soil microbial decomposers can directly assimilates the Nitrogen compounds with a low weight (amino-acids), converting in mineral form the exceeding N. Moreover, microbes can immobilize inorganic N to supply their N demand.

3.1.4 Nitrogen limitations to decomposition

To decompose the organic matter in the soil, the microorganisms need nutrients to balance the organic carbon assimilated through the SOM decomposition (Weill & Brady, 2016). Hence, the availability of organic N is crucial not only for the N dynamics, but also for the C fluxes.

CENTURY manages the limitations due to the N lack on decomposition as a function of the availability of the soil mineral N. At each time step (e.g. daily, monthly or annual) and for each flux from a pool to another, whenever the inorganic N is insufficient to satisfy the eventually N demand by microbes, the C decomposition is stopped (*Fig.10*). Otherwise, if the soil stores enough mineral N to sustain the eventually microbial demand, the process can proceed.

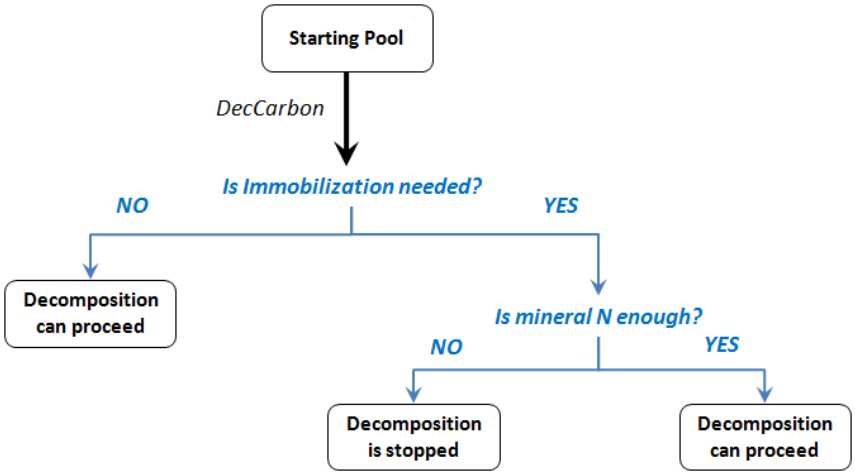

Figure 10. *Nitrogen limitations on decomposition in CENTURY (v.4)(derived by model code)*

3.2 The "SoilR" package

The soil sub-model of the version 4 of CENTURY has been implemented in R language (https://cran.rstudio.com). The aim has been to have a useful tool to carry out the uncertainty analysis on the soil temperature and moisture effects on the soil organic matter decomposition. The implementation of the model in R has been carried out using "*SoilR*" (https://cran.rstudio.com/web/packages/SoilR/index.html), a modelling framework to simulate the soil organic matter decomposition in terrestrial ecosystems developed by Dr. Carlos Sierra and Dr. Markus Müller at the Max Planck Institute for Biogeochemistry (Jena, Germany) (Sierra et al., 2012). The concept on which *SoilR* is based is that most models of SOM decomposition represent specific cases of linear dynamical systems. This allows defining a general model from which it is possible to derive each single model. For the C dynamics, the general model assumes the following form:

$$\frac{dC(t)}{dt} = I(t) + A(t) \cdot C(t) \qquad \textit{(Eq. 3.19)}$$

where $C(t)$ is the soil carbon amount at the time *t*, $I(t)$ is the external input to the system, $A(t)$ is a matrix containing the decay rates of the pools and the transfer fractions among pools. The equation 3.19 allows having a particularly flexible tool to simulate the SOM decomposition for different number of pools and different fluxes. However, at the moment the *SoilR* package is available only to simulate the C dynamics. Thus, for the present work has been necessary to adapt *SoilR* for the simulation of coupled C and N cycles, solving the following system, already described in the previous section:

$$\dot{X} = \begin{pmatrix} X_C \\ X_N \end{pmatrix} = \begin{pmatrix} I_C \\ I_N \end{pmatrix} + \xi(t) \cdot \begin{pmatrix} A_C & A_0 \\ A_0 & A_N \end{pmatrix} \cdot \begin{pmatrix} C \\ N \end{pmatrix} \qquad \textit{(Eq. 3.20)}$$

To solve the system *(Eq. 3.20)*, three scripts in R language have been implemented (*Fig.11*). The first script (‘*model_fluxlist*’) contains the carbon and nitrogen fluxes for the external inputs entering the system (litter input), the internal fluxes among the pools (organic C and N transfer, as well as nitrogen pathways) and the output fluxes from the system (CO_2 emission, N plant uptake and denitrification). Each flux is a function that calls further functions (implemented in another R language script, ’*model_functions*‘), derived from CENTURY v.4, which allow to manage the computation of the C:N ratios of the SOM pools, the N limitations on decomposition, the fractionation of litter input in metabolic and structural litter, the schedule of N pathways (*Tab.S3.3, Supplementary Material*). A third script ’*general_model*’ calls the element to build the general model and solve the system *(3.20)*.

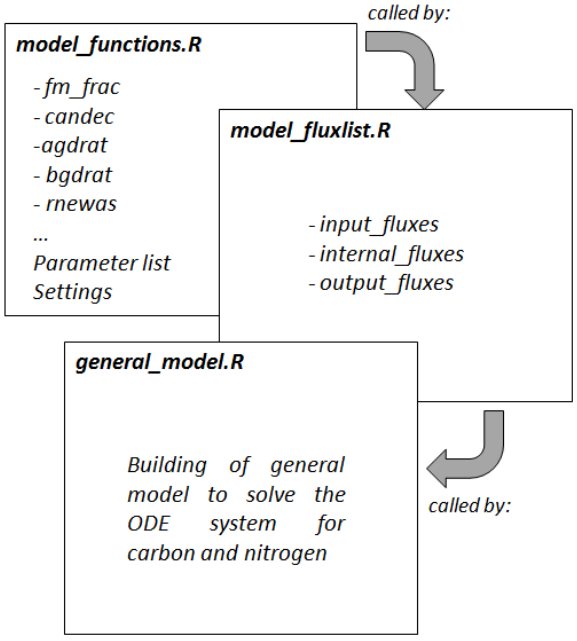

Figure 11. *Scheme of the CENTURY model implemented in R.*

3.3 The experimental set-up

3.3.1 Study sites

<u>Hainich</u>

The Hainich forest (440 m a.s.l.) is a mixed temperate forest located in Germany (51°4’45.36’’N, 10°27’7.20’’E) in the ’Hainich National Park‘ (Braakhekke et al., 2013) (*Fig.12*). The forest has been unmanaged for the last 60-70 years, due to the establishment of a military base (Kutsch et al., 2010; Marconi et al., 2017). The prevalent species are constituted for 65% by beech (*Fagus sylvatica* L.), for 25% by ash (*Fraxinus excelsior* L.) and for 7% by maple (*Acer pseudoplatanus* L. and *Acer platanoides* L.). The forest floor is characterized by herbaceous vegetation constituted by *Allium ursinum* L., *Mercurialis perennis* L. and *Anemone nemorosa* L. The trees are characterized

by different age classes reaching a maximum of 250 years and by a tree height varying between 30 and 35 m (Kutsch et al., 2010; Marconi et al., 2017).

On the site, characterized by a suboceanic/subcontinental climate, an average annual precipitation (MAP) of 800 mm m^{-2} $year^{-1}$ is registered, with an average annual potential evapotranspiration (PET) equal to 600 mm m^{-2} $year^{-1}$ and a mean annual air temperature (MAT) of 7-8 °C (Braakhekke et al., 2013).

Soils are classified as Luvisol or Cambisol, formed in limestone overlain by a layer of loess. The organic layer, a mull or F-Mull, shows a high biological activity of the soil fauna. The soil texture has a predominance of clay (70%) and silt (29%), with a low percentage of sand (1%) (Braakhekke et al., 2013).

Figure 12. *Location of Hainich forest (Germany)*

<u>Ankasa</u>

Ankasa is a tropical primary rainforest in the south-western Ghana (*Fig.13*). The site, which became a wildlife protected area in 1976, covers a surface of about 500 Km^2 (Chiti et al., 2010). The mean annual temperature (MAT) is about 25°C, while the annual precipitation (MAP), mainly concentrated from March to mid-July and in the period September-November, is equal to 2000 mm m^{-2} $year^{-1}$ (Chiti et al., 2010).

The soil, classified as Oxisols, is deeply weathered and highly acid, with a pH ranging from 3.5 and 4.0. The upland soil is characterized by coherent biotite-rich granites. The soil texture shows a predominance of sand (56%), with a percentage of clay and silt equal to 26% and 18% respectively (Chiti et al., 2010).

Figure 13. *Location of Ankasa forest (Ghana)*

3.3.2 Model spin-up

The model implemented in R language has been ran both at daily and monthly time step on two contrasting forest sites, a temperate European beech forest (Hainich) located in Germany and a mixed tropical forest (Ankasa) located in south-western Ghana.

To compute the initial soil C and N stocks for the litter and SOM pools, a spin-up ran has been performed, starting from zero C and N amount for all pools and reaching the values at equilibrium, that is the condition in which the input C and N fluxes into the soil are equal to the output ones. The simulated C and N stocks at equilibrium have been compared to the values measured at 60 cm soil depth for Hainich and at 1 meter for Ankasa (Chiti et al., 2010, 2014). The model has been parameterized with the parameter values found in literature or provided in the original CENTURY model.

3.3.3 Model validation

To evaluate the performance to simulate the heterotrophic respiration fluxes, the model has been validated at monthly time scale, using the original EF to simulate the process. Setting both the soil C and the N stocks computed at steady-state, the monthly heterotrophic respiration has been simulated for the years in which the measured values were available, two years at both sites: from 2005 to 2006 for Hainich, and from 2012 to 2013 for Ankasa, respectively.

The model also ran at daily time scale (i.e. 2005-2006 for Hainich, 2012-2013 for Ankasa, respectively) to compare the performance of both models to simulate the R_{het} fluxes in a finer time scale.

3.3.4 Simulation under climate change scenario

The parameter settings found in the validation step have been used to run the model under climate change scenario from 2006 until 2099 and basing on the Representative Concentration Pathways (RCPs) 2.6, 4.5, 6.0 and 8.5 (Moss et al., 2010; van Vuuren et al., 2011) provided by the Coupled Model Intercomparison Project 5 (CMIP5), a standard experimental protocol for studying the output of coupled atmosphere-ocean general circulation models. To reproduce the fertilization effect of the atmospheric CO_2 concentration enhancement (Collalti et al., 2018), the litterfall input has been artificially increased (*Fig.14*), while the residue C:N ratio has been kept constant. The litterfall increment ($litfal_{incr\,,frac}$) has been computed as function of the atmospheric CO_2 concentration for the three RCP climate scenarios:

$$litfal_{incr\,,frac} = \frac{[CO_2]_i{}^{0.5}}{[CO_2]_{2000}{}^{0.5}} \qquad \textit{(Eq. 3.21)}$$

where $[CO_2]_i$ and $[CO_2]_{2000}$ are the atmospheric CO_2 concentration (ppm) of year i (~421 ppm under RCP 2.6, ~538 ppm under RCP 4.5, ~666 ppm under RCP 6.0 and ~950 ppm under RCP 8.5 at 2099) and 2000 (~369 ppm), respectively.

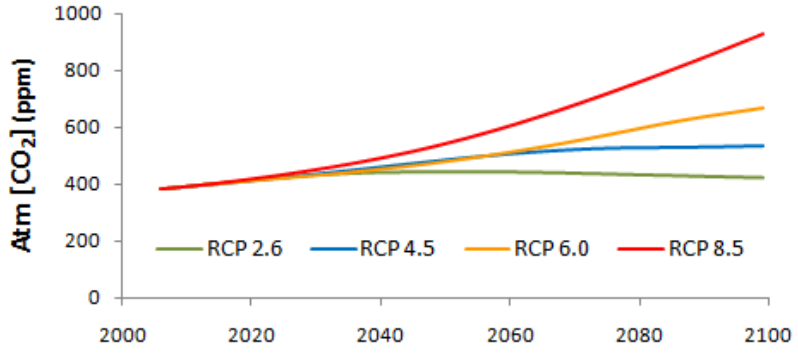

Figure 14. *Carbon dioxide concentration under RCP2.6, 4.5, 6.0 and 8.5 climate scenarios.*

3.3.5 The data

<u>Climate forcing data</u>

The model needs as input the daily (*Fig.15, 16*) or monthly (*Fig.17, 18*) (depending on the time scale at which the model runs) soil temperature (°C), total precipitation (PPT, mm m^{-2} $time^{-1}$) and potential evapotranspiration (PET, mm m^{-2} $time^{-1}$). The first variable has been used to compute the temperature modifier on decomposed carbon flux from litter and SOM pools. Instead, PPT and PET has been used to simulate the soil moisture effect on decomposition, following the original formulation implemented in CENTURY 4.0.

For both sites, Hainich and Ankasa, the meteorological data under current climate come from the FLUXNET2015 data set (http://fluxnet.fluxdata.org/).

The soil temperature under climate change scenario has been previously computed using the original routine of CENTURY, as function of the mean, minimum and maximum monthly air temperature of four Earth System Models (ESMs): HadGEM2-ES, MIROC5, IPSL-CM5A-LR and GFDL-ESM2M. The data belong to the CMIP5 outputs downloaded from the *Earth System Grid Federation* (*ESGF*) website (https://esgf-node.llnl.gov/projects/cmip5/; data accessed 10th October 2019).

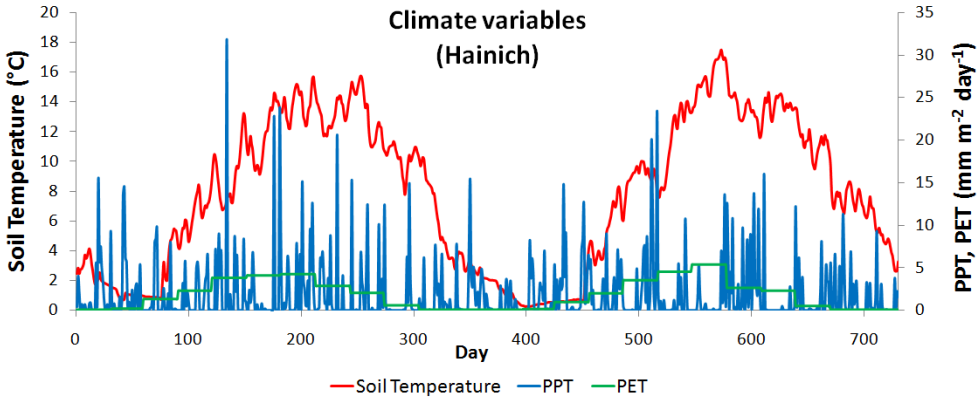

Figure 15. *Daily trend of soil temperature, total precipitation (PPT) and potential evapotranspiration (PET) during 2005 and 2006 at Hainich.*

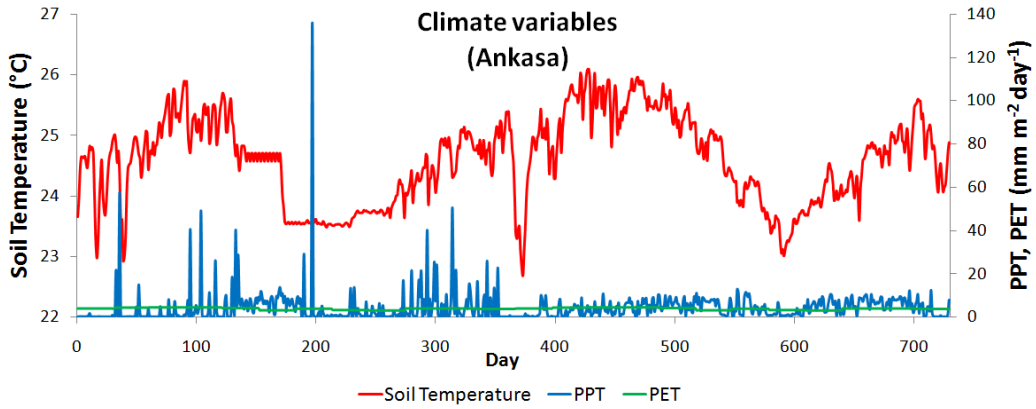

Figure 16. *Daily trend of soil temperature, total precipitation (PPT) and potential evapotranspiration (PET) during 2012 and 2013 at Ankasa.*

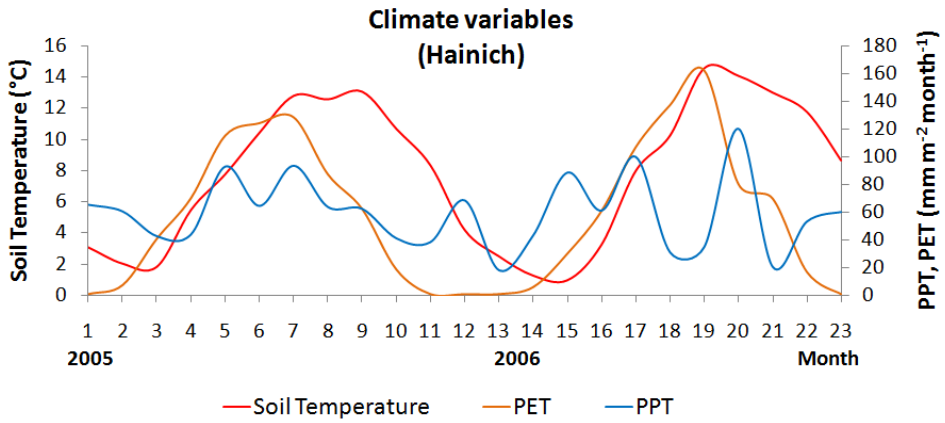

Figure 17. *Monthly trend of soil temperature, total precipitation (PPT) and potential evapotranspiration (PET) during 2005 and 2006 at Hainich.*

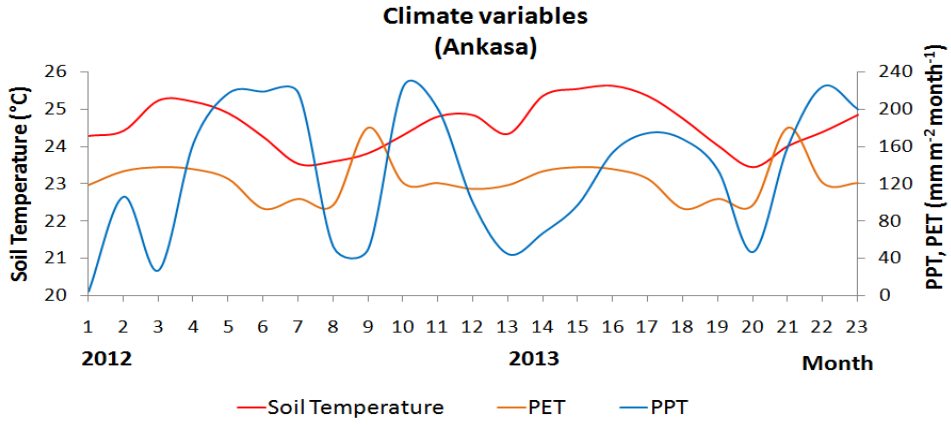

Figure 18. *Monthly trend of soil temperature, total precipitation (PPT) and potential evapotranspiration (PET) during 2012 and 2013 at Ankasa.*

Litterfall data

The litterfall data are constituted by the input residue fluxes reaching the soil. Litterfall is subdivided into above- and below-ground fresh litter (leaves and fine roots, respectively), above- and below-ground woody litter (stems + branches and coarse roots, respectively).

For the spin-up simulations, the average monthly values have been used (*Fig.19, 20*), while to run the model under current climate condition the measured daily and monthly values have been set (2005-2006 at Hainich and 2012-2103 at Ankasa). For Hainich, the data have been provided by the Max Planck Institute for Biogeochemistry (Jena, Germany), while for Ankasa by the University of Tuscia (Viterbo, Italy).

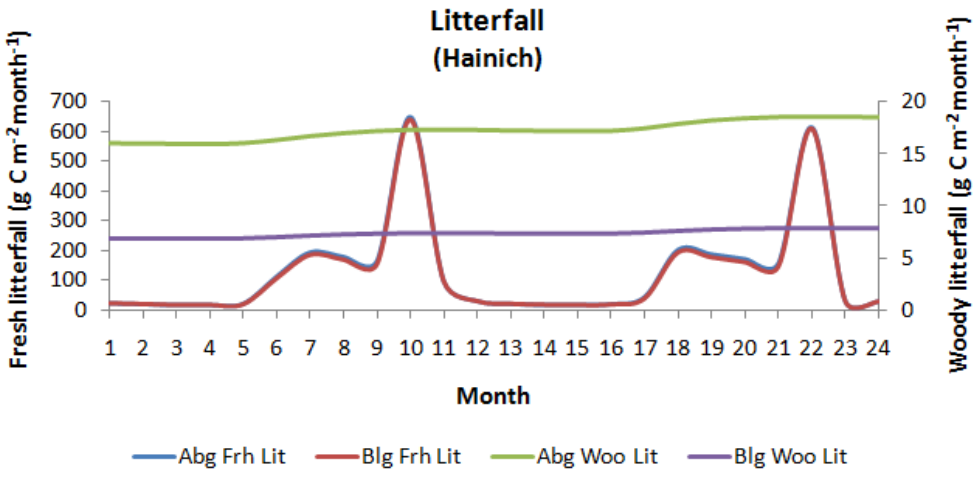

Figure 19. *Monthly trend for above- (Abg) and below- (Blg) ground fresh (Frh) and woody (Woo) litterfall at Hainich during 2005-2006.*

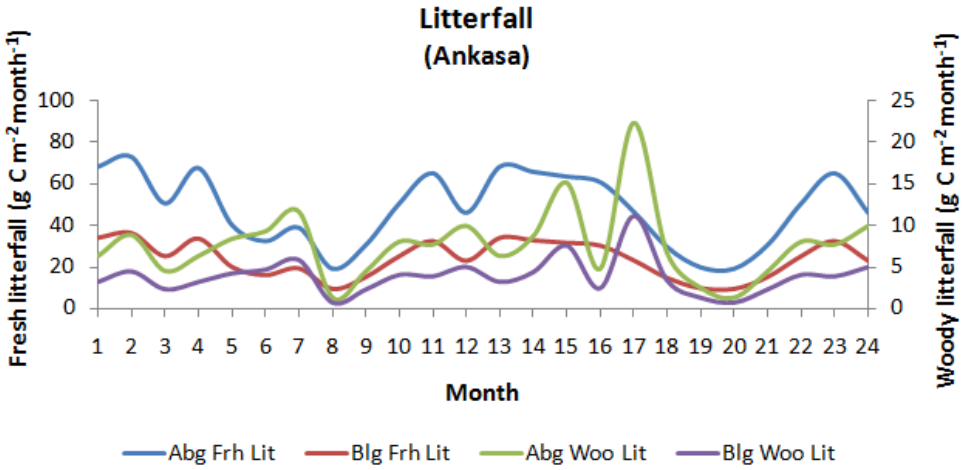

Figure 20. *Monthly trend for above- (Abg) and below- (Blg) ground fresh (Frh) and woody (Woo) litterfall at Ankasa during 2012-2013.*

<u>Soil carbon and nitrogen stocks</u>

For the Hainich site, the C and N stocks data (Kutsch et al., 2010), provided by the Max Planck Institute for Biogeochemistry (Jena, Germany), have been measured at different soil layers with a thickness of 10 cm, until a depth of 60 cm (*Fig.21*). For Ankasa, the C and N stocks are those published in Chiti et al. (2010) and measured at two soil horizons (Bo1 and Bo2) until 1 m soil depth (*Fig.22*). The measured soil C and N stocks have been used to validate the C and N stocks simulated by the model at steady-state during the spin-up simulations.

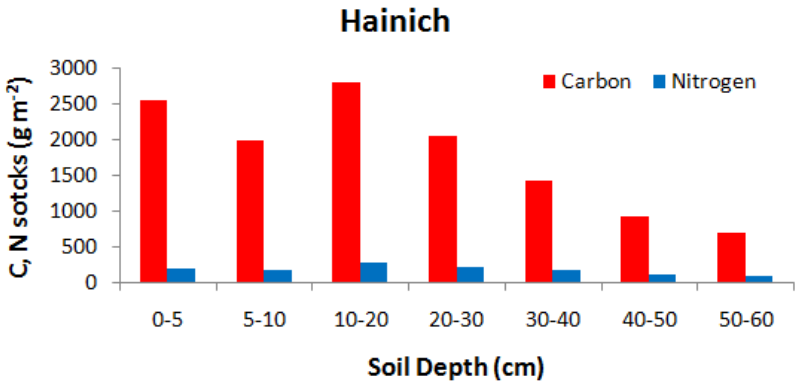

Figure 21. *Measured soil Carbon and Nitrogen stocks (g m^{-2}) at different depth (0-60 cm) at Hainich*

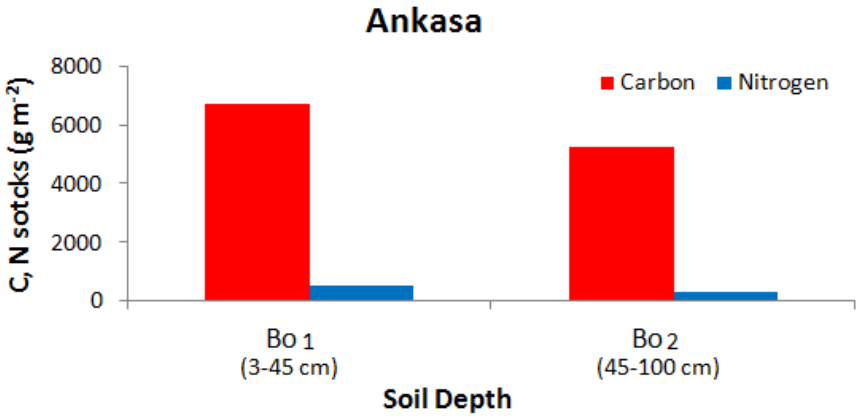

Figure 22. *Measured soil Carbon and Nitrogen stocks (g m^{-2}) at Bo1 (3-45 cm) and Bo2 (45-100 cm) horizons at Ankasa*

<u>Heterotrophic respiration fluxes</u>

For Hainich, the heterotrophic respiration fluxes, provided by Fernando Moyano and published in Kutsch et al. (2010), have been measured for 2005 and 2006. Totally, 14 values were available, measured at April, July, August, September and November for 2005, respectively, while from March to November for 2006 (*Fig.23*), respectively. The measurements have been done using a soil chamber and a infrared gas analyzer (LICOR-LI-6400-09) (Kutsch et al., 2010).

At Ankasa, the measured monthly heterotrophic respiration values have been provided by the University of Tuscia (Viterbo, Italy). The data have been measured by a infrared gas analyzer (SRC-1 IRGA) within a sealed chamber (Marthews et al., 2012). Totally, 14 values were available, measured at June, July, August, November and December for 2012, respectively, and at January, February, from April to July, from September to November for 2013 (*Fig.24*), respectively.

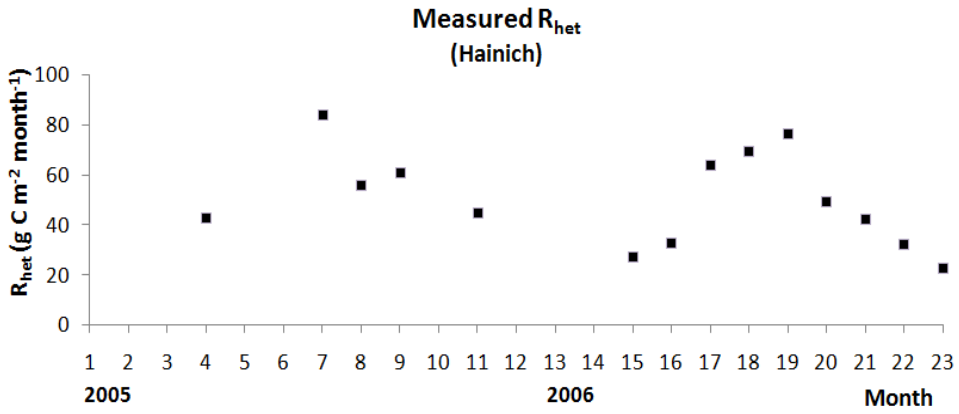

Figure 23. *Monthly heterotrophic respiration (g C m^{-2} $month^{-1}$) at Hainich*

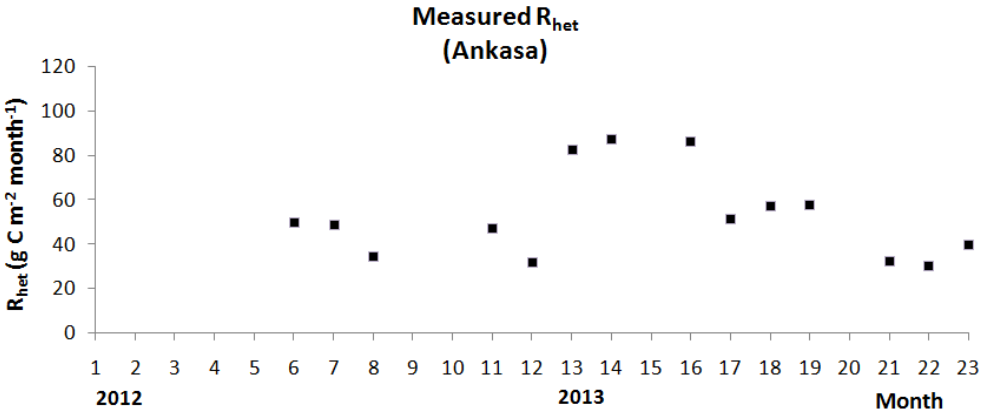

Figure 24. *Monthly heterotrophic respiration (g C m^{-2} $month^{-1}$) at Ankasa*

3.3.6 Model parameterization

For both forest sites, the model has been parameterized basing on the original CENTURY model (v.4) or using the values found in literature for the same forest ecosystems (*Tab.S3.4, Supplementary Material*).

One of the most relevant parameter is the turnover rate (τ, $time^{-1}$) of litter and soil organic matter pools. For both sites, the aboveground and belowground metabolic litter are characterized by the highest turnover rate (about two and three weeks, respectively), while the turnover rates of SOM slow and passive pools assume the lowest values, equal to 5 and 222 years, respectively. For Ankasa, only the turnover rate for the SOM slow pool (equal to 10 years) differs from Hainich.

For both sites, the lignin fractions of above- and below-ground structural residues, as well as the dead fine and coarse root wood, have been set equal to the values used in CENTURY v.4 for the temperate and tropical forests. Also the fixed fractions of respired carbon by the litter and SOM pools are the same as the original CENTURY v.4 model.

The C:N ratios of the residues, in particular for leaves, stem, fine and coarse root wood assume different values for the temperate and the tropical forest. The C:N ratios have been set basing on the

measured values and verified on literature (Snowdon et al., 2005). At Hainich, a deciduous forest, they are equal to 50, 40 and 200, respectively, while at Ankasa, assume higher values (70, 60, 200, respectively).

The denitrification of inorganic N is simulated as in CENTURY v.4. A fraction equal to 5% of mineral N is lost due to denitrification.

In the model, other relevant parameters are the minimum and maximum values in which the C:N ratios of the SOM pools can vary. At Hainich, the range is comprised between 10-16 for surface microbes, 3-15 for the soil microbes, 12-20 for the slow SOM and 10-12 for the passive SOM. At Ankasa, the C:N ratios range differs only for the slow (12-40) and passive SOM (8-20).

The parameters of the exponential function, the slope *par_a* and the exponent *par_b*, have been set with the values of the original CENTURY model computed at a reference temperature of 25°C. Instead, the value of the parameters used in the MMRT equation, the changes in enthalpy (ΔH_0) and in entropy (ΔS_0), have been found by fitting the MMRT to the exponential function until a temperature of 25°C. The fit has been carried out using the 'Non-Linear Least Square regression' package available in R (v.3.6.1) (https://stat.ethz.ch/R-manual/R-devel/library/stats/html/nls.html).

The value of the other parameter, ΔC_p, has been computed running the model with different ΔC_p values (varying from 0 to -10) and comparing the simulated heterotrophic respiration (R_{het}) for each ΔC_p with the measured data. The ΔC_p value for which the simulated R_{het} showed the highest fit with the measured data (hence, highest correlation coefficient and lowest NRMSE and AICc) has been used to run all simulations.

3.4 Sensitivity analysis

The sensitivity analysis can be defined as '*the study of how the uncertainty in the model output can be subdivided into different sources of uncertainty in the model input*' (Saltelli et al., 2019). This definition is particularly useful to understand the relationship between the sensitivity and the uncertainty analysis – which are linked to each other – but are completely different and reflect different purposes. While the sensitivity analysis allows understanding the weight exerted by the parameters on the model, the main goal of the uncertainty analysis is to quantify the uncertainty in the model estimates.

In the present work, the sensitivity analysis is a crucial step (*Fig.26*). The 'one[factor]-at-a-time' (OAT) method (Morris, 1991) allowed to detect the model parameters exerting the major weight on the simulated output CO_2 emission from the soil due to heterotrophic respiration (R_{het},). From the initial parameter set (overall constituted by 93 different parameters), a list of 56 elements has been selected on which carry out the sensitivity analysis. The list of selected parameters excludes the ones assuming a unchangeable value, fixed in the original CENTURY version used (v.4). An

example is constituted by the fractions of decomposed carbon flux, from a litter or SOM pool, that is converted into CO_2.

The OAT method consists in the variation of the default value of the selected parameters by a small fixed fraction (in the present work by –10% and +10% as in Collalti et al., 2019), estimating the effect of such variation on the model output. Hence, for both the exponential and MMRT approaches, overall 112 parameter sets have been obtained (*Fig.25*), each of which contains all parameters with the default value and only one parameter modified 'one-at-time' by –10% or +10%:

$$
\begin{aligned}
pset1 &= f\left(\mathbf{p1}_{-10\%}, p2_{def}, p3_{def}, \dots, pn_{def}\right)\\
pset2 &= f\left(\mathbf{p1}_{+10\%}, p2_{def}, p3_{def}, \dots, pn_{def}\right)\\
pset3 &= f\left(p1_{def}, \mathbf{p2}_{-10\%}, p3_{def}, \dots, pn_{def}\right)\\
pset4 &= f\left(p1_{def}, \mathbf{p2}_{+10\%}, p3_{def}, \dots, pn_{def}\right)\\
&\dots\\
pset111 &= f\left(p1_{def}, p2_{def}, p3_{def}, \dots, \mathbf{p56}_{-10\%}\right)\\
pset112 &= f\left(p1_{def}, p2_{def}, p3_{def}, \dots, \mathbf{p56}_{+10\%}\right)
\end{aligned}
$$

Figure 25 . *Parameter sets in the sensitivity analysis*

where '*pset'* is the parameter set, '*p'* the generic parameter, '*def'* the default value.

To the 112 parameter sets produced, the default set containing the default value for all parameters has been added, hence, without any perturbation. The model has been ran at monthly time step for each parameter set, simulating 113 heterotrophic respiration series, which have been compared to the observed values through the calculation of the percentage bias (*pBias*). The parameters for which the variation of ±10% generates the highest *pBias*, hence the lowest accuracy in the model estimates of R_{het}, have been extracted as the elements with the main effect on the model. The parameters extracted have been used to subsequently carry out the uncertainty analysis.

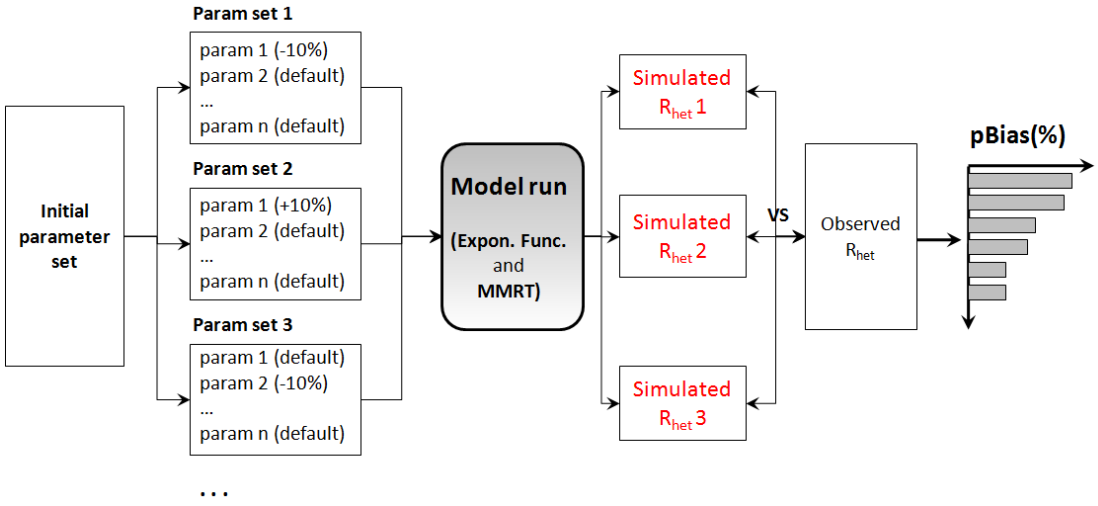

Figure 26. *Scheme adopted in the present work to carry out the sensitivity analysis*

The OAT is a local method. It means that only the effects of each single parameter are evaluated, excluding from the analysis all possible interactions among the parameters. However, this method has several advantages. In particular, the OAT allows analyzing the effect (e.g. linearity) that each parameter exert on the model estimates, setting the same variation of the default value for all parameters. Furthermore, the OAT has been widely applied in the field of ecological modelling (Medlyn et al., 2005; Collalti et al., 2019).

3.5 Uncertainty analysis

Our incomplete knowledge about soil biogeochemical processes is source of uncertainty (Van Oijen et al., 2005). The uncertainty in the representation of the processes arises from the structures on which models are built, hence from the parameters involved in each structure. For these reasons, quantifying the uncertainty in the model projections of soil C and N stocks and fluxes arising from different sources, is crucial to understand the reliability of model estimates. The uncertainty quantification is fundamental especially in the case of process-based models, which are based on the knowledge of the processes in terms of structural connectivity and functional mechanisms (Thakur, 1991) and in which the parameters assume a physical meaning.

In general, the uncertainty in model simulation can be defined as '*the quantitative measure of systematic and random variation from the "true" value of a simulated entity*' (Aubinet et al., 2012). In the models, the uncertainty derives from three main sources: structure, parameters and data (Migliavacca et al., 2012). The uncertainty arising from the structure assumes particularly importance when the aim is to use a model to make predictions under different conditions or to detect the key drivers of the system behavior (Medlyn et al., 2005). Models are built with different structures, depending on the assumptions they are based on. A specific structure contains a specific

set of parameters that, in turn, is a further source of uncertainty (the intrinsic uncertainty) (Collalti et al., 2019).

The uncertainty associated to model estimates is strongly linked to the complexity of model structure. Ultimately, the progressively increase of model complexity generates an increase in the errors produced in estimating an output variable, given by the superposition of two errors: the inadequacy and the propagation errors (*Fig.27*; Saltelli, 2019).

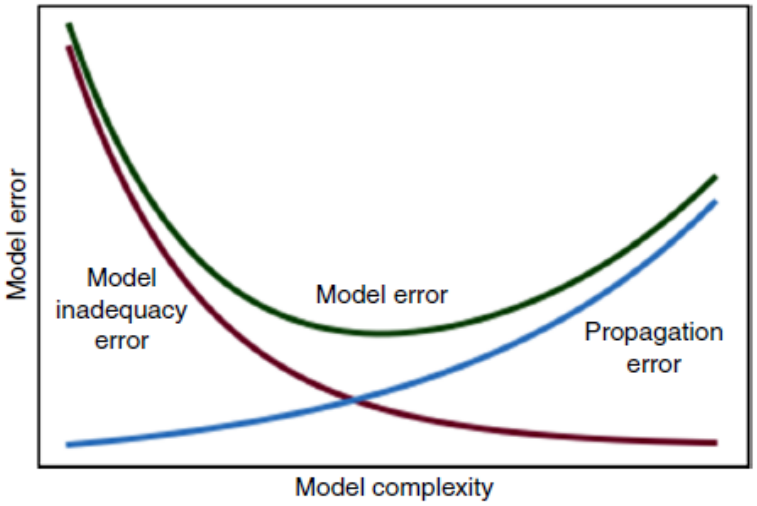

Figure 27. *Relationship between model complexity and model error (from Saltelli, 2019)*

Far too simple structures could inadequately reproduce the processes, becoming a source of inadequacy error. Instead, a too complex structure becomes a mean in which the uncertainty in the input variables propagates to the model output. Models based on more complex structures are able to reproduce more aspects of the process. However, a more complex structure introduces a higher number of parameters, increasing uncertainty on the process simulation.

A particularly clear example is represented by the work of Shi et al. (2018), in which they quantify the uncertainty in the projection of future soil carbon stocks related to the model structure. They simulate the soil carbon stocks at steady-state, under current conditions and climate change scenarios, taking into account three different structures: a conventional CENTURY-like model, a vertically resolved model and a microbial explicit model. The conventional model, despite missing of a detailed representation of the processes, is able to estimate the C stocks under climate change scenario with a lower uncertainty than the two other models with a more complex structure (*Fig.28*).

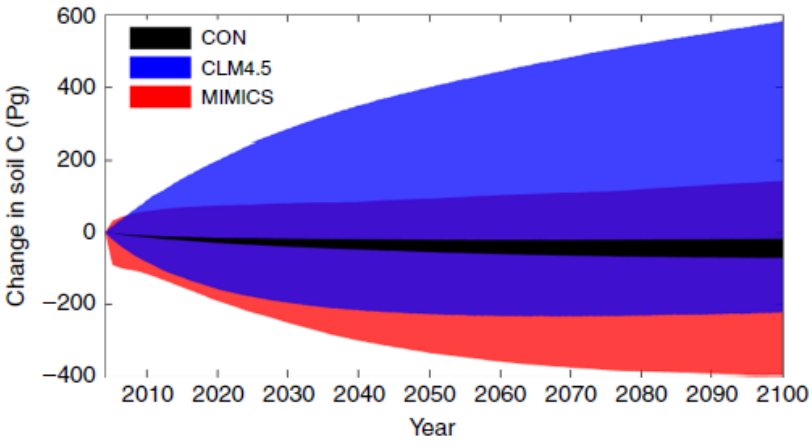

Figure 28. *Changes in global total soil carbon estimated by a conventional CENTURY-type model (CON), a vertically resolved model (CLM4.5) and a microbial explicit model (MIMICS)(from Shi et al., 2018)*

3.5.1 The Bayesian theorem

In the present work, the uncertainty in model estimation of the heterotrophic respiration fluxes has been quantified under current climate and climate change scenario(s). Two main sources of uncertainty, deeply interconnected to each other, have been analyzed: model structural and model parametric uncertainties (Medlyn et al., 2005). The two approaches adopted, to simulate the temperature effect on litter and SOM decomposition, in the present study on the conventional model structure generates itself two different structures. Each of them involves a different set of parameters, which can exert different cascade effects on the model outputs.

To quantify the uncertainty produced by the two approaches taken into account, the Bayes' theorem has been applied (Xu et al., 2006):

$$p(\theta|Z) = \frac{p(Z|\theta)\times p(\theta)}{p(Z)} \qquad \textit{(Eq. 3.22)}$$

where $p(\theta|Z)$ is the posterior probability distribution of the parameter θ conditioned to the observed variable *Z*. In the present work, Z is the monthly heterotrophic respiration.

The theorem is based on the assumption that the posterior distribution can be expressed as function of the prior probability distribution of the parameter ($p(\theta)$) and the probability of the variable Z ($p(Z)$). Usually, the term ($p(Z)^{-1}$) is equal to a fixed value. The term $p(Z|\theta)$, the distribution of Z conditioned to the parameter θ, is represented by the likelihood function for a parameter set. The theorem states that the estimation of an uncertain quantity of the parameters is linked to the data set. For this reason, the Bayes' theorem is defined as '*probabilistic inversion*' (Van Oijen et al., 2005) because it inherently explains how to infer the parameter values from the data considering how the data are determined by the parameters.

The uncertainty analysis has been carried out taking into account only the parameters selected at the end of the sensitivity analysis. In particular, the selection involved the parameters with the highest effect on the model in the simulation of the heterotrophic respiration, hence the parameters significantly affecting the model accuracy (the percentage bias, *pBias*) (*Paragraph 3.6*).

3.5.2 Prior distribution and parameter ranges

The computation of the prior probability distribution implied the definition of a range within a lower and an upper layer for each parameter. Within this range, the prior distribution for each parameter is uniform (*Fig.29*). It means that each value has the same probability to occur.

The ranges in which the parameters can vary have been carried out basing on the values described in literature and some ecological considerations.

The lower and upper values of the slope (*par_a*) and exponent (*par_b*) in the EF have been found basing on some applications of CENTURY on forest ecosystems (Holland et al., 2000; Kelly et al., 2000). The range of decomposition rates of surface microbial (*par_k_srfmic*) and slow (*par_k_slo*) SOM pools are the same as in Shi et al. (2018). In this publication, indeed, the default value of the decay rates for the fast and slow organic matter pools, characterizing the same conventional structure of CENTURY, have the same magnitude of the value set in the present work. For the decay rate of the aboveground metabolic litter (*par_k_am*), the minimum and maximum values have been arbitrary set equal to –20% and +20% of the default value, respectively, basing on some works of Parton about CENTURY (see for example Parton et al., 1987, 1988, 1993).

The definition of the range for some parameters has been difficult, in particular for those involved in the MMRT equation, hence ΔH_0 (changes in enthalpy) and ΔS_0 (changes in entropy). Indeed, for these parameters there is no available literature about similar applications to the present work. Thus, considering that the MMRT equation has been fitted on the EF up to 25°C to find the values of ΔH_0 and ΔS_0, the lower and upper layers for the MMRT parameters have been set arbitrarily equal to –30% and +30% of the default value, respectively, to have the same percentage of variation of the exponent *par_b* used in the exponential equation. However, the plausibility of the ranges set for $\Delta H0$ and ΔS_0 has been verified basing on some works found in literature (e.g. Steffen & Apostolakis, 2007; Schipper et al., 2014; Kraakman, 2017; Liang et al., 2018).

3.5.3 Posterior probability distribution

The posterior probability distribution has been computed for each parameter following a Monte Carlo Markov Chain (MCMC) technique, the same used in Xu et al. (2006) to quantify the uncertainty in the soil carbon estimates. At each run, the method computes the new parameter value basing on the previous value, as well as the lower and upper extremes set at the beginning. In this

way, after each run, the prior distribution is progressively modified and the posterior distribution is computed. In the present work, 1000 iterations have been carried out.

The likelihood function used to calculate the distribution of Z conditioned to the parameter θ ($p(Z|\theta)$) has a log-normal distribution and assumes the following form:

$$p(Z|\theta) = \sum_{i=1}^{N} \left(-0.5 \left(\frac{Obs_i - Sim_i}{\sigma_i} \right)^2 - 0.5 \cdot log(2\pi) - log(\sigma_i) \right) \qquad \textit{(Eq. 3.23)}$$

where *Obs* and *Sim* are the observed and simulated values, respectively, σ_i the standard deviation.

The likelihood function allows quantifying the model performance in simulating the output variable. Hence, the followed method allows finding the parameter values that maximize the likelihood function.

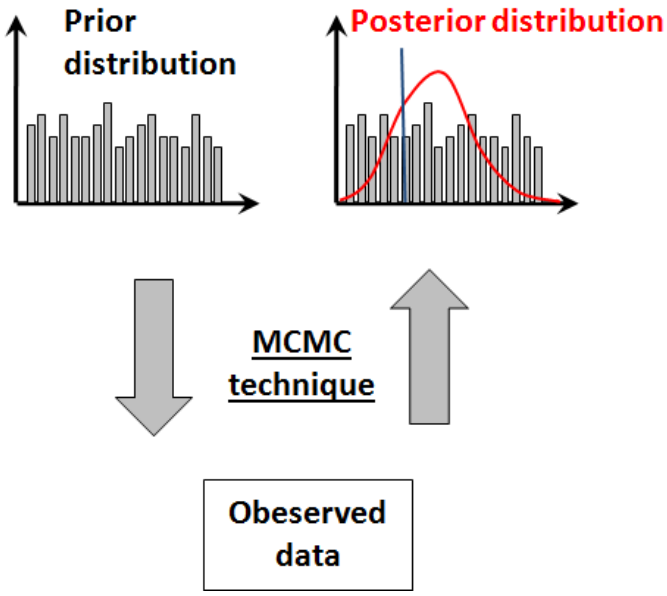

Figure 29. *Scheme adopted to quantify the posterior distribution of model parameters*

3.5.4 Uncertainty under present-day climate

The MCMC technique allowed to generate 1000 series for the monthly heterotrophic respiration (R_{het}) simulated each by both the EF and MMRT approaches at Hainich (2005-2006) and Ankasa (2012-2013) under present-day climate. To quantify the uncertainty produced by the two approaches, basing on the 1000 series, the 5th, 25th, 75th and 95th percentiles, as well as the minimum and maximum simulated R_{het}, have been computed for both approaches at both sites.

3.5.5 Uncertainty under climate change scenario

For each of the 1000 series generated by the MCMC method for both the EF and MMRT approaches at both sites, the simulated R_{het} has been compared to the measured values to calculate

the percentage bias error (*pBias*) and to detect the series that produce the lowest and the highest *pBias*. These series represent the minimum and maximum bounds of the simulated R_{het}. The corresponding parameter sets have been used to run the model under the RCP 2.6, 4.5, 6.0 and 8.5 climate change scenario(s) and to define the minimum and maximum bounds of the simulated R_{het} within the time range 2006-2099.

Considering that the temperature data of four Earth System Models (ESMs) have been used, the total annual simulated heterotrophic respiration ($F_{t,y}$) flux has been computed as a weighted mean of the single fluxes simulated for the year *y* using the ESM *j* ($F_{j,y}$), following Luyssaert et al. (2009):

$$F_{t,y} = \sum_{j=1}^{N} \left(\frac{w_j \cdot F_{j,y}}{\sum_{j=1}^{N} w_j} \right) \quad \textit{(Eq. 3.24)}$$

The term w_j is the weight of the uncertainty linked to each ESM and it has been computed as:

$$w_j = \frac{1}{{s_j}^2} \quad \textit{(Eq. 3.25)}$$

where s_j is the standard deviation calculated basing on the annual R_{het} series 2006-2099 of each ESM.

3.6 Statistical analysis

A statistical analysis has been carried out for the model validation, with the aim to evaluate the model performance to simulate the monthly heterotrophic respiration both for the EF and the MMRT formulation.

Three indices have been computed: the Pearson correlation coefficient (*rPea*), the Normalized Root Mean Square Error (*NRMSE*) and the Akaike Information Criterion (*AICc*).

The Pearson correlation coefficient explains the linear correlation between simulated and observed data, assuming values ranging between –1 (total negative linear correlation) and +1 (total positive linear correlation). A value of *rPea* equal to zero means no correlation between simulated and measured data. The coefficient is expressed as the ratio between the covariance of the two variables ($cov(Sim, Obs)$) and the product of their standard deviation (σ):

$$rPea = \frac{cov(Sim, Obs)}{\sigma_{Sim} \cdot \sigma_{Obs}} \quad \textit{(Eq. 3.26)}$$

The Normalized Root Mean Square Error (*NRMSE*) explains the difference between modeled and observed data (Collalti et al., 2016). This index is computed as:

$$NRMSE = \frac{\sqrt{\frac{1}{N}\sum_1^N (Sim - Obs)^2}}{\sigma_{Obs}} \quad \textit{(Eq. 3.27)}$$

The lower the *NRMSE* value, the lower the difference between simulated and observed data.

To compare the approaches measuring the goodness-of-fit, but also taking into account their complexity, in particular the number of parameters, the Akaike Information Criterion (*AIC*) has been computed. The *AIC* has been used also in Medlyn et al. (2005) and Migliavacca et al. (2012) to compare the performance of different model structures. Considering the small size of the data sample available, the modified version of the coefficient, the *AICc* (Burnham & Anderson, 2002), for few data has been calculated. The *AICc* should be computed when the ratio between the number of data (n) and the number of parameters (p) is lower than 40. In the present work the n/p ratio is equal to 14/2 = 7 for the exponential function, while 14/3 = 4.7 for MMRT.

The expression that allows calculating the *AICc* is:

$$AICc = nlog(\sigma^2) + 2p + \frac{2p(p+1)}{n-p-1} \quad \textit{(Eq. 3.28)}$$

where σ^2 is the residual sum of square. The approach with the lowest *AICc* indicates the approach best supported by the data.

In a different step of the work, another statistical index has been calculated: the percentage bias error (*pBias*). This index allows quantifying the accuracy of model estimates and it has been crucial in the sensitivity analysis to evaluate the model sensitivity for parameter values on the model outputs. The *pBias*, expressed in percentage, indicates about the average tendency of the simulated data to be larger or smaller than the observed values. The *pBias* has been calculated as:

$$pBias = \frac{\sum_1^n (Sim - Obs)}{\sum_1^n Obs} \cdot 100 \quad \textit{(Eq. 3.29)}$$

The best *pBias* is equal to zero. Positive values indicate overestimation, while negative values mean underestimation. In general, low-magnitude values of *pBias* mean accurate simulated outputs.

The *pBias* and the *NRMSE* have been computed in R using the pBias and NRMSE functions, respectively, of the 'hydroGOF' package (v.0.3-10) (https://www.rdocumentation.org/packages/hydroGOF/versions/0.3-10/), while the AICc has been calculated by the 'MuMIn' package (v.1.15.6) (https://www.rdocumentation.org/packages/MuMIn/versions/1.15.6/topics/AICc).

4. Results

4.1 C and N pools after the model spin-up

The soil C and N stocks at the steady-state used for the simulations has been obtained by the model spin-up phase. At Hainich forest (*Fig.30*), the metabolic and the structural litter pools (above- and below-ground) reach the equilibrium after 20 and 40 years respectively (*Fig.31-32*). The fine woody litter (fine branches) reaches the equilibrium after 150 years, while the above- (stems) and below-ground (coarse roots) woody pools stop after 300 years. For the SOM pools, the surface and the soil microbial pools reach the steady-state condition after 250 years and 600 years respectively. As expected, the longest time is required for the slow and the passive SOM, 2500 and 5000 years respectively.

The fresh litter pools, above- and below-ground, metabolic and structural, are characterized by the lowest C and N stocks, varying between 7.86 g C m^{-2} (in aboveground structural litter) to 62.9 g C m^{-2} (in belowground structural litter), between 0.75 g N m^{-2} to 1.6 g N m^{-2} (*Tab.1-2*). The soil microbial pool stores more C and N (425.7 g C m^{-2} and 15.3 g N m^{-2}) than surface microbes (116.3 g C m^{-2} and 8.4 g N m^{-2}). Most of the C and N are stored into the slow pool (5122 g C m^{-2} and 320.15 g N m^{-2}) and the passive SOM (6230.2 g C m^{-2} and 778.75 g N m^{-2}). The woody litter pools contain organic C ranging from 158.7 g C m^{-2} (fine wood) and 429.5 g C m^{-2} (above-ground coarse wood), while N is between 0.79 g N m^{-2} (fine wood) and 2.14 g N m^{-2} (above-ground coarse wood).

The simulated C:N ratios of fresh and woody litter pools are equal to the C:N ratios of the residues that reach the soil. For the SOM pools, the C:N ratios are definitely lower than litter, with the lowest value of the passive pools (equal to 8) (*Tab.3*).

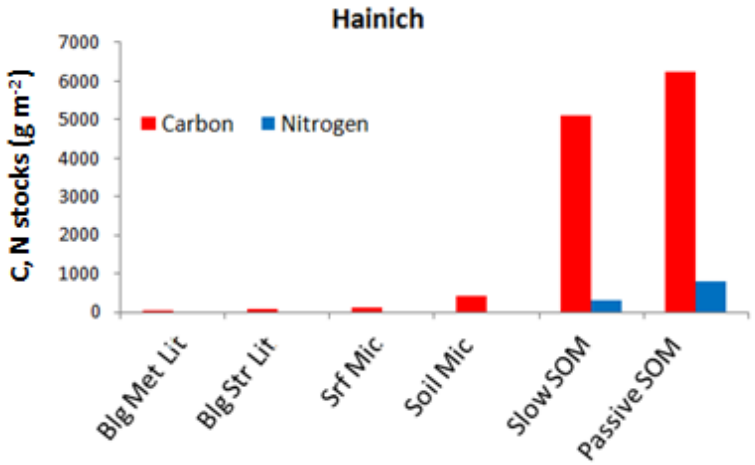

Figure 30. *Simulated Carbon and Nitrogen stocks in Belowground (Blg) Metabolic (Met) and Structural (Str) litter (Lit), Surface (Srf) and Soil Microbes (Mic), Slow and Passive SOM pools at Hainich forest*

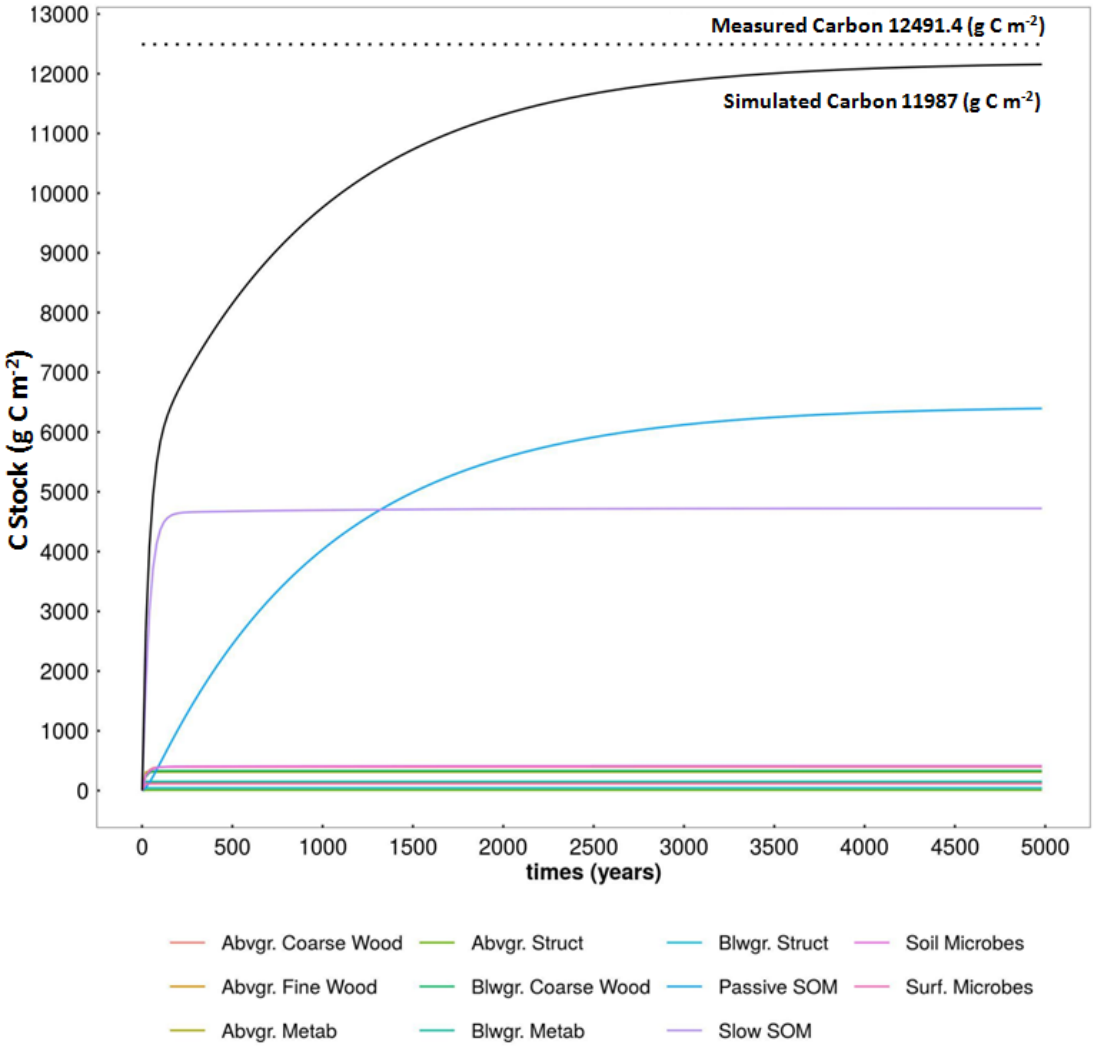

Figure 31. *Simulated Carbon stocks of each litter and SOM pool and the total amount (black curve) at steady-state at Hainich.*

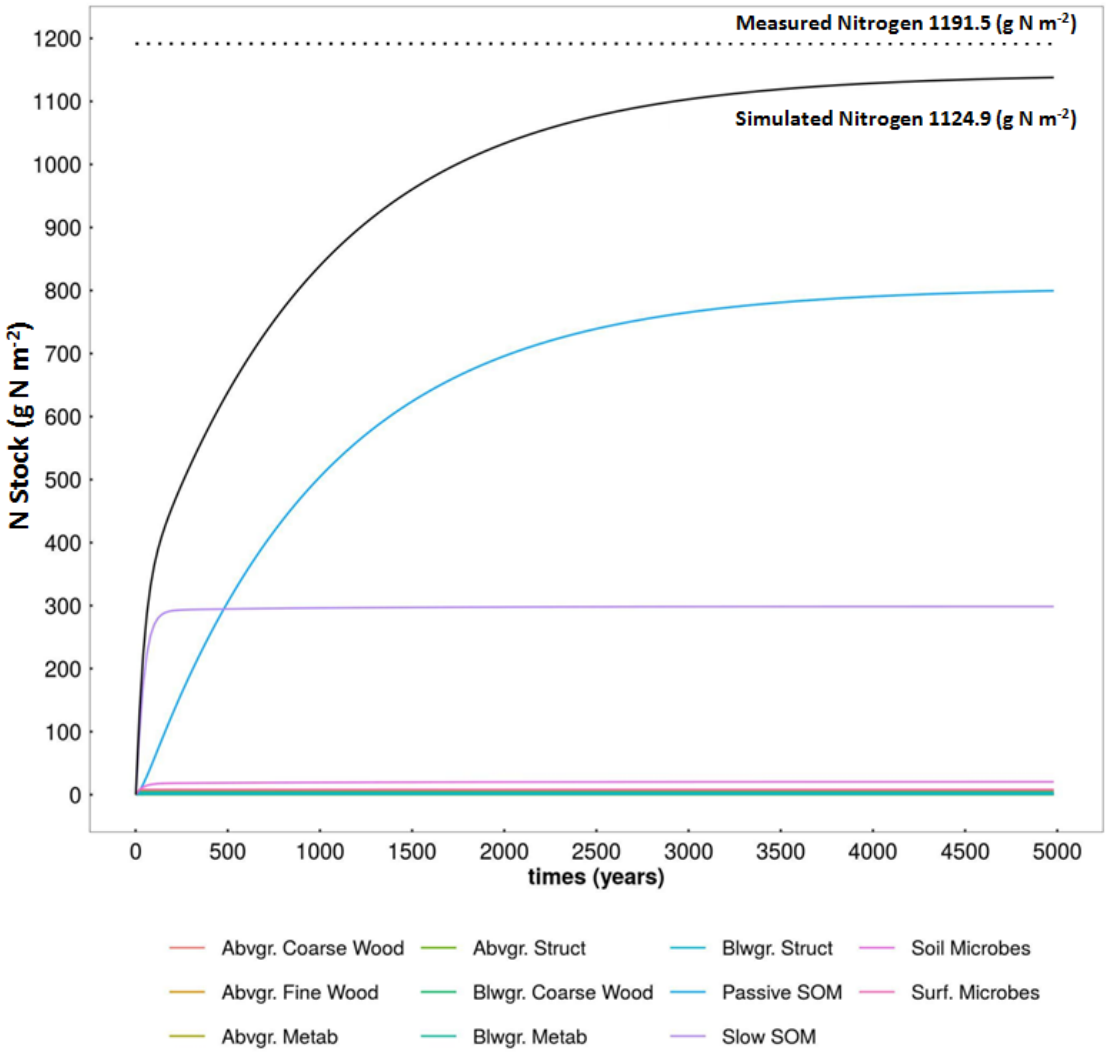

Figure 32. *Simulated Nitrogen stocks of each litter and SOM pool and the total amount (black curve) at steady-state at Hainich.*

Layer		Pool	Time to steady-state (years)	Simulated Carbon		Measured Carbon		
				Carbon Stocks (Steady State) (g C m^{-2})	Total Carbon (g C m^{-2})	Total Carbon (g C m^{-2})	Stocks at different depth (g C m^{-2})	Soil depth (cm)
Fresh Litter	Aboveground	Metabolic	20	50.3	-	-	-	-
		Structural	40	7.9				
	Belowground	Metabolic	20	30.1			2567.4	0-5
		Structural	40	62.9			2002.9	5-10
Soil Organic Matter (SOM)	Surface	Microbes	250	116.3			2806.5	10-20
	Soil	Microbes	600	425.7	**11987.23**	**12491.4**	2060.1	20-30
		Slow	2500	5122.0			1426.6	30-40
		Passive	5000	6230.2			929.4	40-50
							698.4	50-60
Woody Litter	Aboveground	Fine Wood	150	158.7	-	-	-	-
		Coarse Wood	300	429.5				
	Belowground	Coarse Wood	300	410.7				

Table 1. *Measured and simulated Carbon stocks of litter and SOM pools at steady-state at Hainich*

Layer		Pool	Time to steady-state (years)	Simulated Nitrogen		Measured Nitrogen		
				Nitrogen Stocks (Steady State) (g N m^{-2})	Total Nitrogen (g N m^{-2})	Total Nitrogen (g N m^{-2})	Stocks at different depth (g N m^{-2})	Soil depth (cm)
Fresh Litter	Aboveground	Metabolic	20	1.00	-	-	-	-
		Structural	40	0.15				
	Belowground	Metabolic	20	0.75			195.2	0-5
		Structural	40	1.60			167.3	5-10
Soil Organic Matter (SOM)	Surface	Microbes	250	8.40			263.1	10-20
	Soil	Microbes	600	15.30	**1124.95**	**1191.47**	213.5	20-30
		Slow	2500	320.15			158.0	30-40
		Passive	5000	778.75			107.1	40-50
							87.4	50-60
Woody Litter	Aboveground	Fine Wood	150	0.79	-	-	-	-
		Coarse Wood	300	2.14				
	Belowground	Coarse Wood	300	2.05				

Table 2. *Measured and simulated Nitrogen stocks of litter and SOM pools at steady-state at Hainich*

Layer		Pool	Simulated Carbon (Steady State) (g C m^{-2})	Simulated Nitrogen (Steady State) (g N m^{-2})	C:N ratios (unitless)
Fresh Litter	Aboveground	Metabolic	50.3	1.00	50.3
		Structural	7.9	0.15	52.4
	Belowground	Metabolic	30.1	0.75	40.2
		Structural	62.9	1.60	39.3
Soil Organic Matter (SOM)	Surface	Microbes	116.3	8.40	13.8
	Soil	Microbes	425.7	15.30	27.8
		Slow	5122.0	320.15	16.0
		Passive	6230.2	778.75	8.0
Woody Litter	Aboveground	Fine Wood	158.7	0.79	200.9
		Coarse Wood	429.5	2.14	200.7
	Belowground	Coarse Wood	410.7	2.05	200.3

Table 3. *Simulated C:N ratios of litter and SOM pools at Hainich*

Similar to Hainich, also at Ankasa (*Fig.34-35*) the metabolic and the structural litter pools reach the equilibrium after 20 and 40 years respectively. More time is required by fine woody litter (160 years), above- and below-ground woody pools (310 years).

The surface and soil microbial pools need about 210 years and 525 years, respectively, to reach the steady-state condition, while the slow and the passive SOM need 3000 and 5000 years, respectively. The lowest C and N stocks characterize the aboveground structural litter, 7.93 g C m^{-2} and 0.11 g N m^{-2}, respectively (*Fig.33*). The values for the woody litter pool, between 94.1 g C m^{-2} and 281.3 g C m^{-2} for C, between 0.47 g N m^{-2} and 1.41 g N m^{-2} for N, are higher than fresh litter, between 7.93 g C m^{-2} and 92.5 g C m^{-2} for C and between 0.11 g N m^{-2} and 1.54 g N m^{-2} for N, respectively.

Also for Ankasa, the soil microbial pool stores more C (110.1 g C m^{-2}) than surface microbes (67.9 g C m^{-2}) (*Tab.4-5*). The slow pool, 4175.2 g C m^{-2} and 222.09 g N m^{-2}, respectively, and the passive SOM, 8453.6 g C m^{-2} and 828.78 g N m^{-2}, respectively, store the most C and N.

The simulated C:N ratios of fresh and woody litter pools are equal to the C:N ratios of the residues that reach the soil. The C:N ratios of the SOM pools are certainly lower than litter, with the passive pools characterized by the lowest value (equal to 10.2) (*Tab.6*).

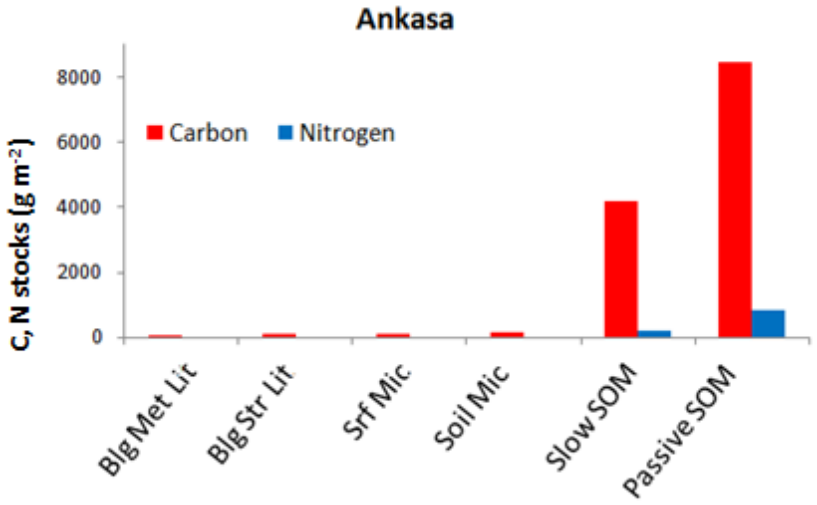

Figure 33. *Simulated Carbon and Nitrogen stocks in Belowground (Blg) Metabolic (Met) and Structural (Str) litter (Lit), Surface (Srf) and Soil Microbes (Mic), Slow and Passive SOM pools at Ankasa forest*

Comparing the two forest sites, the temperate forest of Hainich shows slightly higher amount of C stored in the soil (12491 g C m^{-2}) than the tropical site of Ankasa (12030 g C m^{-2}), and a higher N stock, 1191.47 g N m^{-2} versus 900 g N m^{-2} than that measured at Ankasa. In general, the CENTURY model underestimates the C and N values at Hainich (–4.04% and –5.6%) and overestimates at Ankasa (+7.5% and +17.9%).

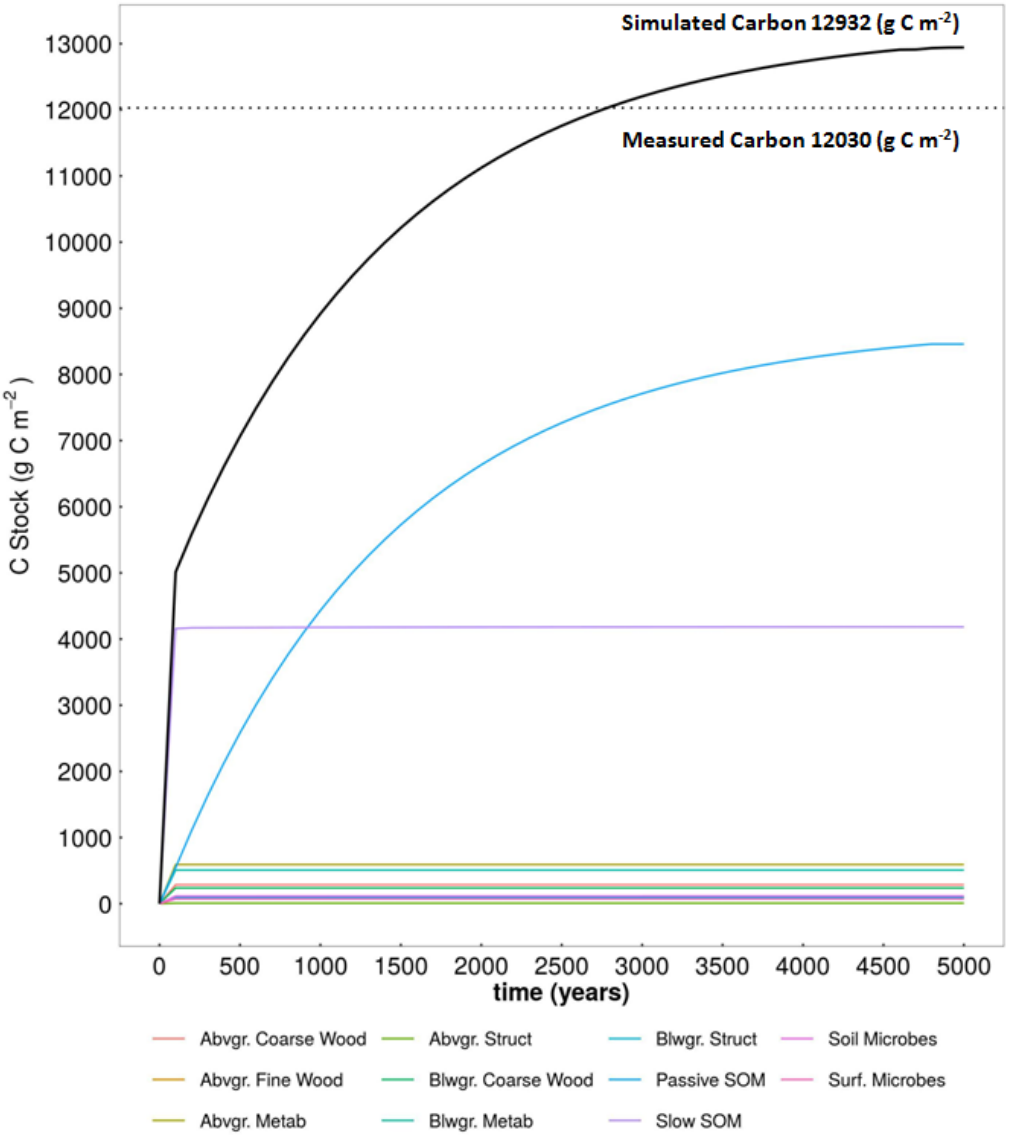

Figure 34. *Simulated Carbon stocks of each litter and SOM pool and the total amount (black curve) at steady-state at Ankasa.*

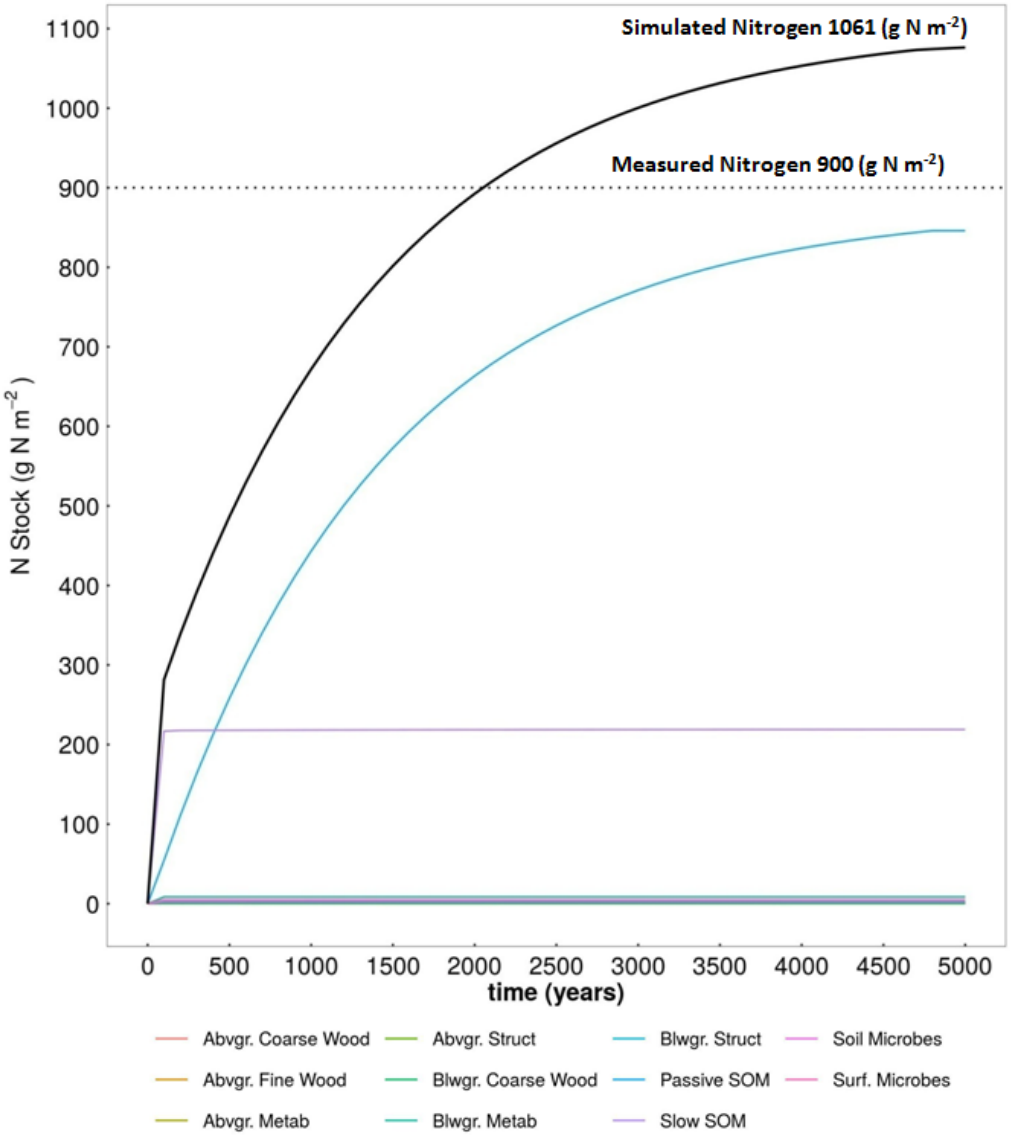

Figure 35. *Simulated Nitrogen stocks of each litter and SOM pool and the total amount (black curve) at steady-state at Ankasa.*

Layer		Pool	Time to steady-state (years)	Simulated Carbon		Measured Carbon		
				Carbon Stocks (Steady State) (g C m^{-2})	Total Carbon (g C m^{-2})	Total Carbon (g C m^{-2})	Stocks at different depth (g C m^{-2})	Horizons
Fresh Litter	Aboveground	Metabolic	20	52.1	-	-	-	-
		Structural	40	7.93				
	Belowground	Metabolic	20	33.4				
		Structural	40	92.5				
Soil Organic Matter (SOM)	Surface	Microbes	210	67.9			6760.0	Bo1
	Soil	Microbes	525	110.1	**12932.7**	**12030**		
		Slow	3000	4175.2			5270.0	Bo2
		Passive	5000	8453.6				
Woody Litter	Aboveground	Fine Wood	160	94.1	-	-	-	-
		Coarse Wood	310	281.3				
	Belowground	Coarse Wood	310	238.4				

Table 4. *Measured and simulated Carbon stocks of litter and SOM pools at steady-state at Ankasa*

Layer		Pool	Time to steady-state (years)	Simulated Nitrogen		Measured Nitrogen		
				Nitrogen Stocks (Steady State) (g N m^{-2})	Total Nitrogen (g N m^{-2})	Total Nitrogen (g N m^{-2})	Stocks at different depth (g N m^{-2})	Horizons
Fresh Litter	Aboveground	Metabolic	20	0.74	-	-	-	-
		Structural	40	0.11				
	Belowground	Metabolic	20	0.55				
		Structural	40	1.54				
Soil Organic Matter (SOM)	Surface	Microbes	210	4.62			550.0	Bo1
	Soil	Microbes	525	3.41	**1061.0**	**900**		
		Slow	3000	222.09			350.0	Bo2
		Passive	5000	828.78				
Woody Litter	Aboveground	Fine Wood	160	0.47	-	-	-	-
		Coarse Wood	310	1.41				
	Belowground	Coarse Wood	310	1.19				

Table 5. *Measured and simulated Nitrogen stocks of litter and SOM pools at steady-state at Ankasa*

Layer		Pool	Simulated Carbon (Steady State) (g C m^{-2})	Simulated Nitrogen (Steady State) (g N m^{-2})	C:N ratios (unitless)
Fresh Litter	Aboveground	Metabolic	52.1	0.74	70.1
		Structural	7.93	0.11	69.6
	Belowground	Metabolic	33.4	0.55	60.2
		Structural	92.5	1.54	60.1
Soil Organic Matter (SOM)	Surface	Microbes	67.9	4.62	14.7
	Soil	Microbes	110.1	3.41	32.3
		Slow	4175.2	222.09	18.8
		Passive	8453.6	828.78	10.2
Woody Litter	Aboveground	Fine Wood	94.1	0.47	200.1
		Coarse Wood	281.3	1.41	200.0
	Belowground	Coarse Wood	238.4	1.19	200.0

Table 6. *Simulated C:N ratios of litter and SOM pools at Ankasa*

The time needed by the model to reach the steady-state condition both for soil C and N stocks varies for the different litter and soil organic matter pools. The equilibrium has been reached for all pools after about 5000 years at both sites.

4.2 Model validation

At both forest sites, the model performances have been evaluated comparing the simulated heterotrophic respiration fluxes (R_{het}) to the values measured at monthly time scale. Unfortunately, both for Hainich and Ankasa, not further measured variables were available to validate the model.

The model ran under present-day climate at monthly time scale for the years for which the measured R_{het} were available, hence 2005 and 2006 at Hainich, 2012 and 2013 at Ankasa.

At Hainich, the measured values ranging between a minimum equal to 22.72 g C m^{-2} $month^{-1}$ to 84 g C m^{-2} $month^{-1}$, while the simulated R_{het} varies between 24.47 and 63.51 g C m^{-2} $month^{-1}$ for the EF and 17.29 and 66.47 g C m^{-2} $month^{-1}$ for the MMRT formulation, respectively (*Tab.7*). The R_{het} values simulated by both approaches are very close each other. The EF underestimates the mean measured R_{het} of about 9 g C m^{-2} $month^{-1}$, while the MMRT underestimates of 12 g C m^{-2} $month^{-1}$.

In general, there is an underestimation of heterotrophic respiration during 2005 and the most of 2006 of about 16 g C m^{-2} $month^{-1}$ for both approaches compared to the mean value computed on that period (*Fig.36*). From August to November 2006, the model, with both configurations, overestimates the measured R_{het} of about 16 g C m^{-2} $month^{-1}$ with the EF and 20 g C m^{-2} $month^{-1}$ with MMRT, respectively.

A particular case is represented by July 2005 in which the heterotrophic respiration reaches the highest value of 84 g C m^{-2} $month^{-1}$. The model is not able to reproduce this spike, simulating a value definitely lower of about 28 g C m^{-2} $month^{-1}$ with both approaches.

Year	Month	Measured R_{het} (g C m^{-2} $month^{-1}$)	Simulated R_{het} (g C m^{-2} $month^{-1}$) (EF)	Simulated R_{het} (g C m^{-2} $month^{-1}$) (MMRT)
2005	1	-	27.933	21.356
2005	2	-	26.087	19.148
2005	3	-	25.848	18.843
2005	4	42.96	33.460	28.039
2005	5	-	39.315	35.403
2005	6	-	47.326	45.645
2005	7	84.00	55.691	56.343
2005	8	55.80	54.609	54.990
2005	9	60.90	56.309	57.168
2005	10	-	47.564	46.057
2005	11	44.70	40.361	36.885
2005	12	-	30.293	24.278
2006	1	-	26.934	20.249
2006	2	-	24.846	17.759
2006	3	27.08	24.473	17.290
2006	4	32.69	28.845	22.432
2006	5	63.82	40.249	36.688
2006	6	69.42	47.140	45.542
2006	7	76.59	63.514	66.467
2006	8	49.5	61.100	63.414
2006	9	42.34	56.470	57.541
2006	10	32.38	51.662	51.410
2006	11	22.72	41.574	38.488
2006	12	-	-	-
Mean		50.35	41.37	38.32

Table 7. *Evaluation of the model performance at Hainich. The red row indicates the month with the highest difference between the simulated and the measured* R_{het}.

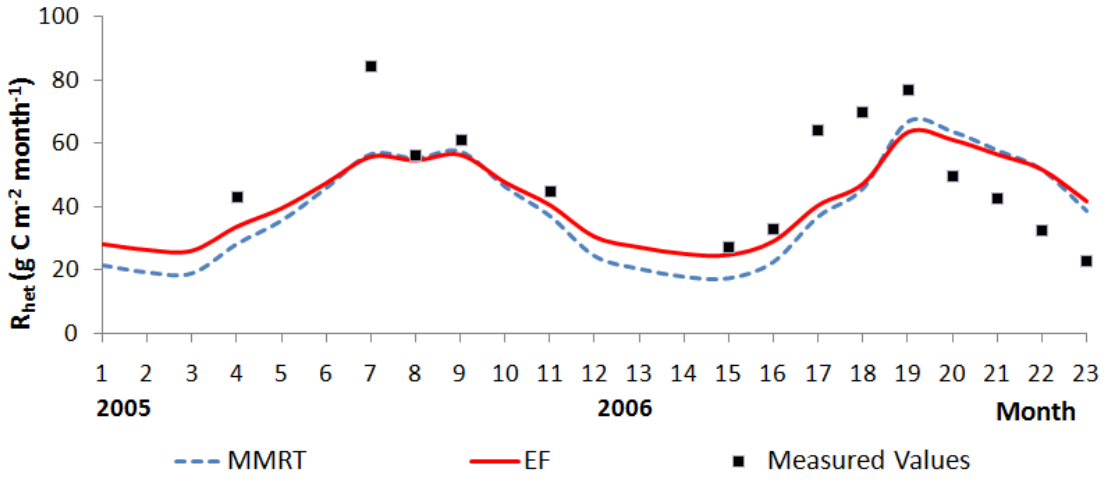

Figure 36. *Comparison between measured monthly R_{het} (g C m^{-2} $month^{-1}$) and simulated values by the EF and MMRT formulation at Hainich.*

Analyzing the monthly trend of soil temperature (T_{soil}), total precipitation (PPT) and potential evapotranspiration (PET), during 2005 and 2006 (*Fig.17*), it is clear how the heterotrophic respiration fluxes mainly follow the temperature trend. The highest R_{het} values are registered in summer, during the hottest period. The plot shows two picks in July 2005, 84 g C m^{-2} $month^{-1}$, with a soil temperature equal to 13°C, and in July 2006, 76.6 g C m^{-2} $month^{-1}$, with a soil temperature equal to 14.5°C, respectively. Instead, during the period between September and November, a decrease of the CO_2 fluxes from the soil is shown (*Tab.7*).

Comparing both approaches the values of the correlation coefficient computed are very close to each other, with a statistical negligible difference of 0.004 (*Tab.8*). Substantially, the heterotrophic respiration data simulated by the model with the two approaches correlate similarly with the measured data, showing the same *rPea*. The value tends to value of 1, hence toward a positive linear correlation between simulated and observed monthly R_{het}.

The lowest *NRMSE* (0.809) has been computed for the EF approach. It means that the model simulates the heterotrophic respiration flux with the lowest difference with the measured data. This is also confirmed by the *AICc* value calculated for the two approaches. Based on the lowest *AICc* (111.41), the EF approach shows a better fit to the measured R_{het}. However, despite the outcome of *NRMSE* and *AICc* values, the low difference between the correlation coefficients indicates that neither of the two approaches shows a statistical prevalence on the other.

	Exponential function	MacroMolecular Rate Theory (MMRT)
Correlation coefficient (rPea)	0.582	**0.578**
Normalized Root Mean Square Error (NRMSE)	**0.809**	0.865
Akaike Information Criterion (AICc)	**111.41**	118.11

Table 8. *Statistical indices computed for EF and MMRT at Hainich*

Regarding the tropical forest site located at Ankasa, the monthly heterotrophic respiration data available for 2012 and 2013 (*Tab.9*) range between 30.13 g C m^{-2} $month^{-1}$ (October, 2013) and 87.26 g C m^{-2} $month^{-1}$ (February, 2013). The mean R_{het} simulated by the EF and the MMRT are close to the mean measured value, with a difference equal to 5.38 g C m^{-2} $month^{-1}$ and 6.86 g C m^{-2} $month^{-1}$, respectively (*Fig.37*).

As at Hainich forest, also at Ankasa both approaches are very close to each other, with a difference between the mean simulated R_{het} values of 1.49 g C m^{-2} $month^{-1}$. Figure 37 shows how the two approaches are practically overlapping.

The maximum difference with the measured R_{het} occurs at May 2013, 37.05 g C m^{-2} $month^{-1}$ for EF and 39.02 g C m^{-2} $month^{-1}$ for MMRT, respectively, while the minimum difference occurs at September 2013 of 0.68 g C m^{-2} $month^{-1}$ and 1.58 g C m^{-2} $month^{-1}$, respectively.

Year	Month	Measured R_{het} (g C m^{-2} $month^{-1}$)	Simulated R_{het} (g C m^{-2} $month^{-1}$) (EF)	Simulated R_{het} (g C m^{-2} $month^{-1}$) (MMRT)
2012	1	-	94.98	97.66
2012	2	-	97.93	100.61
2012	3	-	3.54	3.64
2012	4	-	14.89	15.33
2012	5	-	108.04	110.70
2012	6	49.96	46.56	48.08
2012	7	48.60	32.74	33.84
2012	8	34.60	30.57	31.59
2012	9	-	72.57	74.92
2012	10	-	60.62	62.46
2012	11	47.24	38.18	39.25
2012	12	31.49	38.09	39.13
2013	1	82.62	66.02	67.96
2013	2	87.26	102.93	105.33
2013	3	-	116.33	118.32
2013	4	86.12	111.10	112.89

2013	5	51.49	88.54	90.51
2013	6	57.35	34.56	35.44
2013	7	57.74	32.92	33.84
2013	8	-	39.14	40.27
2013	9	32.27	32.95	33.86
2013	10	30.13	34.20	35.09
2013	11	39.46	35.98	36.84
2013	12	-	-	-
Mean		52.60	57.97	59.46

Table 9. *Evaluation of the model performance at Ankasa. The red row indicates the month with the highest difference between the simulated and the measured R_{het}.*

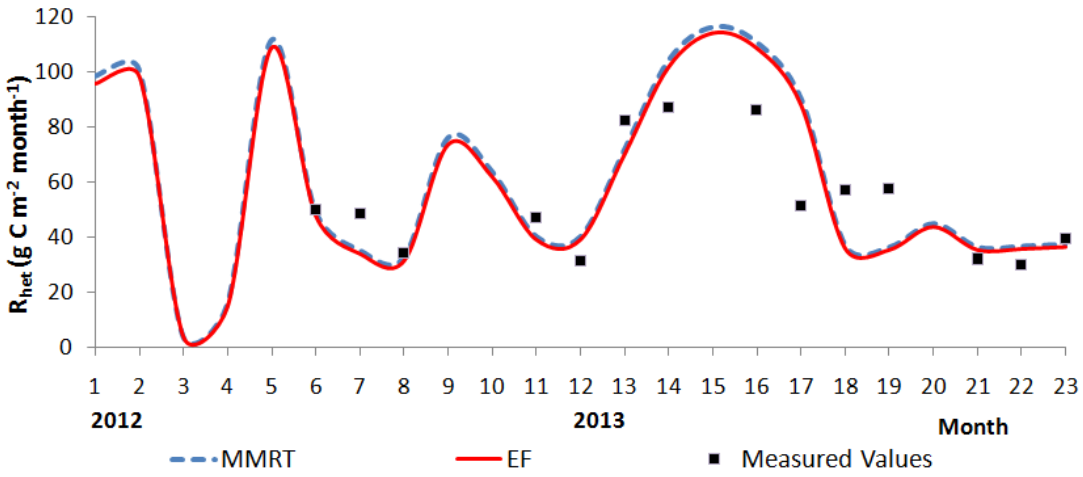

Figure 37. *Comparison between measured monthly R_{het} (g C m^{-2} $month^{-1}$) and simulated values by the EF and MMRT formulation at Ankasa.*

Despite the trend shown at Hainich, for Ankasa it is no possible to distinguish any markedly clear period to evaluate the simulated R_{het} trend. However, the plot shows some months (June and August 2012, September, October and November 2013) in which the model reproduces R_{het} values particularly close to the measured ones.

Despite at Hainich the monthly R_{het} trend is mainly driven by soil temperature, at Ankasa the total monthly precipitation and the potential evapotranspiration exert a higher weight on the trend. Indeed, the temperature values are comprised in a narrow range, ranging between 23.46 °C (August, 2013) and 25.64°C (April, 2013) (*Fig.18*).

The correlation coefficient assumes the highest value for the MMRT formulation, but, as Hainich, there is no a statistical prevalence between the two approaches. Indeed, the difference between the two *rPea* values is equal to 0.0013. The *NRMSE* computed for the EF assumes the lowest value (85.5). Also the lowest *AICc* coefficient (127.33) for the exponential approach confirms that it is the

one best supported by the data. Also for Ankasa, the statistical indices do not allow to assert which approach shows the highest statistical fit with the measured data (*Tab.10*).

	Exponential function	**MacroMolecular Rate Theory (MMRT)**
Correlation coefficient (rPea)	**0.7855**	0.7868
Normalized Root Mean Square Error (NRMSE)	**85.5**	86.9
Akaike Information Criterion (AICc)	**127.33**	127.71

Table 10. *Statistical indices computed for EF and MMRT at Ankasa.*

4.3 Simulation at daily time scale

To compare the performance of the model to simulate the heterotrophic respiration (R_{het}) by the EF and MMRT approaches, the model has been also ran at daily time scale.

At Hainich, the simulated R_{het} assumes an average value of about 0.33 g C m^{-2} day^{-1} using EF and 0.30 g C m^{-2} day^{-1} using MMRT, with the lowest values scattered in February and March (minimum 0.025 g C m^{-2} day^{-1} with EF and 0.016 g C m^{-2} day^{-1} with MMRT) and the highest values during July and August (maximum 2.30 g C m^{-2} day^{-1} with EF and 2.36 g C m^{-2} day^{-1} with MMRT).

At Ankasa, the average R_{het} is equal to 1.45 g C m^{-2} day^{-1} using EF and 1.49 g C m^{-2} day^{-1} using MMRT, with a minimum value of 0.09 g C m^{-2} day^{-1} with EF and 0.1 g C m^{-2} day^{-1} with MMRT. The maximum R_{het} is higher than Hainich, equal to 3.73 g C m^{-2} day^{-1} with EF and 3.82 g C m^{-2} day^{-1} with MMRT.

The daily trend clearly shows that – at both sites – there are not significant differences between the EF and the MMRT approaches in the simulation of R_{het} (*Fig.38-39*). The maximum daily difference between the two approaches is equal to 0.27 g C m^{-2} day^{-1} at Hainich and 0.12 g C m^{-2} day^{-1} at Ankasa. The mean cumulated difference is equal to 15.3 g C m^{-2} at Hainich and 16.9 g C m^{-2} at Ankasa, corresponding to 3.6% and 3.2% of the total annual R_{het}, respectively (*Fig.40*).

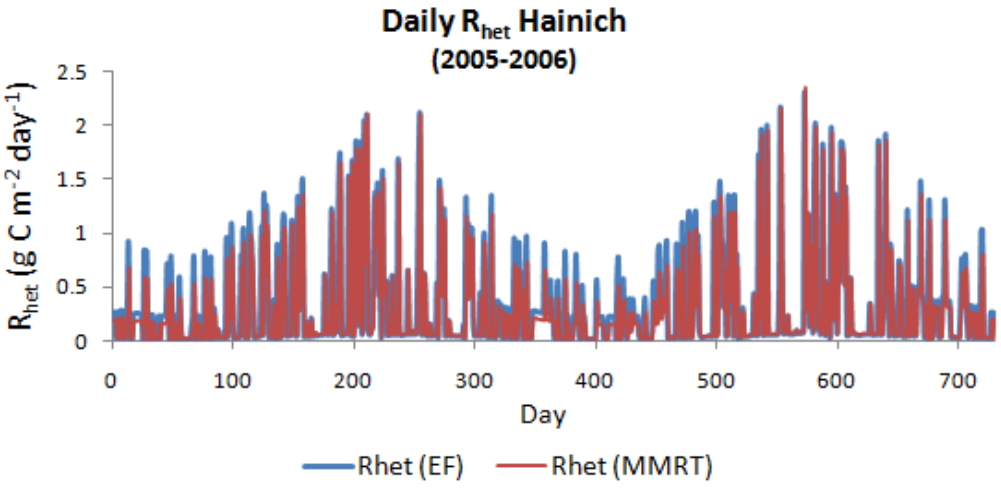

Figure 38. *Daily simulated heterotrophic respiration fluxes applying the EF and the MMRT approach at Hainich forest.*

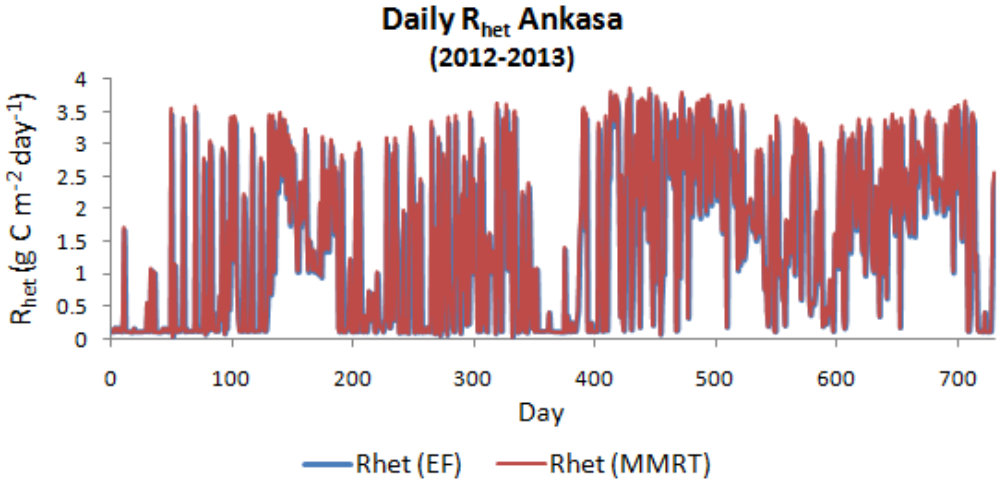

Figure 39. *Daily simulated heterotrophic respiration fluxes applying the EF and the MMRT approach at Ankasa forest.*

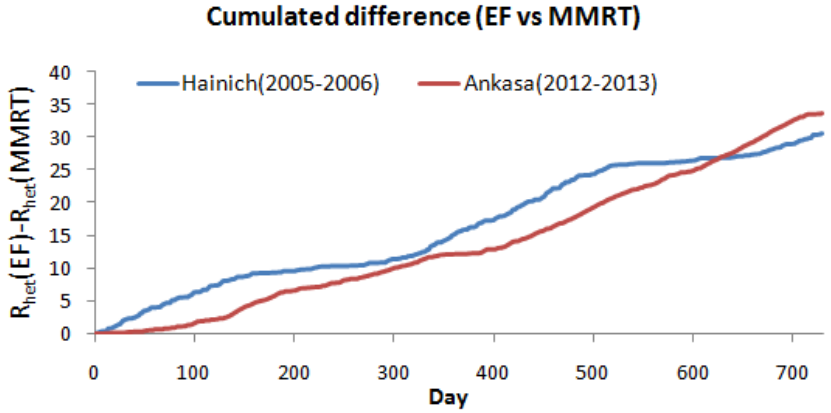

Figure 40. *Cumulated differences between the daily heterotrophic respiration simulated applying the EF and the MMRT approaches at Hainich (2005-2006) and Ankasa (2012-2013).*

4.4 Simulation under climate change scenario

To compare the EF and the MMRT approaches, the heterotrophic respiration fluxes (R_{het}) have been simulated also under three climate change scenarios (RCP 2.6, 4.5, 6.0 and 8.5) both at Hainich and Ankasa over 100 years (from 2000 to 2099).

The enhanced litterfall production – due to CO_2 fertilization effect and increased temperatures – is expected to determine an increase in the simulated R_{het} because of increased substrate. At Hainich the annual R_{het} reaches a maximum of 629.9 g C m^{-2} $year^{-1}$ using the EF approach and 623.8 g C m^{-2} $year^{-1}$ using the MMRT formulation under RCP 2.6. The maximum is equal to 660.6 g C m^{-2} $year^{-1}$ using the EF and 653.6 g C m^{-2} $year^{-1}$ using the MMRT under RCP 4.5. The maximum is equal to 680.9 g C m^{-2} $year^{-1}$ using the EF and 674.9 g C m^{-2} $year^{-1}$ using the MMRT under RCP 6.0. Instead, under the RCP 8.5, the annual R_{het} reaches a maximum of 771.9 g C m^{-2} $year^{-1}$ using the EF and 779.5 g C m^{-2} $year^{-1}$ using the MMRT approach (*Fig.41*).

At Ankasa, considering the highest temperature values, the maximum R_{het} is definitely higher than the temperate site and corresponding to 1059.1 g C m^{-2} $year^{-1}$ and 1053.4 g C m^{-2} $year^{-1}$ for the EF and MMRT approaches, respectively, under RCP 2.6. The maximum is equal to 1164.7 g C m^{-2} $year^{-1}$ using the EF and 1155.0 g C m^{-2} $year^{-1}$ using the MMRT under RCP 4.5. The maximum is equal to 1285.0 g C m^{-2} $year^{-1}$ using the EF and 1261.0 g C m^{-2} $year^{-1}$ using the MMRT under RCP 6.0. The maximum R_{het} is equal to 1431.9 g C m^{-2} $year^{-1}$ and 1407.3 g C m^{-2} $year^{-1}$ for the EF and MMRT approaches, respectively, under RCP 8.5 (*Fig.42*).

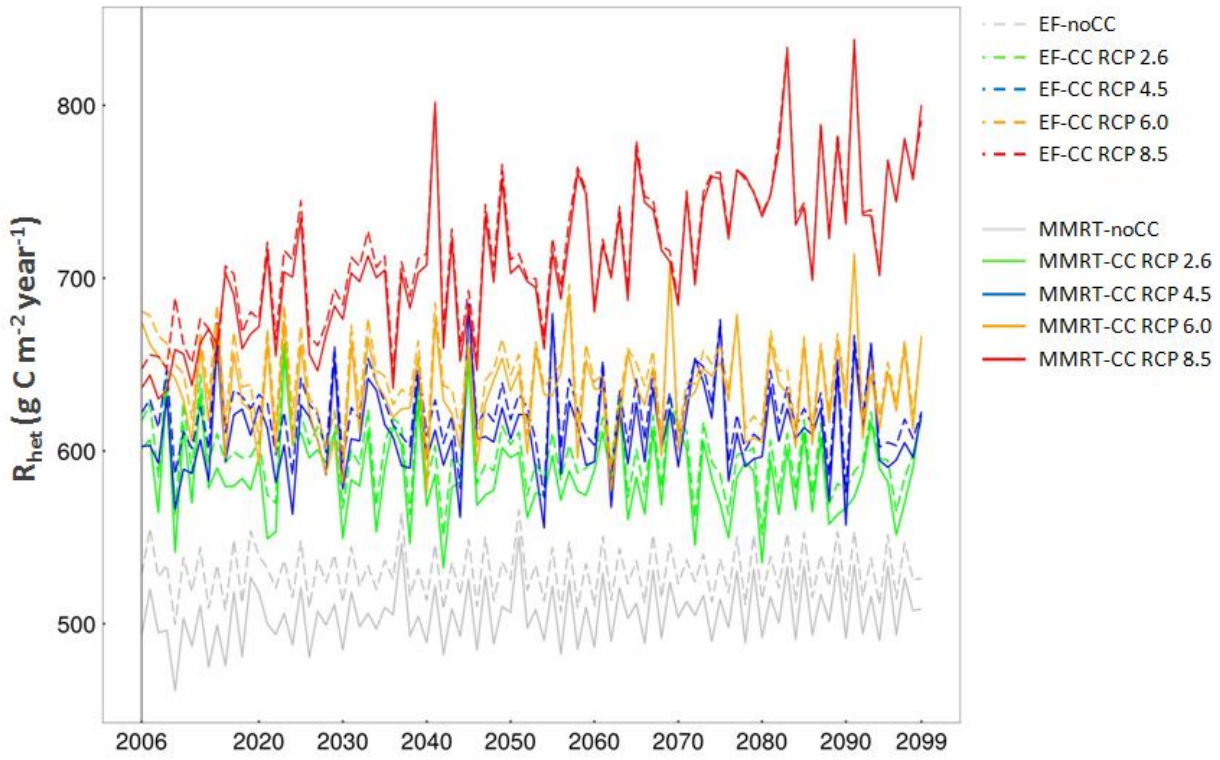

Figure 41. *Simulated annual heterotrophic respiration fluxes R_{het} (g C m^{-2} $year^{-1}$) at Hainich by the EF and MMRT approaches under no climate change scenario (noCC) and the RCP 2.6, 4.5, 6.0 and 8.5 climate change scenarios (CC) (increasing temperature and litterfall, constant C:N residues) 2006-2099.*

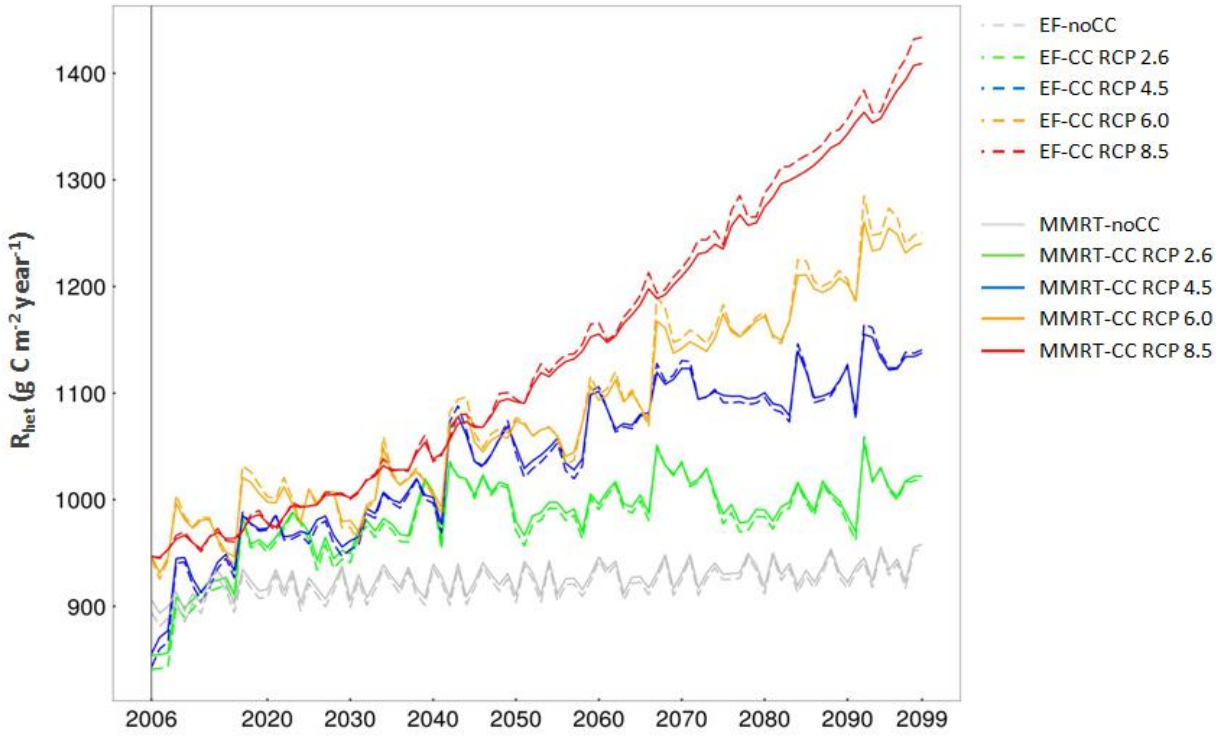

Figure 42. *Simulated annual heterotrophic respiration fluxes R_{het} (g C m^{-2} $year^{-1}$) at Ankasa by the EF and MMRT approaches under no climate change scenario (noCC) and the RCP 2.6, 4.5, 6.0 and 8.5 climate change scenarios (CC) (increasing temperature and litterfall, constant C:N residues) 2006-2099.*

At Hainich, the mean and maximum differences in the simulated heterotrophic respiration between the two approaches are equal to 12.3 g C m^{-2} $year^{-1}$ and 25.3 g C m^{-2} $year^{-1}$ under RCP 2.6, 11.9 g C m^{-2} $year^{-1}$ and 26.8 g C m^{-2} $year^{-1}$ under RCP 4.5, 9.5 g C m^{-2} $year^{-1}$ and 19.3 g C m^{-2} $year^{-1}$ under RCP 6.0, 6.4 g C m^{-2} $year^{-1}$ and 30.1 g C m^{-2} $year^{-1}$ under RCP 8.5. At Ankasa the mean and maximum differences in the simulated heterotrophic respiration between the two approaches are equal to 5.2 g C m^{-2} $year^{-1}$ and 13.1 g C m^{-2} $year^{-1}$ under RCP 2.6, 4.8 g C m^{-2} $year^{-1}$ and 12.6 g C m^{-2} $year^{-1}$ under RCP 4.5, 6.3 g C m^{-2} $year^{-1}$ and 24.1 g C m^{-2} $year^{-1}$ under RCP 6.0, 6.7 g C m^{-2} $year^{-1}$ and 24.6 g C m^{-2} $year^{-1}$ under RCP 8.5 (*Tab.11*).

Site	RCP	Mean Annual Difference (EF - MMRT) (g C m^{-2} $year^{-1}$)	Maximum Annual Difference (EF - MMRT) (g C m^{-2} $year^{-1}$)
Hainich	2.6	12.3	25.3
	4.5	11.9	26.8
	6.0	9.5	19.3
	8.5	6.4	30.1
Ankasa	2.6	5.2	13.1
	4.5	4.8	12.6
	6.0	6.3	24.1
	8.5	6.7	24.6

Table 11. *Mean and Maximum difference of annual R_{het} between the EF and MMRT approaches at Hainich and Ankasa under the RCP 2.6, 4.5, 6.0 and 8.5 climate change scenarios*

While on the short-term both approaches show to reproduce similar results, some difference between the two approaches can be detected taking into account the cumulated differences over 100 years. At the tropical site, the total cumulated difference within the whole period 2006-2099 is equal to 485.5 g C m^{-2} under RCP 2.6, 452.0 g C m^{-2} under RCP 4.5, 591.7 g C m^{-2} under RCP 6.0 and 628.1 g C m^{-2} under RCP 8.5. At Hainich the difference is higher and equal to 1158.3 g C m^{-2} under RCP 2.6, 1115.4 g C m^{-2} under RCP 4.5, 898.1 g C m^{-2} under RCP 6.0 and 603.0 g C m^{-2} under RCP 8.5.

It is interesting to analyze the cumulated difference of two intervals, 2006-2050 (near future) and 2051-2099 (far future), computing the percentage over the entire period, 2006-2099 (*Tab.12*). The tropical site shows a cumulated difference in the near future corresponding to 259.0 g C m^{-2} (53.4% of the total) under RCP 2.6, 227.7 g C m^{-2} (50.4% of the total) under RCP 4.5, 228.9 g C m^{-2} (38.7% of the total) under RCP 6.0 and 109.3 g C m^{-2} (17.4% of the total) under RCP 8.5, which becomes 226.5 g C m^{-2} (46.6% of the total) under RCP 2.6, 224.3 g C m^{-2} (49.6% of the total)

under RCP 4.5, 362.8 g C m^{-2} (61.3% of the total) under RCP 6.0 and 518.8 g C m^{-2} (82.6% of the total) under RCP 8.5 when computed in the far future. Instead, the temperate site shows a cumulated difference in the near future corresponding to 621.3 g C m^{-2} (53.6% of the total) under RCP 2.6, 637.3 g C m^{-2} (57.1% of the total) under RCP 4.5, 526.4 g C m^{-2} (58.6% of the total) under RCP 6.0 and 430.4 g C m^{-2} (71.4% of the total) under RCP 8.5, which becomes 536.9 g C m^{-2} (46.4% of the total) under RCP 2.6, 478.1 g C m^{-2} (42.9% of the total) under RCP 4.5, 371.7 g C m^{-2} (41.4% of the total) under RCP 6.0 and 172.6 g C m^{-2} (28.6% of the total) under RCP 8.5 when computed in the far future (*Fig.43*).

Site	RCP	Cumulated Difference (EF - MMRT) (g C m^{-2})		
		2006-2050	**2051-2099**	**Total**
Hainich	2.6	621.3	536.9	**1158.3**
	4.5	637.3	478.1	**1115.4**
	6.0	526.4	371.7	**898.1**
	8.5	430.4	172.6	**603.0**
Ankasa	2.6	259.0	226.5	**485.5**
	4.5	227.7	224.3	**452.0**
	6.0	228.9	362.8	**591.7**
	8.5	109.3	518.8	**628.1**

Table 12. *Cumulated differences of annual R_{het} between the exponential and MMRT approaches at Hainich and Ankasa under the RCP 2.6, 4.5, 6.0 and 8.5 climate change scenarios. The differences are referred to 2006-2050, 2051-2099 and to the entire period (Total).*

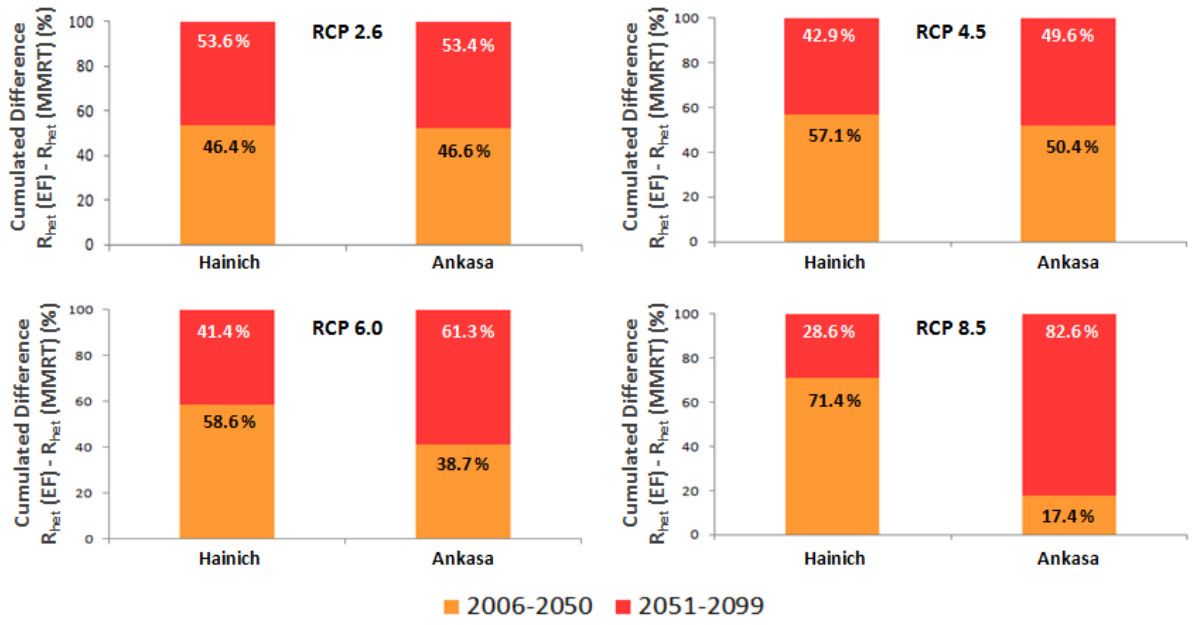

Figure 43. *Cumulated percentage differences on the total value for 2006-2050 and 2051-2099 of annual R_{het} between the EF and MMRT approaches at Hainich and Ankasa under RCP 2.6, 4.5, 6.0 and 8.5.climate change scenarios.*

4.5 Sensitivity analysis

The perturbation by ±10% to the model parameters through the application of the Morris method allowed detecting the parameters that exert the highest weight on the simulated monthly heterotrophic respiration fluxes under current climate at both the temperate and the tropical forests.

At Hainich, the parameters to which the model is more sensitive for both approaches are summarized in the *Table 13* and *Table 14*.

When the exponential approach is applied, the parameters with the highest effect are *par_a* and *par_b*, the slope and the exponent of the exponential equation, respectively. A perturbation in the default values determines the lowest accuracy of the simulated R_{het}, translated in a *pBias* up to –14.5% for *par_a* (–10% of the default value) (*Fig.44*).

The model is also sensitive to the maximum decay rates of aboveground metabolic litter, as well as the surface microbial and slow SOM pools, with a pBias ranging from –7.6% and –8.5%.

Exponential Function approach			
Parameter	**Description**	**Variation** (%)	**pBias** (%)
par_a	Slope of exponential equation.	–10	–14.5
		+10	+2.2
par_b	Exponent of exponential equation.	–10	–12.3
		+10	+0.6
par_k_slo	Maximum decay rate of slow SOM	–10	–8.5
par_k_am	Maximum decay rate of aboveground metabolic litter	–10	–7.7
par_k_srfmic	Maximum decay rate of surface microbial SOM	–10	–7.6

Table 13. *Parameters to which the model is more sensitive when the EF is applied at Hainich forest.*

The model structure with the MMRT approach is more sensitive to the changes in enthalpy (ΔH_0) and entropy (ΔS_0) of the system (*Fig.45*). However, these parameters exert a relevant effect on the model. A variation of –10% determines a *pBias* equal to +280.5% and +124.1% for ΔH_0 and ΔS_0, respectively. When these two parameters are perturbed by +10%, the model underestimates the heterotrophic respiration fluxes until –85.8% (ΔH_0) and –70.4% (ΔS_0).

Parameter	MMRT approach Description	Variation (%)	pBias (%)
ΔH_0	Changes in the enthalpy of the system	–10	+280.5
		+10	–85.8
ΔS_0	Changes in the entropy of the system	–10	+124.1
		+10	–70.4

Table 14. *Parameters to which the model is more sensitive when the MMRT approach is applied at Hainich forest.*

(a)

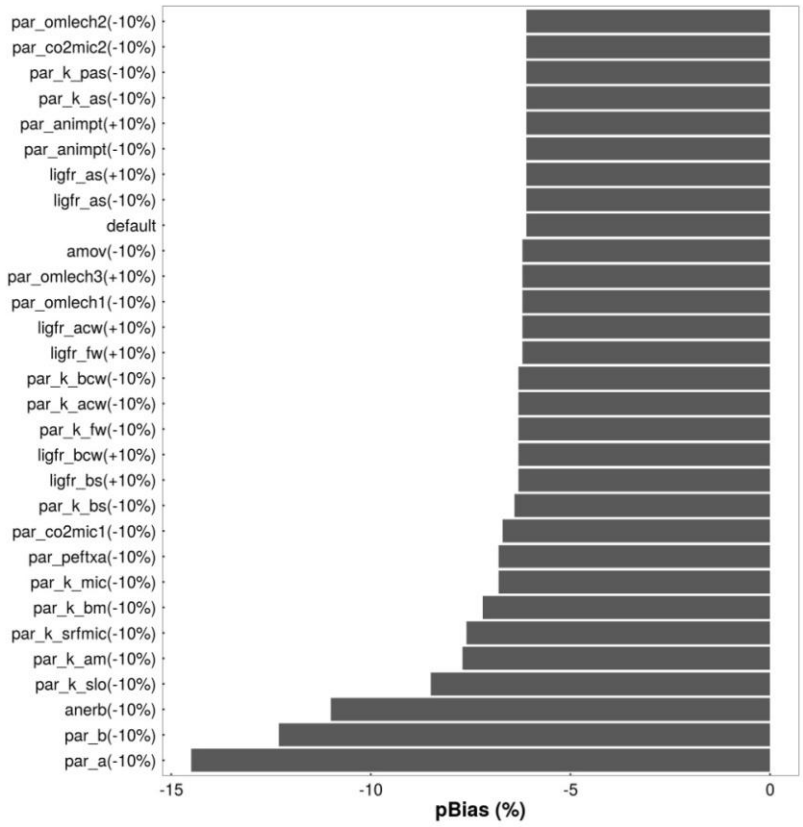

(b)

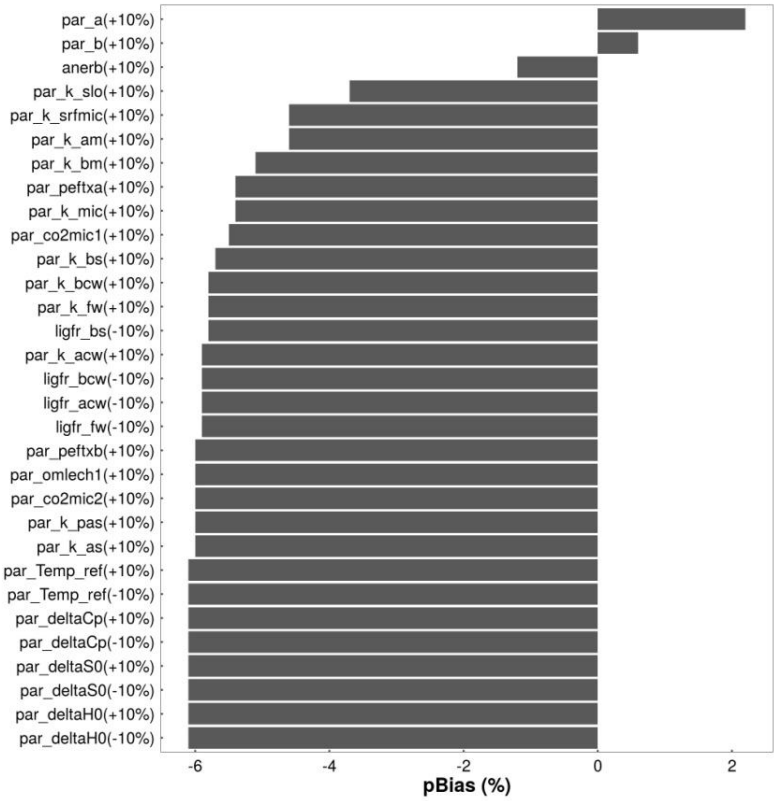

Figure 44. *Parameter sensitivity when the EF approach is applied. Negative (a) and Positive (b) pBias at Hainich forest.*

(a)

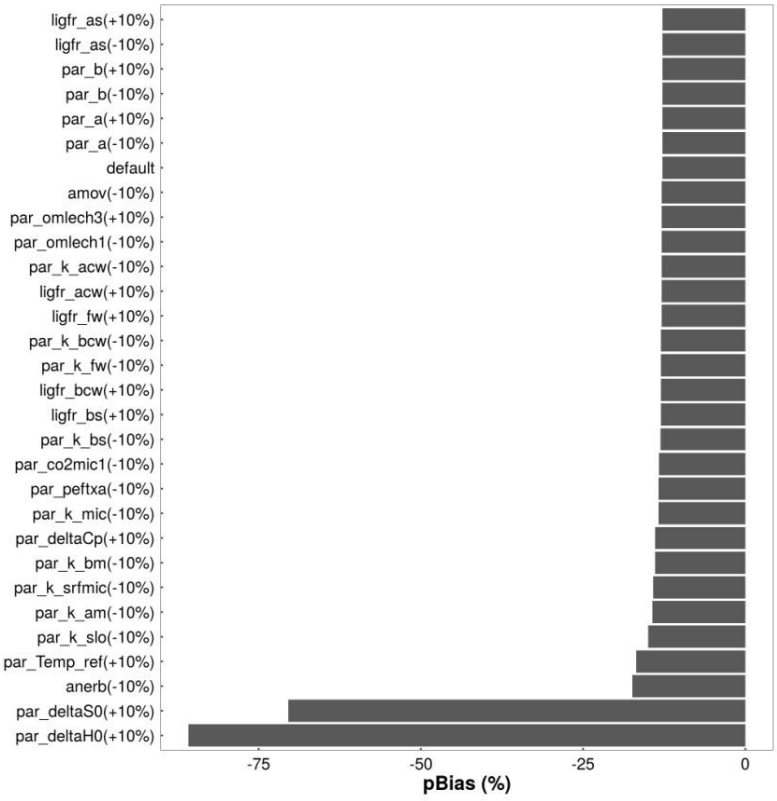

(b)

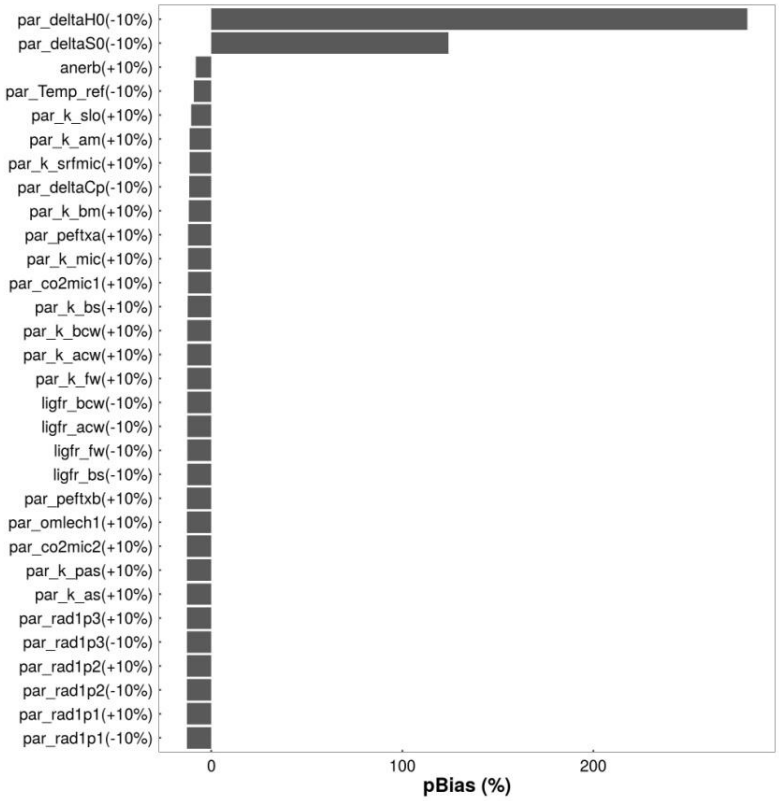

Figure 45. *Parameter sensitivity when the MMRT approach is applied. Negative (a) and Positive (b) pBias at Hainich forest.*

At Ankasa, the model is particularly sensitive to the parameters *par_a*, *par_b* and *par_k_am* for the exponential approach and ΔH_0 and ΔS_0 for the MMRT approach (*Tab.15-16*). The slope and the exponent of the exponential equation determine a *pBias* equal to –14.4% (for a –10% perturbation) and +12.6% (for +10% perturbation) for *par_b*, –9.5% (for a –10% perturbation) and +6.1% (for +10% perturbation) for *par_a*. The maximum decay rate of aboveground metabolic litter (*par_k_am*) generates a pBias ranging from –3.7% and +0.5% (*Fig.46*).

As for Hainich, also at Ankasa the parameters of the MMRT approach exert a relevant effect on the model. Indeed the changes in enthalpy (ΔH_0) and entropy (ΔS_0) of the process produce an overestimation in the outputs corresponding to +229.8% for ΔH_0 and +126.9% for ΔS_0, respectively. A variation of +10% of the default values generates an underestimation of -80.1% for ΔH_0 and -62.7% for ΔS_0, respectively (*Fig.47*).

Exponential Function approach			
Parameter	**Description**	**Variation** (%)	**pBias** (%)
par_b	Exponent of exponential equation. It represents the temperature sensitivity of decomposition	–10	–14.4
		+10	+12.6
par_a	Slope of exponential equation. It is the decay rate measured at the reference temperature	–10	–9.5
		+10	+6.1
par_k_am	Maximum decay rate of aboveground metabolic litter	–10	–3.7
		+10	+0.5

Table 15. *Parameters to which the model is more sensitive when the EF is applied at Ankasa forest.*

MMRT approach			
Parameter	**Description**	**Variation** (%)	**pBias** (%)
ΔH_0	Changes in the enthalpy of the system	–10%	+229.8
		+10%	–80.1
ΔS_0	Changes in the entropy of the system	–10%	+126.9
		+10%	–62.7

Table 16. *Parameters to which the model is more sensitive when the MMRT is applied at Ankasa forest.*

(a)

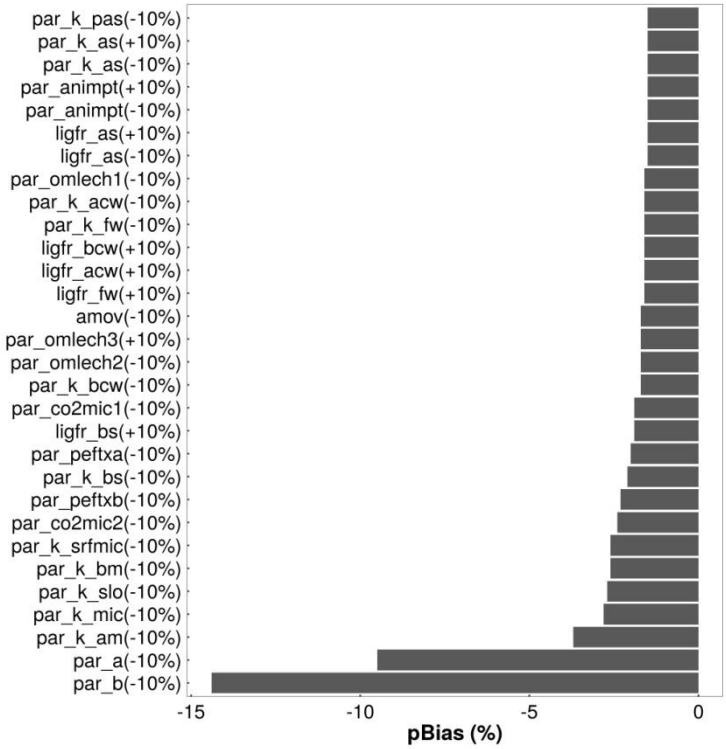

(b)

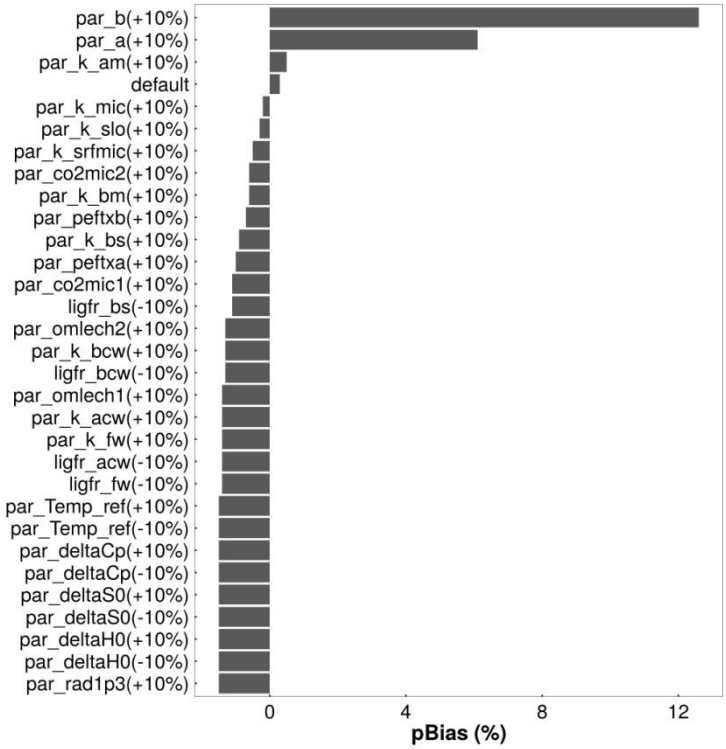

Figure 46. *Parameter sensitivity when the EF approach is applied. Negative (a) and Positive (b) pBias at Ankasa forest.*

(a)

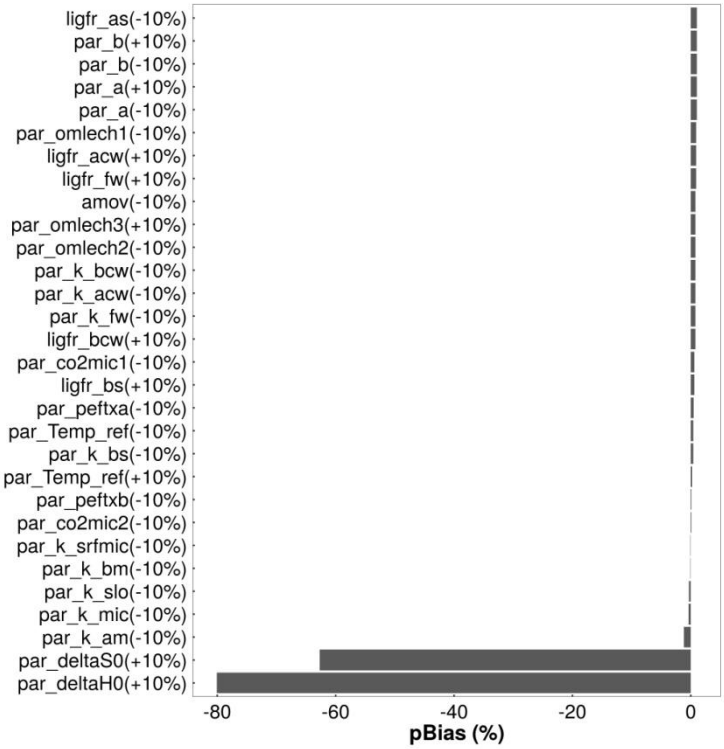

(b)

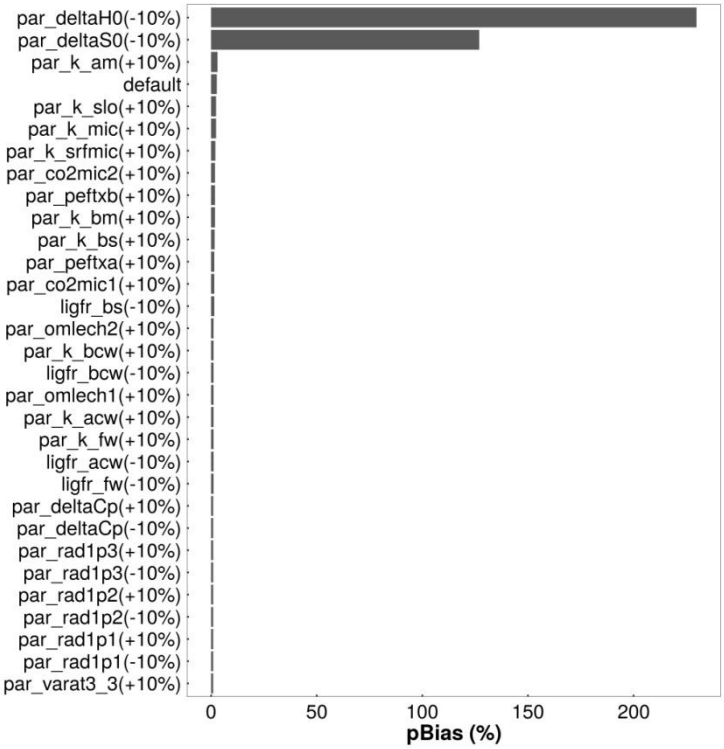

Figure 47. *Parameter sensitivity when the MMRT approach is applied. Negative (a) and Positive (b) pBias at Ankasa forest.*

4.6 Uncertainty analysis under current and climate change scenario

Through the application of the Bayes' theorem (Van Oijen et al., 2005), the prior and posterior distributions of the parameters selected during the sensitivity analysis have been computed within the lower and upper limits set for each parameter (*Tab.17*):

Parameter	default	Value lower limit	upper limit	Reference
par_a	0.125	0.063	0.354	Holland et al. (2000); Kelly et al. (2000)
par_b	0.07	0.043	0.095	Holland et al. (2000); Kelly et al. (2000)
par_k_am	1.23	1	1.48	Parton et al. (1987, 1988, 1993)
par_k_srfmic	0.5	0.083	1	Shi et al. (2018)
par_k_slo	0.02	0.0083	0.042	Shi et al. (2018)
ΔH_0	45.1	31.6	58.6	Steffen & Apostolakis (2007); Schipper et al. (2014); Kraakman (2017); Liang et al. (2018)
ΔS_0	–0.096	–0.125	–0.067	Steffen & Apostolakis (2007); Schipper et al. (2014); Kraakman (2017); Liang et al. (2018)

Table 17. *Parameter default, lower and upper values*

<u>Uncertainty under current climate</u>

At Ankasa, the decay rate of aboveground metabolic litter (*par_k_am*) is characterized by a wide posterior distribution, which covers the entire range of variation with high values of the Probability Density Function (PDF) (*Fig.48-49*). This parameter is particularly uncertain for both EF and MMRT approaches. When the EF is applied, the slope *par_a* of the exponential equation is well constrained, with a posterior distribution concentrated around the peak value. Instead, when the MMRT is enabled (*Fig.49*), ΔH_0 (changes in enthalpy) shows a narrower probability, while ΔS_0 (changes in entropy) is definitely more uncertain, showing a wide distribution with high PDF values (up to 25).

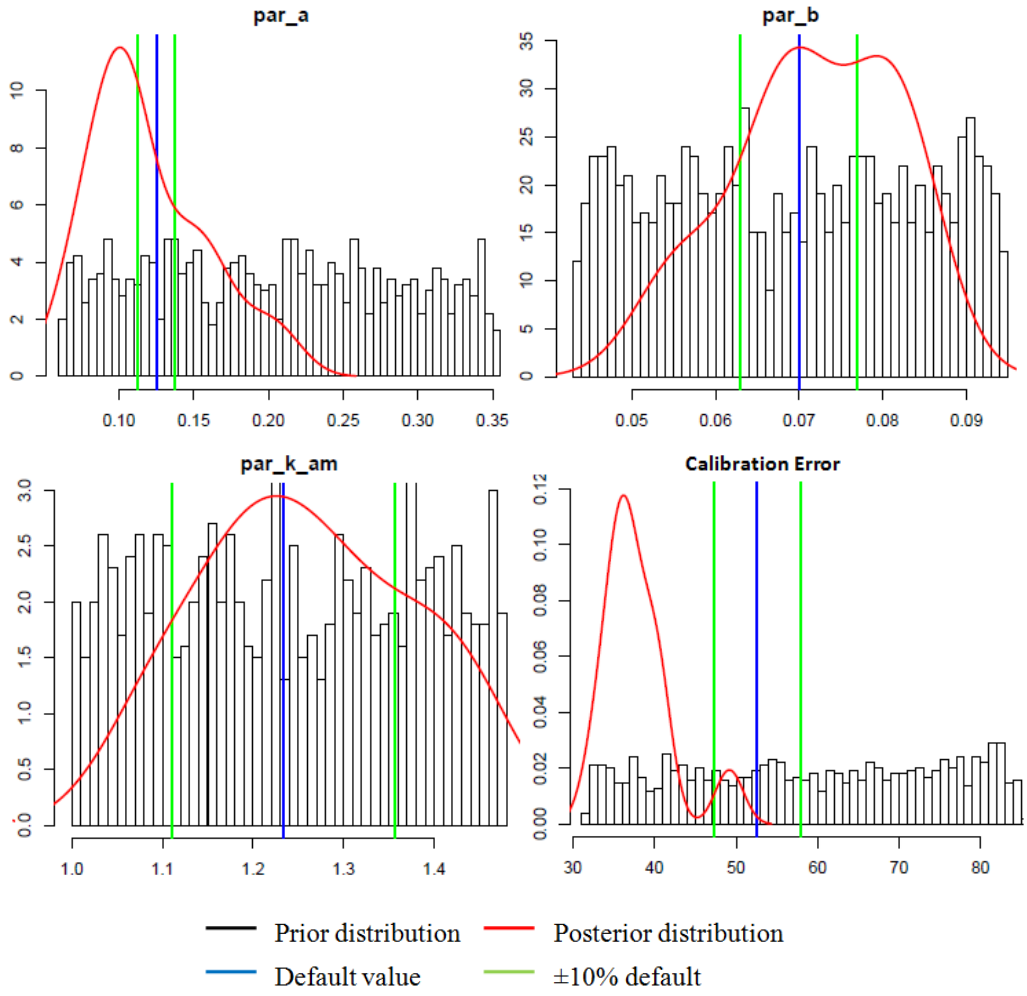

Figure 48. *Prior (black rectangles) and posterior (red curve) probability distributions. Probability values on y-axis. Parameter values on x-axis. Default parameter value (blue vertical line) and sensitivity range (±10%, green vertical lines) for the parameters to which the model is more sensitive applying the EF approach at Ankasa site. The last plot (Calibration Error) is referred to the probability distribution of the error in the R_{het} estimate during the calibration phase.*

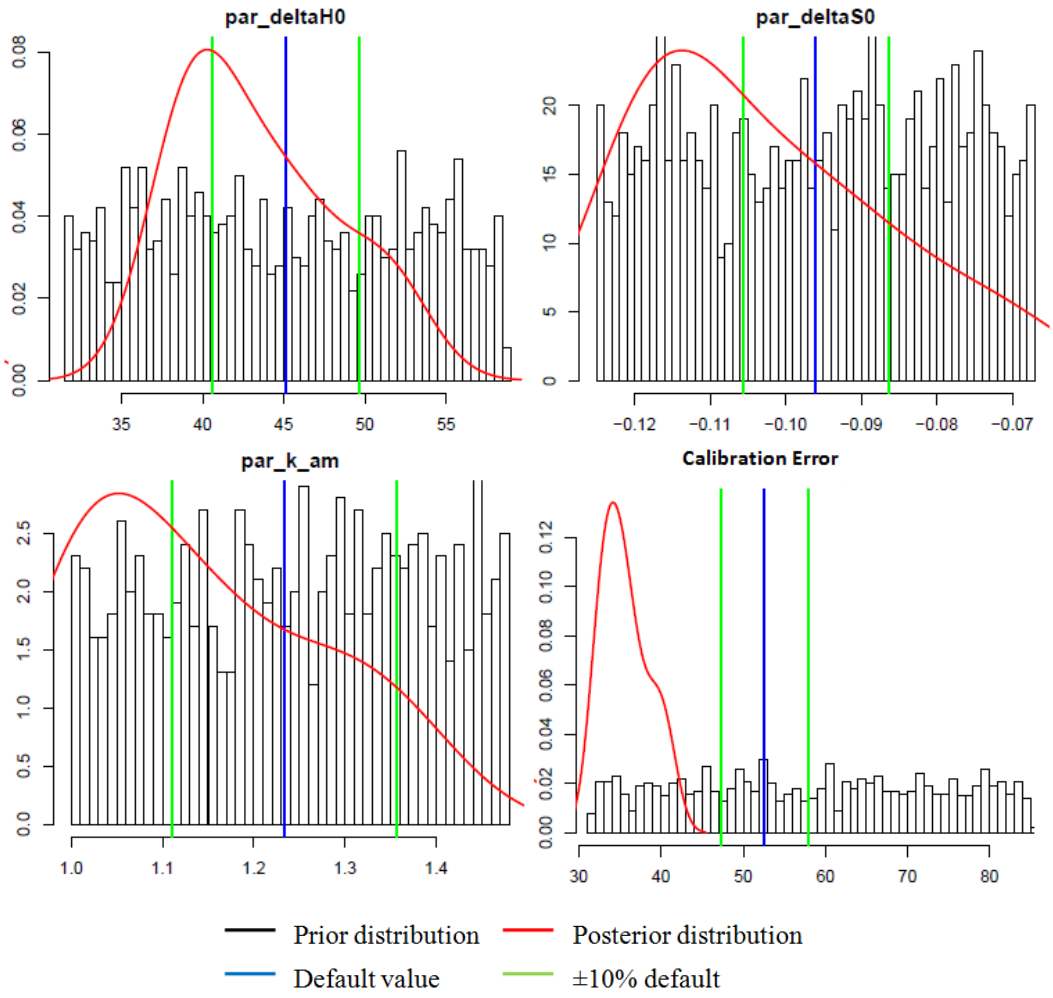

Figure 49. *Prior (black rectangles) and posterior (red curve) probability distributions. Probability values on y-axis. Parameter values on x-axis. Default parameter value (blue vertical line) and sensitivity range (±10%, green vertical lines) for the parameters to which the model is more sensitive applying the MMRT approach at Ankasa site. The last plot (Calibration Error) is referred to the probability distribution of the error in the R_{het} estimate during the calibration phase.*

To quantify the uncertainty generated by the two approaches in the R_{het} simulation, the monthly trend of R_{het} has been analyzed, evaluating the extension of the areas comprised between the 5th and 95th, the 25th and 75th percentiles, as well as within the minimum and the maximum simulated values (Fig.50, *Tab.18*).

The uncertainty produced by the parameters when the MMRT approach is applied generates larger differences than the EF between the minimum and maximum simulated R_{het} and the values at 5th and 95th percentiles corresponding to 121.5 and 66.5 g C m^{-2} month^{-1}, respectively. Only the difference between the R_{het} values simulated by MMRT at 25th and 75th percentiles is lower than the difference generated by EF and is equal to 22 g C m^{-2} month^{-1}. Hence, at Ankasa, under present-day climate, the MMRT shows to be more uncertain than the EF approach, except between the 75th and 25th percentiles.

Approach	Difference (g C m^{-2} $month^{-1}$)		
	R_{het} (Max) – R_{het} (Min)	R_{het} (75^{th}) – R_{het} (25^{th})	R_{het} (95^{th}) – R_{het} (5^{th})
EF	91.7	**26.7**	60.7
MMRT	**121.5**	22.0	**66.5**

Table 18. *Average difference between Minimum and Maximum, 25^{th} and 75^{th}, 5^{th} and 95^{th} percentiles of simulated R_{het} (g C m^{-2} $month^{-1}$) by the EF and MMRT approaches at Ankasa. The differences are computed as the mean of the differences of all single months*

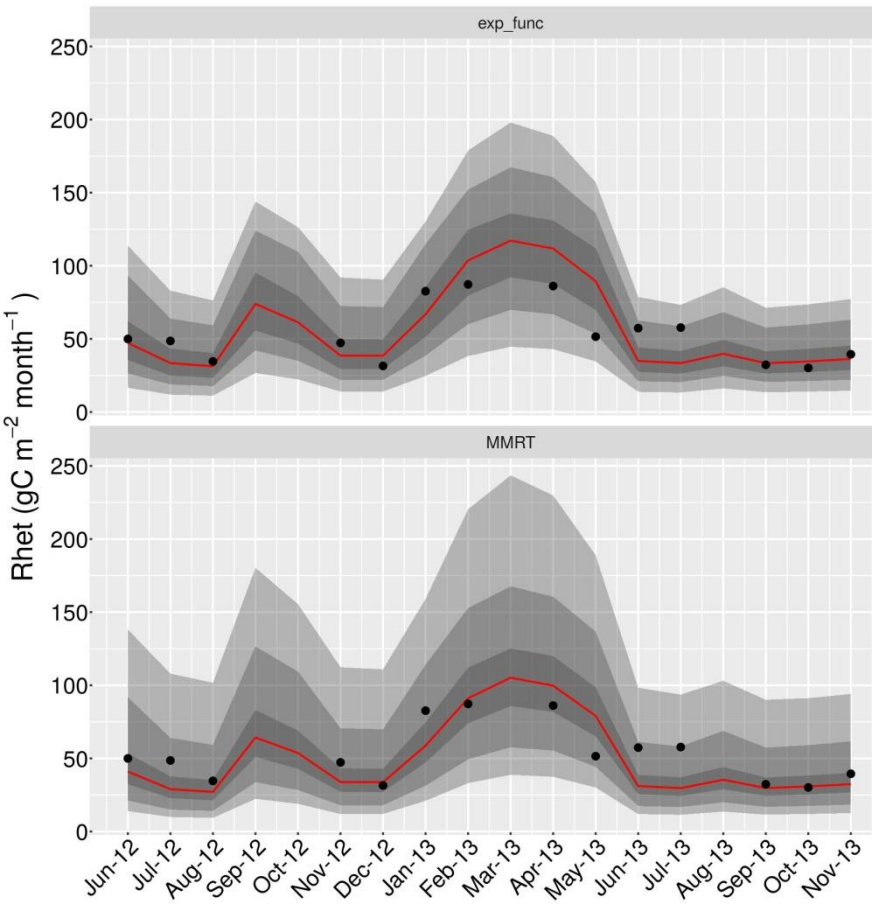

Figure 50. *Uncertainty in monthly R_{het} trend produced by the EF (upper panel) and MMRT (lower panel) approaches at Ankasa. The shaded areas represent, starting from the bottom, the minimum, the 5^{th}, 25^{th}, 50^{th} (red line), 75^{th}, 95^{th} percentiles, the maximum value. The black points represent the measured values.*

At Hainich, among the common parameters, the decay rate *par_k_am* is highly uncertain for both the EF (*Fig.51*) and MMRT approaches (*Fig.52*), while *par_k_srfmic* and *par_k_slo* show a larger distribution with MMRT than the EF approach.

The slope of the exponential equation (*par_a*) is more constrained than *par_b*, which is characterized by a wide posterior distribution. Instead, regarding the parameters contained in the MMRT equation, $\Delta H0$ and $\Delta S0$, the first is well constrained, while the second shows to be potentially much uncertain.

As Ankasa, also at Hainich the peak of the distribution of the calibration error is definitely lower than the default value set to carried out the iterations (30 g C m^{-2} $month^{-1}$).

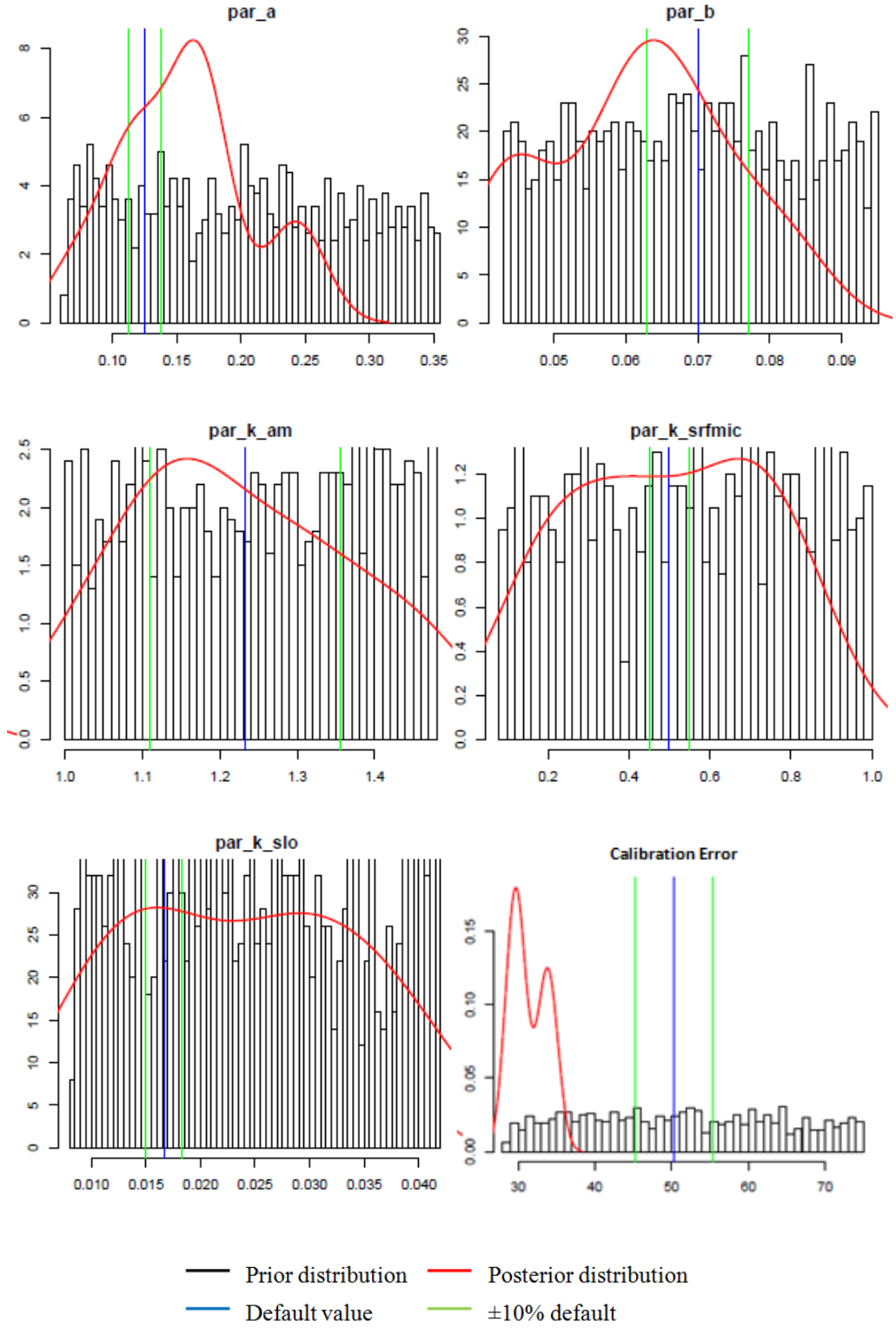

Figure 51. *Prior (black rectangles) and posterior (red curve) probability distributions. Probability values on y-axis. Parameter values on x-axis. Default parameter value (blue vertical line) and sensitivity range (±10%, green vertical lines) for the parameters to which the model is more sensitive applying the EF approach at Hainich site. The last plot (Calibration Error) is referred to the probability distribution of the error in the R_{het} estimate during the calibration phase.*

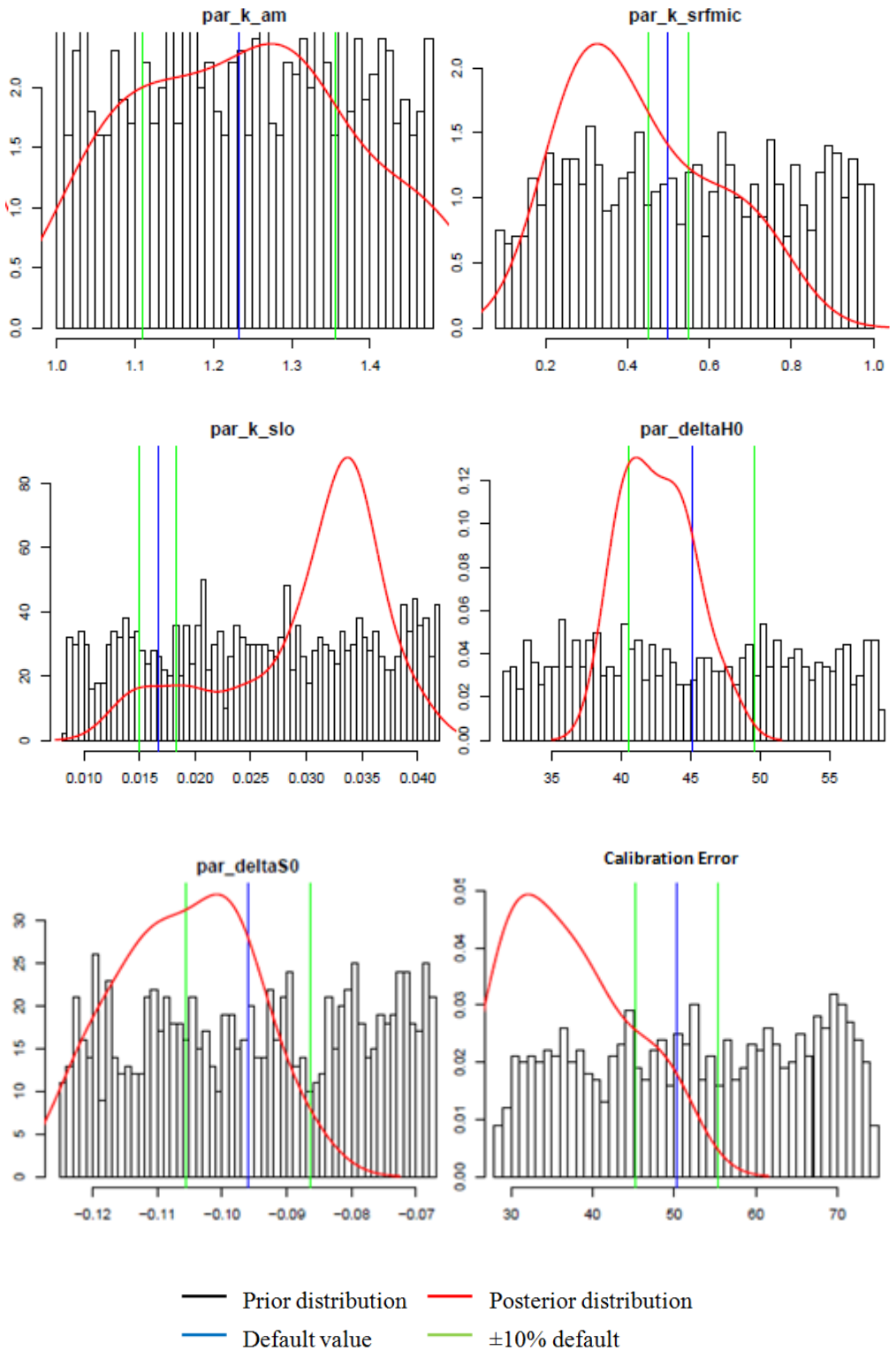

Figure 52. *Prior (black rectangles) and posterior (red curve) probability distributions. Probability values on y-axis. Parameter values on x-axis. Default parameter value (blue vertical line) and sensitivity range (±10%, green vertical lines) for the parameters to which the model is more sensitive applying the MMRT approach at Hainich site. The last plot (Calibration Error) is referred to the probability distribution of the error in the R_{het} estimate during the calibration phase.*

The analysis of the extension of the areas comprised between the 5th and 95th, the 25th and 75th percentiles, as well as within the minimum and the maximum, clearly shows that, also for Hainich,

the MMRT is the most uncertain between the two approaches taken into account (*Tab.19*). The difference in the simulated R_{het} values at 25th and 75th percentiles is 27.9 g C m^{-2} month^{-1} for MMRT and 16.1 g C m^{-2} month^{-1} for the EF. Instead, the difference between the 5th and 95th percentiles is equal to 95.5 g C m^{-2} month^{-1} for MMRT and 47.4 g C m^{-2} month^{-1} for the EF. As for Ankasa, the difference between the maximum and the minimum R_{het} (200.9 g C m^{-2} month^{-1} for MMRT and 100.8 g C m^{-2} month^{-1} for the EF approach) clearly shows that the MMRT, also at Hainich under present-day climate, is the most uncertain approach (*Fig.53*).

Approach	Difference (g C m^{-2} month^{-1})		
	R_{het} (Max) – R_{het} (Min)	R_{het} (75th) – R_{het} (25th)	R_{het} (95th) – R_{het} (5th)
EF	100.8	16.1	47.4
MMRT	**200.9**	**27.9**	**95.5**

Table 19. *Average difference between Minimum and Maximum, 25th and 75th, 5th and 95th percentiles of simulated R_{het} (g C m^{-2} month^{-1}) by the EF and MMRT approaches at Hainich. The differences are computed as the mean of the differences of all single months*

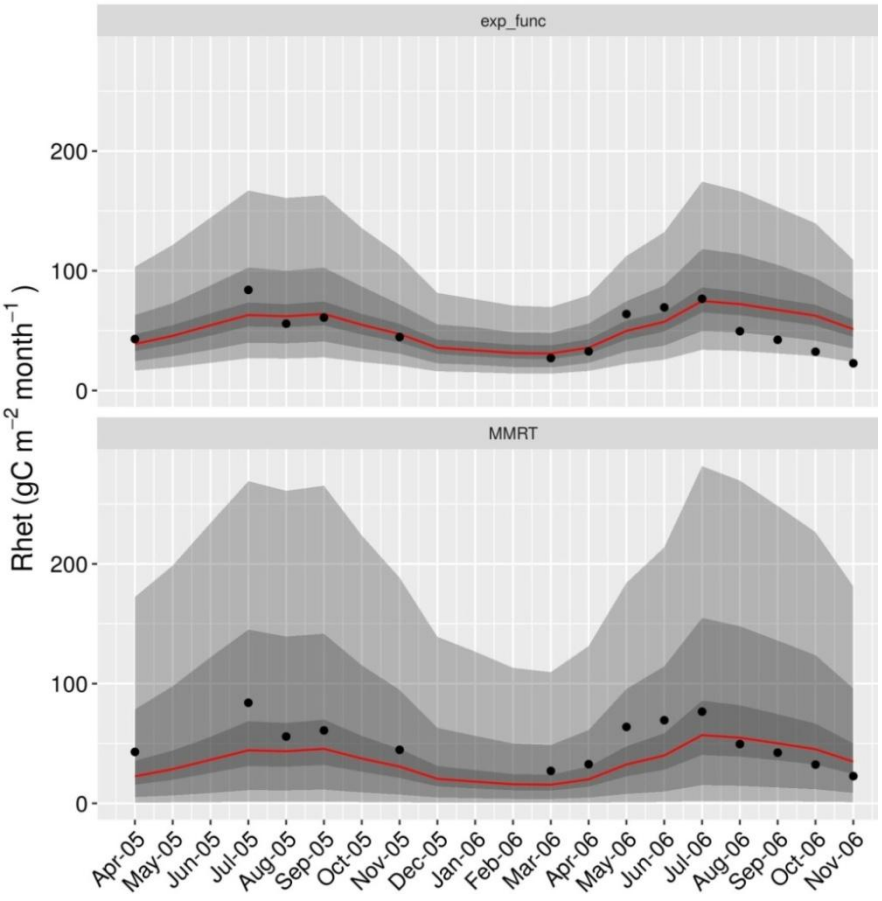

Figure 53. *Uncertainty in monthly R_{het} trend produced by the EF (upper panel) and MMRT (lower panel) approaches at Hainich. The shaded areas represent, starting from the bottom, the minimum, the 5th, 25th, 50th (red line), 75th, 95th percentiles, the maximum value. The black points represent the measured values.*

Uncertainty under climate change scenario

The uncertainty in simulating R_{het} has been quantified both at Hainich and Ankasa running the model under no-climate (no increasing temperature and litterfall) and climate change scenario (2006-2099) – under RCP 2.6, 4.5, 6.0 and 8.5 – to disentangle, when possible, the effects of temperature and CO_2 fertilization on R_{het}.

At Hainich the MMRT approach shows to be more uncertain than the EF for both no-climate and climate change scenario under all RCPs (*Fig.54*). Indeed, under no-climate change scenario, the mean difference between the R_{het} simulated by the maximum and minimum parameter sets is equal to 451.7 g C m^{-2} $year^{-1}$ using the EF approach and 756.2 g C m^{-2} $year^{-1}$ using the MMRT. Under the RCP 2.6 climate change scenario, the difference is 519.7 g C m^{-2} $year^{-1}$ using the EF approach and 831.7 g C m^{-2} $year^{-1}$ using the MMRT. The RCP 4.5, instead, shows a mean difference equal to 528.4 g C m^{-2} $year^{-1}$ using the EF approach and 851.0 g C m^{-2} $year^{-1}$ using the MMRT. Under the RCP 6.0 climate change scenario, the difference is 546.7 g C m^{-2} $year^{-1}$ using the EF approach and 870.5 g C m^{-2} $year^{-1}$ using the MMRT. For the RCP 8.5 climate change scenario, the difference is 585.5 g C m^{-2} $year^{-1}$ using the EF approach and 906.7 g C m^{-2} $year^{-1}$ using the MMRT.

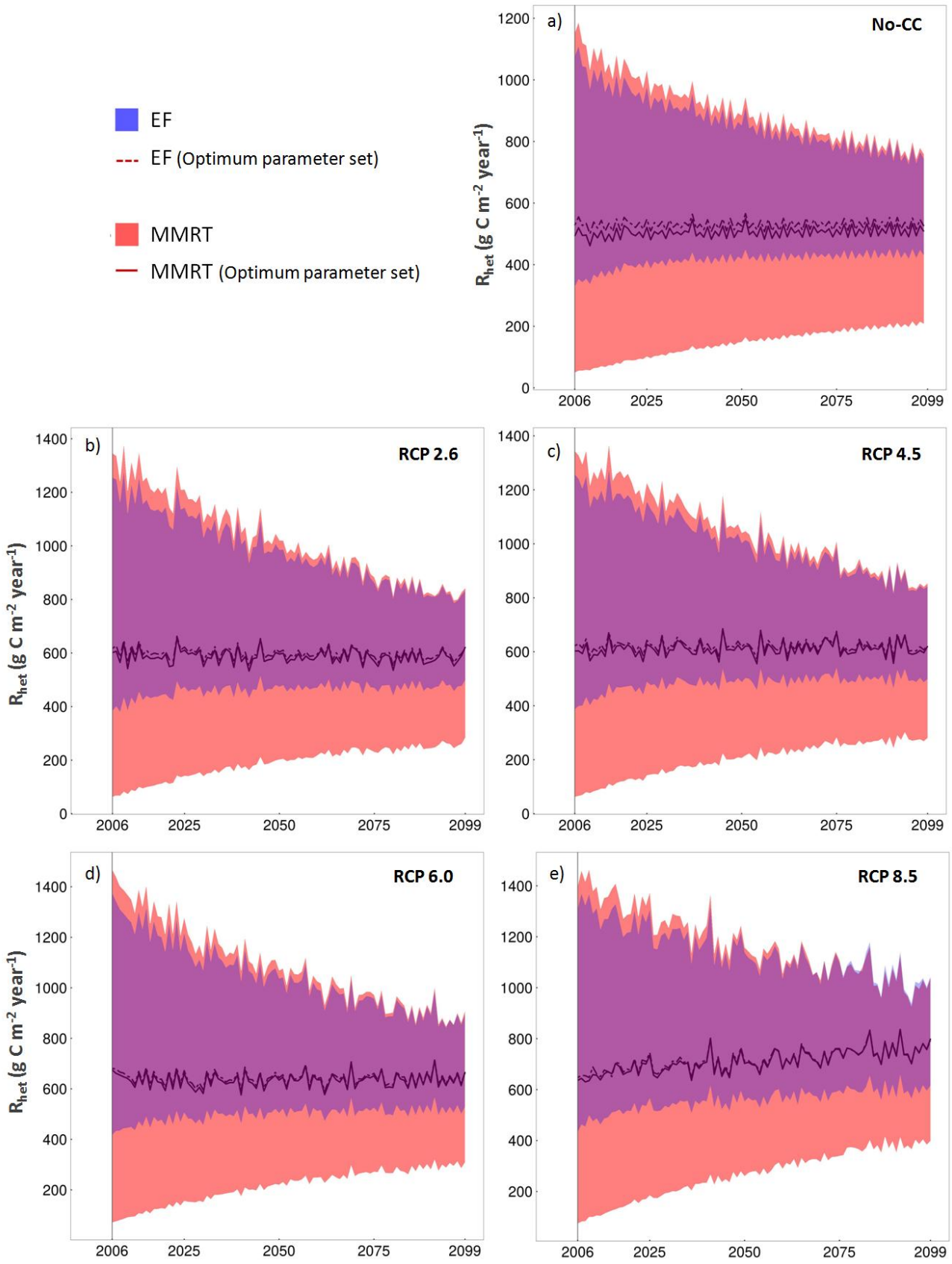

Figure 54. *Uncertainty in the annual R_{het} trend produced by the exponential (EF) and MMRT approaches at Hainich under no-climate change scenario (a), RCP2.6 (b), RCP4.5 (c), RCP6.0 (d) and the RCP8.5 (e) climate change scenarios. The solid and dashed lines are the R_{het} simulated by the MMRT and EF, respectively, using the optimum parameter set.*

Also at Ankasa the MMRT approach is more uncertain than EF under no-climate change scenario, showing a mean difference in the simulated heterotrophic respiration between the maximum and minimum parameter sets equal to 438.1 g C m^{-2} $year^{-1}$, slightly higher than the EF of 107.0 g C m^{-2} $year^{-1}$, respectively (*Fig.55*). Under RCP 2.6, 4.5, 6.0 and 8.5 climate change scenarios, the MMRT is more uncertain than EF. Under RCP 2.6, the mean difference is equal to 448.0 g C m^{-2} $year^{-1}$ for MMRT and 110.5 g C m^{-2} $year^{-1}$ for EF. Under RCP 4.5, the mean difference is equal to 460.0 g C m^{-2} $year^{-1}$ for MMRT and 117.4 g C m^{-2} $year^{-1}$ for EF. Under RCP 6.0, the mean difference is equal to 469.4 g C m^{-2} $year^{-1}$ for MMRT and 124.9 g C m^{-2} $year^{-1}$ for EF. Under RCP 8.5, the mean difference is equal to 483.5 g C m^{-2} $year^{-1}$ for MMRT and 129.1 g C m^{-2} $year^{-1}$ for EF.

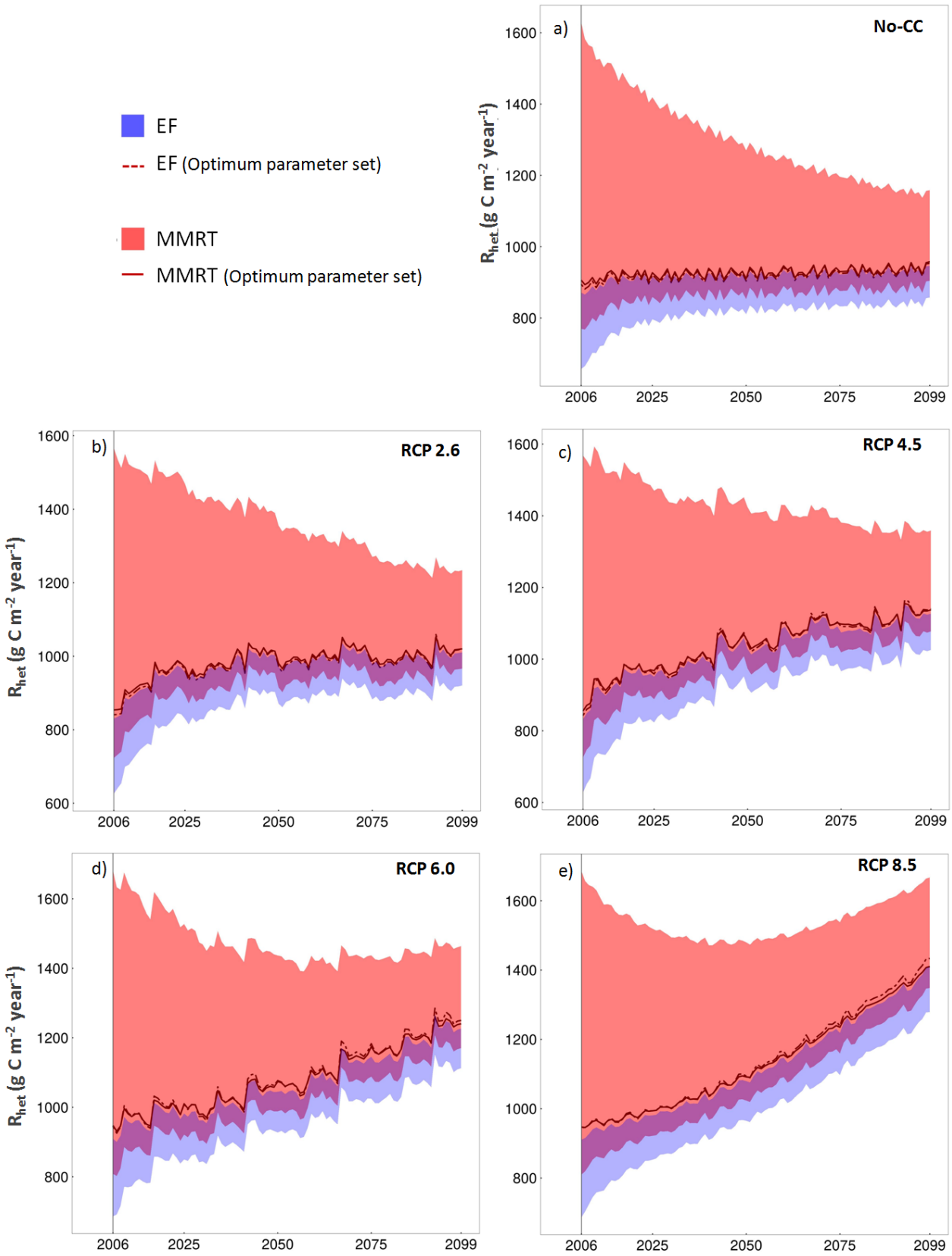

Figure 55. *Uncertainty in the annual R_{het} trend produced by the exponential (EF) and MMRT approaches at Ankasa under no-climate change scenario (a), RCP2.6 (b), RCP4.5 (c), RCP6.0 (d) and the RCP8.5 (e) climate change scenarios. The solid and dashed lines are the R_{het} simulated by the MMRT and EF, respectively, using the optimum parameter set.*

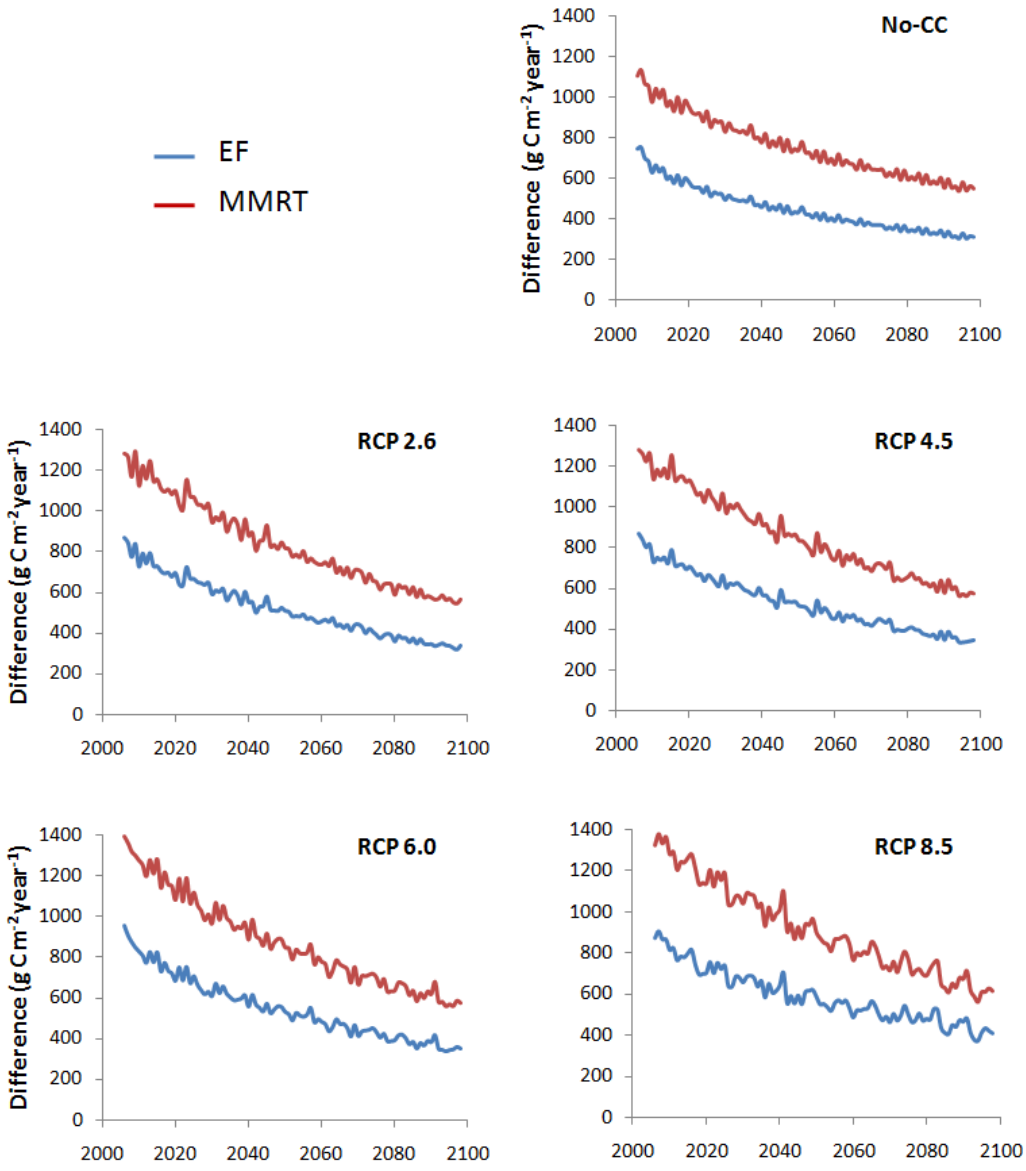

Figure 56. *Differences of annual R_{het} under no-climate change scenario (No-CC), RCP 2.6, 4.5, 6.0 and 8.5 climate change scenarios between the maximum and minimum parameter sets for the EF and MMRT approaches at Hainich.*

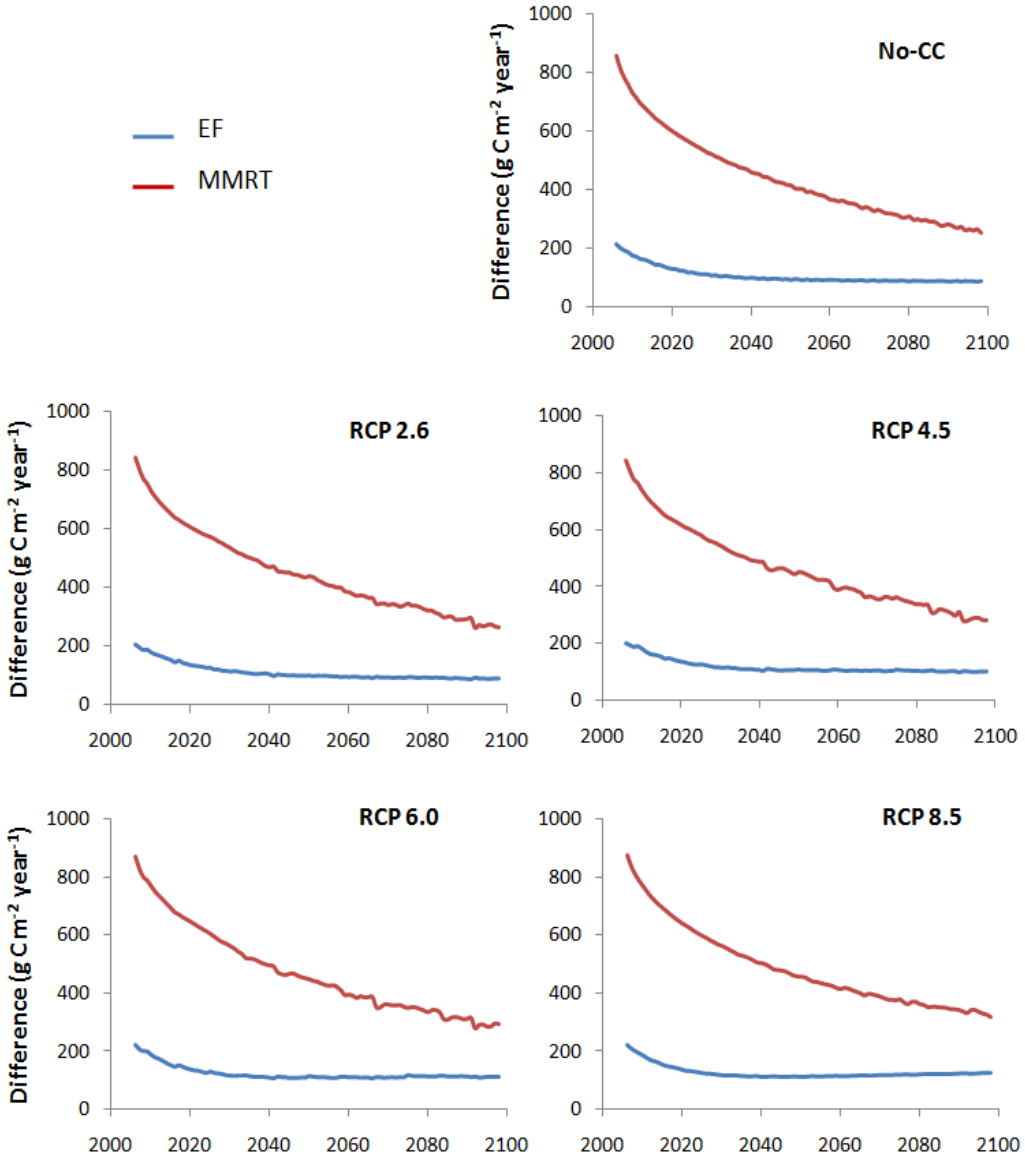

Figure 57. *Differences of annual R_{het} under no-climate change scenario (No-CC), RCP 2.6, 4.5, 6.0 and 8.5 climate change scenarios between the maximum and minimum parameter sets for the EF and MMRT approaches at Ankasa.*

5. Discussions

5.1 C and N stocks at steady-state

The C and N stocks obtained by the model spin-up phase are in line with Thornton & Rosenbloom (2005) where the spin-up of the BIOME-BGC model was carried out for different evergreen forests and the equilibrium was reached after a mean time for the analyzed forests corresponding to 4911 years run. Nevertheless, BIOME-BGC has a similar structure of CENTURY, with several litter and SOM pools subdivided basing on the degree of decomposability.

5.2 Model validation

The trend of the monthly R_{het} at Hainich highlights how both configurations of the CENTURY model tend to underestimate the measured values for most of the two analyzed years (2005 and 2006) and to overestimate in the last months of 2006 (*Fig.36*). Reasons for a such underestimation could be found in the logic behind how the model simulates hydrology. Indeed, the soil moisture modifier, i.e. the effects exerted by soil moisture on litter and SOM decomposition, is simulated by a function based on the ratio between total precipitation (PPT) and potential evapotranspiration (PET) (*Fig.8*). The soil moisture modifier increases up to a PPT/PET ratio equal to 1, and subsequently decreases at higher ratios. Analyzing the PPT and PET values registered in the analyzed period, a cumulated PPT equal to 462.7 mm m^{-2} $month^{-1}$ occurs in the first period of 2005 (from January to July), about 90 mm more than the same period of the next year. Furthermore, the cumulated PET (January-July) is lower in 2005 (485.2 mm m^{-2} $month^{-1}$) than 2006 (mm m^{-2} $month^{-1}$). The high PPT and the low PET occurring in the first period of 2005 generate PPT/PET ratios higher than 1 and a soil moisture modifier with low values. This effect is dragged until August 2006, determining low simulated R_{het} fluxes. At August 2006, a particular high precipitation event occurs (120.4 mm m^{-2} $month^{-1}$) with an increase of the PPT/PET ratio, but without exceeding 1. The higher ratios determine higher values for the soil moisture modifier, hence, a higher simulated R_{het}, with an overestimation compared to the measured fluxes. It is possible that the function implemented in the model is not able to reproduce correctly the hydrological dynamic when high PPT/PET ratios occur. Similarly, the model is not able to reproduce the peak R_{het} at July 2005 (84 g C m^{-2} $month^{-1}$). The too high PPT/PET ratios until that month determine a soil moisture modifier with low values and, consequently, a low simulated R_{het} when compared to measured data, 55.7 g C m^{-2} $month^{-1}$ with the EF, 56.3 g C m^{-2} $month^{-1}$ with MMRT, respectively.

It is important to highlight that in the present work the original scheme of hydrological dynamics has been maintained, even if this is a simplified approach as build in the original CENTURY model (v.4), with the aim to compare (only) the EF and the MMRT approach. This is a much used

experimental scheme also adopted in other works to more clearly, and more easily, disentangle the effect of changing one single approach to the other(s) (Collalti et al., 2020)

5.3 Heterotrophic respiration estimates under climate change scenario

Over the period 2006-2099, under climate change scenario - that is with increasing soil temperature and litterfall production – taking the warmest RCP (8.5) as reference – the CENTURY model simulates an increase of mean annual R_{het} compared to the one simulated under no climate change scenario – i.e. with current soil temperature and litterfall – equal to +35.1% using the EF and +34.0% using the MMRT at Hainich, +23.4% with EF and +22.8% with MMRT at Ankasa. These results are in line with Wang et al. (2014), which analyzed 202 R_{het} datasets from 50 ecosystem warming experiments across several terrestrial ecosystems, including temperate forests located in U.S.A., Austria and Japan. Warming by 2°C caused a R_{het} increment of 21% (Wang et al., 2014).
The results are also comparable with the ones found by Schindlbacher et al. (2009) regarding a warming experiment conducted on a mature Norway spruce (*Picea abies* (L.) H.Karst) forest located in Austria. They found that a soil temperature enhancement of 4°C increased the mean annual R_{het} fluxes between +39% and +45%.
The R_{het} increment under the warmest climate change scenario simulated by the CENTURY model in this work is also in line with Wu et al. (2016). They registered a mean annual R_{het} enhancement of +22.9% in a subtropical forest in southwestern China with a soil temperature increase by 2.1°C.
In the present work, the annual R_{het} simulated at Hainich by the CENTURY model under RCP 8.5 climate change scenario can reach a maximum percentage equal to +66.4% using the EF and +75.4% by the MMRT compared to the R_{het} simulated under no climate change scenario. These results are in line with Aguilos et al. (2011) who measured an annual R_{het} increment up to +74% in a mixed temperate forest in northern Japan when soil temperature increased of 3°C.

5.4 Does MMRT improve the simulation of R_{het}?

The statistical analysis carried out to compare the EF and the MMRT approach, at monthly time scale, shows that there is not a better approach than the other. The correlation coefficient (*rPea*) has similar values at both sites, with a difference equal to 0.004 at Hainich and 0.0013 at Ankasa between the *rPea* values computed for the EF and MMRT functions at each site. It means that the two approaches produce substantially equal results.
The MMRT formulation has been applied to simulate the soil respiration fluxes in several recent studies and compared to the empirical exponential functions classically used by models. Alster et al. (2016) compared the MMRT and the Arrhenius function basing on soil respiration data measured at different temperatures in three grassland sites, across the U.S. Great Plains: Makoce Washte Prairie

in South Dakota, Shortgrass Steppe in Colorado and Sevilleta in New Mexico. The Arrhenius approach was more complex than the EF equation used in this work and it was based on the concept of activation energy, i.e. the energy barrier that the reactants of a reaction must to overcome to be converted into products. The MMRT was able to simulate the data with a higher fit than the Arrhenius equation, with a high difference between the R^2 computed with the two approaches that, in some cases, was equal to 0.68.

Schipper et al. (2014) applied the MMRT to fit soil respiration data published in Davidson et al. (2006) and measured in a mature conifer forest at Howland (ME, USA). They demonstrated – at least in their study cases – that the MMRT predicted an optimum temperature with a R^2 equal to 0.817.

In the present work, the soil temperature range at Hainich (even under the warmest climate change scenario) is likely too low to have a higher fit between the simulated and measured R_{het} using the MMRT rather than the EF. In the temperate forest, indeed, the MMRT does not simulate the acclimation, showing an exponential behavior. At Ankasa, instead, the soil temperature range is certainly much higher than at Hainich, but is in any case insufficient to show some relevant difference between the two approaches. Hence, in the present work, the MMRT does not improve the simulation of R_{het}.

5.5 Which differences between EF and MMRT?

Under present-day climate, at monthly time step, there are no statistically significant differences between the two formulations. One possible explanation for this result could be related to the soil temperature range characterizing the two sites. At Hainich, the soil temperature varies between 0.98 °C and 14.53 °C at which the two approaches simulate an exponential increase of the process rate. Conversely, at Ankasa, the soil temperature is comprised within a range in which the acclimation of the process can be simulated, but it is insufficient to detect relevant differences between the EF and the MMRT.

At daily time scale there are some differences, even if they are relatively low. The mean cumulated difference between the R_{het} simulated by the MMRT and the fluxes reproduced using the EF approach is equal to 3.6% at Hainich and 3.2% at Ankasa of the total annual R_{het}.

It is interesting to highlight that, despite the soil temperature range registered at Ankasa is ultimately higher than at Hainich, i.e. from 0.98 °C to 14.53 °C at Hainich and from 24.13°C to 25.38°C at Ankasa, the incorporation of the acclimation seems to produce very narrow percentage differences between the two sites. This could be explained considering the Figure 4 with the curves referred to the temperature-decomposition rate relationship of the two approaches. The plot shows

how the curves of the EF and the MMRT approach differ not only at high temperatures (after the optimum temperature) but also within the temperature range registered at Hainich (between 0°C and 15°C).

Despite the differences between the two approaches – both qualitatively and quantitatively – are relatively low if considered at short term (i.e. days or months), the results obtained under climate change scenario show more relevant differences when analyzed under longer term, but only for the warmest RCP (8.5) and if the results are scaled on the entire surface of the analyzed forests. The R_{het} simulated over 100 years under RCP 8.5 by the EF is higher of 593.9 g C m^{-2} at Hainich and 614.1 g C m^{-2} at Ankasa than the values simulated by the MMRT. Computing the R_{het} values for the entire surface of the two sites, ~160 Km^2 Hainich and ~500 Km^2 Ankasa, and converting in tons of C, the R_{het} estimated by the EF over the entire period (2006-2099) is higher of $95 \cdot 10^3$ tons C at Hainich and $307 \cdot 10^3$ tons C at Ankasa than the values simulated by the MMRT.
It is possible to analyze the cumulated differences between the two approaches to simulate the annual R_{het} over the two periods taken into account (2006-2050 and 2051-2099). The results show that the main differences are detected under RCP 8.5, for which they are equal to 71.4% of the total in the first period at Hainich and to 82.6% of the total in the second interval at Ankasa. At Hainich, in the near future interval (2006-2050), the soil temperature range is comprised between 7.8° C and 10.2 °C in which the values of the soil temperature modifier simulated by the two approaches differ from each other of about 0.05 (*Fig.4*). A low difference but that becomes not negligible over the entire period (2006-2050). Instead, in the far future (2051-2099), the soil temperature varies in the range 9.7 - 14.1 °C, in which the differences in the soil temperature modifier values between the two approaches are almost zero.

5.6 Is MMRT more or less uncertain than EF?

Both at the temperate and at the tropical forest sites, the parameters exerting the highest weight on the model are those directly involved in the equation used to simulate the R_{het}. Indeed, in a conventional model as CENTURY, the decomposed carbon is simulated by a first-order kinetic (Sierra et al., 2012) in which the decay rate of the litter and SOM pools plays a key role (Manzoni & Porporato, 2007). In particular, the model is sensitive to the decomposition rate of the aboveground metabolic litter. This pool directly receives the litterfall input and it is constituted by the more labile C and N compounds, which are rapidly degraded by soil microorganisms (Weil & Brady, 2017).
The model is also sensitive to decomposition rates of surface microbes and slow SOM pools. These parameters are relevant because regulate the amount of C (and N linked to C through the C:N ratio)

decomposed at each time step. This result is in line with Shi et al. (2018). With the aim to quantify the uncertainty – due to model parameters – in the simulation of soil C and N stocks at steady-state, they carried out a sensitivity analysis on a conventional CENTURY-like model. They found that – at least in their study cases – the maximum decay rates of the microbial and slow SOM pools are the parameters to which the model is more sensitive.

Other relevant parameters that exert a relevant weight on the model are represented by those involved in the equations used to compute the soil temperature modifier of litter and SOM decomposition, hence the EF and the MMRT equations. For the first equation the parameters are the slope (*par_a*) and the exponent (*par_b*), while ΔH_0 and ΔS_0 are comprised in the MMRT formulation. In the CENTURY model, the soil temperature modifier is one of the most important factors in the simulation of decomposition, hence of R_{het} (Parton et al., 1987; Sierra et al., 2012). In particular, the parameters involved in the MMRT approach depend on the microbial communities that decompose the soil organic matter in the ecosystem and also on the enzymes produced by microorganisms (Hobbs et al., 2013; Schipper et al., 2014). Regarding this important point, Schipper et al. (2014) suggest the hypothesis – which finds somehow support also in Alster et al. (2016) – that the ecosystem, to avoid irreversible damages due to denaturation, naturally selects for microbial communities that can reach, in the enzyme production, an optimum temperature optimized with the local temperature variations.

In general, the present work shows that MMRT is more uncertain than EF in the analyzed cases, i.e. under present-day climate and climate change scenario – RCP 2.6, 4.5, 6.0 and 8.5 – at Hainich and Ankasa forests.

5.7 Scientific implications and future perspective

At the beginning of this work I questioned:

1. Is it possible to improve the simulation of the heterotrophic respiration fluxes taking into account the acclimation process at higher temperatures?

2. By comparing the MMRT approach to the classical empirical EF, is there any difference, and to what extent, in the simulated heterotrophic respiration fluxes under different climate conditions and different time scales?

3. How large is the uncertainty in the simulation of the heterotrophic respiration due to the implementation of the MMRT and how large is by using the EF one? And which generates the largest uncertainty in the model estimates at different temporal scale?

These questions stem from the expectation that potentially obtain significantly different results in the R_{het} simulation when comparing two approaches – the EF and the MMRT – under present-day climate and, theoretically even more, under warmer climate change scenarios. The initial hypothesis was promising because of the two approaches are particularly different from each other, and reanimating the ancient debate between *mechanism* (rationalism) from one side and *empiricism* to the other (Bies et al., 2016). Distinguishing mechanism from empiricism with a clear line is extremely difficult, because in general a purely mechanistic or empirical approach does not exist (Nestorov & Rowland, 1999). The distinction is only relative, basing on the degree of preponderance of one of the two realities on the other in a specific approach. However, in the present work, the EF has been defined as an *empirical* approach because it is actually based on the data – the R_{het} usually observed in a specific range of temperature up to 25°C – that show an exponential relationship between R_{het} and soil temperature. Conversely, the MMRT has been defined as a *mechanistic* approach that, because also of incorporating the R_{het} acclimation to enhancing soil temperature, should explain the process on a 'rational knowledge' which tends to overcome the specificity of observations. Hence, while the empirical EF is more inclined to predict the current patterns as observed in nature, the mechanistic MMRT is – or it should theoretically be – characterized by a better predictive potential, with better effects of the soil temperature increment in predicting R_{het}.

Despite the diversity of these two approaches, the results achieved related to the R_{het} simulation under both present-day and climate change scenarios, as well as under different time scales (from daily to monthly), at Hainich and Ankasa, seem to deny the initial hypothesis. The MMRT and EF simulate the R_{het} fluxes without any statistically relevant differences, notwithstanding the first approach reproduces the process in a more sophisticated way than the second one, basing on the thermodynamic properties of the phenomenon and on a higher number of parameters with a specific physical meaning. In the cases analyzed in the present work, the implementation of a more complex mechanistic approach has not translated in a significant improvement of the results, despite the R_{het} acclimation has been widely observed in the experiments (Davidson et al., 2006; Hobbs et al., 2013; Schipper et al., 2014).

A possible reason to explain the denial of the initial hypothesis is the base structure used to compare the EF and the MMRT, that is, the scheme introduced by CENTURY. The lack of significant differences in the results between the two approaches, especially under warming climate change scenarios, puts in doubt the possibility to catch the effects produced by the R_{het} acclimation implementing the MMRT on the 'conventional' scheme of soil C and N cycles. The R_{het} acclimation at increasing soil temperature has been simulated by models, but using a microbial-enzyme scheme

(Allison et al., 2010) in which, conversely to the ’conventional‘ one used in this work, the microbial processes are explicitly reproduced. This point is relevant because the CENTURY scheme represents the base structure of several other models of the soil C and N processes developed since the late 1980s (e.g. Manzoni & Porporato, 2009), among which BIOME-BGC (Thornton et al, 2002), CENW (Kirschbaum & Paul, 2002), 3D-CMCC-FEM (Collalti et al., 2014; Marconi et al., 2017), CASA (Wang et al., 2010), CLM (Yang et al., 2014) and ORCHIDEE (Krinner et al., 2005).

6. Conclusions

The acclimation of soil respiration (in both autotrophic and heterotrophic components) because of the increment of soil temperature has been widely observed in forest, for several other ecosystems, in laboratory experiments and simulated by models. Hence, the R_{het} acclimation is a relevant process to simulate to predict reliable CO_2 fluxes from the soil at enhancing soil temperature.

In the present work, the implementation of the mechanistic MMRT approach – embedding the R_{het} acclimation at increasing soil temperature – does not improve the simulation of the R_{het} process. The results achieved in this work put in doubt the possibility to improve the simulation of the enhancing soil temperature effect on R_{het} by the models that embed the CENTURY scheme. This is crucial to understand the reliability of the estimates of the CO_2 fluxes from the soil by those models and to better define the role of the forest soils in contributing to climate change mitigation.

Acknowledgements

The list of people to thank is particularly and fortunately long. At the end of the journey, looking back I realize how this experience has been an absolutely unique opportunity of personal and professional growth. Along the way, I have met a number (I would dare to say) enormous of people whose support has been crucial to overcome the several difficulties encountered.

Thank to Alessio Collalti, constant and patient guide. He has taught me a lot from a professional and personal point of view. Especially during the crucial moments, his support has been fundamental to reach the goal in the best way.

A huge thank to Dario Papale, the compass to follow the right direction during the last three years.

Thank Carlo Trotta, a further guide, man of great humanity and always available to support me, especially in the crucial moments.

I will never forget the experience at the *Max Planck Institute for Biogeochemistry* in Jena (Germany). Six months whit extraordinary people. Among many, thank to Marion Schrumpf and Sönke Zaehle, two wonderful group leaders. Thank to Markus Reichstein, Bernhard Ahrens, Marleen Pallandt, Lin Yu, Thomas Wutzler and Melanie Kern for their time, knowledge and skills. Thank to Mirco Migliavacca, Carlos Sierra and all members of *Soil Biogeochemistry* and *Terrestrial Biosphere Modelling* groups for the constant dialogues, the precious support and for all the teachings that I had the honor and luck to receive.

Thank Markus Müller, a further guide, extremely prepared, patient and of great humanity.

Thank Sungmin, Lina, Nora, Naixin, Helvi, Junzhi, Xuanlong, Jasper and Daniel for the wonderful moments lived together.

This experience has given me a big friend, Ali Fallah, healthy carrier of joy and essential point of reference during my stay in Jena.

Thank to the people that I have met in the last three years at *CMCC* and, in particular, at *CMCC-IAFES* in Viterbo. Thank Monia, Antonio, Lucia, Alessandra, Arianna, Elisa, Alessio (Ribeca), Cinzia, Sergio, Matteo, Guido, Luca, Giulia for welcoming me from the first moment making me feel at home.

The support and the dialogue with the Internal Evaluation Commission have been fundamental. Thank Maria Cristina Moscatelli, Anna Barbati and Alessandro D'Annibale for the precious questions that allowed me to better understand several aspects of the work.

Thank to Fernando Moyano, Monia Santini, Tommaso Chiti and Giacomo Nicolini for their availability in sending me the requested data promptly.

Thank Daniela Dalmonech for giving me some important advices.

Thank to the members of the *Forest Modelling Lab.* for their constant and fundamental support.

It was good to live this experience with other Ph.D. students, sharing with them pleasant moments and also fears and concerns. Thank Adriana, Francesco, Angelo, Valentina, Rosa, Federica, Serena and Matteo.

In general, thank to the people that I have met during this experience and who has helped me to growth and improve.

I am a very lucky person to have a fantastic family and wonderful friends that have supported me.

Et dulcis in fundo, a big thank to my Annamaria who, during this important journey, has walked with me along the way, never leaving me alone.

Code availability

The model code is available at https://github.com/cbiondo84/CENTURY_model_R

Author contacts: corrado.biondo@cmcc.it

References

Aguilos M., Takagi K., Liang N., Watanabe Y., Goto S., Takahashi Y., Mukai H. and Sasa K. 2011 Soil warming in a cool-temperate mixed forest with peat soil enhanced heterotrophic and basal respiration rates but Q_{10} remained unchanged. Biogeosciences Discussions, 8, 6415–6445.

Allison S.D., Wallenstein M.D. and Bradford M.A. 2010. Soil-carbon response to warming dependent on microbial physiology. Nature Geoscience. 3, 336-340.

Alster C.J., Koyama A., Johnson N.G., Wallenstein M.D. and von Fischer J.C. 2016. Temperature sensitivity of soil microbial communities: an application of macromolecular rate theory to microbial respiration. Journal of geophysical research: biogeosciences. 121, 1420-1433.

Anderson, J.M. 1973. Carbon dioxide evolution from two temperate deciduous woodland soils. Journal of Applied Ecology, 10, 361-378.

Aubinet M., Vesala T. and Papale D. 2012. Eddy covariance: a practical guide to measurement and data analysis. Springer, Dordrecht, The Netherlands.

Bies R., Cook S. and Duffull S. 2016. The pharmacometrician's dilemma: the tension between mechanistic and empirical approaches in mathematical modelling and simulation – a continuation of the age-old dispute between rationalism and empiricism? British Journal of Clinical Pharmacology. 82, 580-582.

Blagodatskaya E. and Kuzyakov. Y. 2008. Mechanisms of real and apparent priming effects and their dependence on soil microbial biomass and community structure: critical review. Biology and fertility of soils. 45, 115-131.

Bond-Lamberty B. and Thomson A., 2010. Temperature-associated increases in the global soil respiration record. Nature. 464, 579-582.

Braakhekke M.C., Wutzler T., Beer C., Kattge J., Schrumpf M., Ahrens B., Schoning I., Hoosbeek M.R., Kruijt B., Kabat P. and Reichstein M. 2013. Modeling the vertical soil organic matter profile using Bayesian parameter estimation. Biogeosciences. 10, 399-420.

Bradford M.A., Wieder W.R., Bonan G.B., Fierer N., Raymond P.A. and Crowther T.W. 2016. Managing uncertainty in soil carbon feedbacks to climate change. Nature Climate Change. 6, 751-758.

Bradford M.A., Watts B.W. and Davies C.A. 2010. Thermal adaptation of heterotrophic soil respiration in laboratory microcosms. Global Change Biology. 16, 1576-1588.

Bradford M.A., Davies C.A., Frey S.D., Maddox T.R., Melillo J.M., Mohan J.E., Reynolds J.F., Treseder K.K. and Wallenstein M.D. 2008. Thermal adaptation of soil microbial respiration to elevated temperature. Ecology Letters. 11, 1316-1327.

Bridge, B.J., Mott, J.J. & Hartigan, R.J. 1983. The formation of degraded areas in dry savanna woodlands of northern Australia. Australian Journal of Soil Research, 21, 91-104.

Burnham K.P. and Anderson D.E.. 2002. Model selection and multimodel inference: A practical information-theoretic approach. Springer.

Burns R.G. 2010. How do microbial extracellular enzymes locate and degrade natural and synthetic polymers in soil. Molecular environmental soil science at the interfaces in the Earth's critical zone. 294-297.

Chapman, S.B. 1979. Some interrelationships between soil and root respiration in lowland Calluna heathland in southern England. Journal of Ecology, 67, 1-20.

Chen H. and Tian H.Q. 2005. Does a general temperature-dependent Q_{10} model of soil respiration exist at biome and global scale? Journal of Integrative Plant Biology. 47, 1288-1302.

Chiti T., Grieco E., Perugini L., Rey A and Valentini R. 2014. Effect of the replacement of tropical forests with tree plantations on soil organic carbon levels in the Jomoro district, Ghana. Plant Soil. 375, 47-59.

Chiti T., Certini G., Grieco E. and Valentini R. 2010. The role of soil in storing carbon in tropical rainforests: the case of Ankasa Park, Ghana. Plant Soil. 331, 453-461.

Ciais, P., C. Sabine, G. Bala, L. Bopp, V. Brovkin, J. Canadell, A. Chhabra, R. DeFries, J. Galloway, M. Heimann, C. Jones, C. Le Quéré, R.B. Myneni, S. Piao and P. Thornton, 2013: Carbon and Other Biogeochemical Cycles. In: Climate Change 2013: The Physical Science Basis. Contribution of Working Group I to the Fifth Assessment Report of the Intergovernmental Panel on Climate Change [Stocker, T.F., D. Qin, G.-K. Plattner, M. Tignor, S.K. Allen, J. Boschung, A. Nauels, Y. Xia, V. Bex and P.M. Midgley (eds.)]. Cambridge University Press, Cambridge, United Kingdom and New York, NY, USA.

Collalti A., Tjoelker M.G., Hoch, G., Mäkelä A., Guidolotti G., Heskel M., et al., 2020. Plant respiration: Controlled by photosynthesis or biomass?. Global Change Biology. 26, 1739-1753. doi.org/10.1111/gcb.14857.

Collalti A., Thornton P.E., Cescatti A., Rita A., Borghetti M., Nolè A., Trotta C., Ciais P. and Matteucci G. 2019. The sensitivity of the forest carbon budget shifts across processes along with stand development and climate change. Ecological Applications. 29 (2). doi.org/10.1002/eap.1837.

Collalti A., Trotta C., Keenan T.F., Ibrom A., Bond-Lamberty B., Grote R., Vicca S., Reyer C.P.O., Migliavacca M., Veroustraete F., Anav A., Campioli M., Scoccimarro E., Šigut L., Grieco E., Cescatti A. and Matteucci G. 2018. Thinning Can Reduce Losses in Carbon Use Efficiency and Carbon Stocks in Managed Forests Under Warmer Climate. Journal of Advances in Modeling Earth Systems. 10, 2427-2452.

Collalti A., Marconi S., Ibrom A., Trotta C., Anav A., D'Andrea E., Matteucci G. , Montagnani L., Gielen B., Mammarella I., Grunwald T., Knohl A., Berninger F., Zhao Y., Valentini R., and Santini M. 2016. Validation of 3D-CMCC Forest Ecosystem Model (v.5.1) against eddy covariance data for 10 European forest sites. Geoscientific Model Development. 9, 479-504.

Collalti A., Perugini L., Santini M., Chiti T., Nolè A., Matteucci G. and Valentini R. 2014. A process-based model to simulate growth in forests with complex structure: Evaluation and use of 3D-CMCC Forest Ecosystem Model in a deciduous forest in Central Italy. Ecological Modelling. 272, 362-378.

Crowther T.W. and Bradford M.A. 2013. Thermal acclimation in widespread heterotrophic soil microbes. Ecology Letters. 16, 469-477.

Davidson E.A. and Janssen I.A. 2006. Temperature sensitivity of soil carbon decomposition and feedbacks to climate change. Nature. 440, 165-173.

Dörr, H. & Münnich, K.O. 1987. Annual variation is soil respiration from selected areas of the temperate zone. Tellus, 39B, 114-121.

Eliasson P.E., McMurtrie R.E., Pepper D.A., Stroemgren M., Linder S. and Agren G.I. 2005. The response of heterotrophic CO_2 flux to soil warming. Global Change Biology. 11, 167-181.

Evans M.G. & Polanyi M. 1935. Some applications of the transition state method to the calculation of reaction velocities, especially in solution. Transactions of the Faraday Society. 31, 875-894.

Fang C., Smith P., Moncrieff J.B. and Smith J.U. 2005. Similar response of labile and resistant soil organic matter pools to changes in temperature. Nature. 433, 57-59.

Fang X., Luo S. and Lyu S. 2019. Observed soil temperature trends associated with climate change in the Tibetan Plateau, 1960-2014. Theoretical and Applied Climatology. 135, 169-181.

FAO. 2015. Global forest resources assessment.

Fields P.A., 2001. Review: Protein function at thermal extremes: balancing stability and flexibility. Comparative Biogeochemistry and Physiology. 129, 417-431.

Friedlingstein P., Meinshausen M., Arora V.K., Jones C.D., Anav A., Liddicoat S.K. and Knutti R. 2014. Uncertainties in CMIP5 Climate Projections due to Carbon Cycle Feedbacks. Journal of Applied Meteorology and Climatology. 27, 511-526.

Gessner M.O., Swan C.M., Dang C.K., McKie B.G., Bardgett R.D., Wall D.H. and Hattenschwiler S. 2010. Diversity meets decomposition. Tree. 1230.

Gielen B., Mammarella I., Grünwald T., Knohl A., Berninger F., Zhao Y., Valentini R., and Santini M. 2016. Validation of 3D-CMCC Forest Ecosystem Model (v.5.1) against eddy covariance data for 10 European forest sites. Geoscientific Model Development. 9, 479-504.

Golinkoff. 2010. Biome-BGC version 4.2: theoretical framework of Biome-BGC.

Goll D.S., Brovkin V., Parida B.R., Reick C.H., Kattge J., Reich P.B., van Bodegom P.M. and Niinemets U. 2012. Nutrient limitation reduces carbon uptake in simulations with a model of combined carbon, nitrogen and phosphorus cycling. Biogeosciences. 9, 3547-3569.

Hersterberg, R. & Seigenthaler, U. 1991. Production and stable isotopic composition of CO2 in a soil near Bern, Switzerland. Tellus, 43B, 197-205.

Hobbs J.K., Jiao W., Easter A.D., Parker E.J., Schipper L.A. and Arcus V.L. 2013. Change in heat capacity for enzyme catalysis determines temperature dependence of enzyme catalyzed rates. ACS Chemical Biology. 8, 2388-2393.

Holland E.A., Neff J.C., Townsend A.R. and McKeown B. 2000. Uncertainty in the temperature sensitivity of decomposition in tropical and subtropical ecosystems: implications for models. Global biogeochemical cycles. 14, 1137-1151.

IPCC Special Report 2018. Global Warming of 1.5°C.Intergovernmental Panel on Climate Change.

Janssen I.A. and Pilegaard K., 2003. Large seasonal changes in Q10 of soil respiration in a beech forest. Global Change Biology. 9, 911-918.

Kelly R.H., Parton W.J., Hartman M.D., Stretch L.K., Ojima D.S., and Schimel D.S. 2000. Intra-annual and interannual variability of ecosystem processes in shortgrass steppe. Journal of geophysical research. 105, 93-100.

Kirschbaum M.U.F. 2004. Soil respiration under prolonged soil warming: are rate reductions caused by acclimation or substrate loss? Global Change Biology. 10, 1870-1877.

Kirschbaum M.U.F. and Paul K.I. 2002. Modelling C and N dynamics in forest soils with a modified version of the CENTURY model. Soil biology and biogeochemistry. 34, 341-354.

Kirschbaum M.U.F. 2000a. Will changes in soil organic carbon act as a positive or negative feedback on global warming? Biogeochemistry. 48, 21-51.

Kirschbaum M.U.F. 1995. The temperature dependence of soil organic matter decomposition, and the effect of global warming on soil organic storage. Soil Biology and Biogeochemistry. 27, 753-760.

Kleber M. 2010. What is the recalcitrant soil organic matter? Environmental chemistry. 7, 320-332.

Krinner N. V., de Noblet-Ducoudré N., Ogée J., Polcher J., Friedlingstein P., Ciais P., Sitch P., and Prentice I. C. 2005. A dynamic global vegetation model for studies of the coupled atmosphere-biosphere system. Global biogeochemical cycles. 19.

Kucera, C. & Kirkham, D. 1971. Soil respiration studies in tallgrass prairie in Missouri. Ecology, 52, 912-915.

Kutsch W.L., Persson T., Schrumpf M., Moyano F.E., Mund M., Andersson S., Schulze E-D. 2010. Heterotrophic soil respiration and soil carbon dynamics in the deciduous Hainich forest obtained by three approaches. Biogeochemistry. 100, 167-183.

Kuzyakov Y., Horwath W., Dorodnikov M. and Blagodatskaya E. 2018. Review and synthesis of the effects of elevated atmospheric CO2 on soil processes: No changes in pools, but increased fluxes and accelerated cycles. Soil Biology and Biochemistry. 128, 66-78.

Li C. and Aber J., Stange F., Butterbach-Bahl K. and Papen H. 2000. A process-oriented model of N2O and NO emissions from forest soils: 1. model development. Journal of geophysical research. 105, 4369-4384.

Li J., Nie M., Pendall E., Reich P.B., Pei J., Noh N.J., Zhu T., Li B., and Fang C. 2019. Biogeografic variation in temperature sensitivity of decomposition in forest soils. Global Change Biology. 0, 1-13.

Liang L.L., Arcus V.L., Heskel M.A., O'Sullivan O.S., Weerasinghe L.K., Creek D., Egerton J.J.G., Tjolker M.G., Atkin O.K., Schipper L.A. 2018. Macromolecular rate theory (MMRT) provides a thermodynamics rationale to underpin the convergent temperature response in plant leaf respiration. Global Change Biology. 24, 1538-1547.

Lloyd J. and Taylor J.A. 1994. On the temperature dependence of soil respiration. Functional ecology. 8, 315-323.

Luo Y., Wan S., Hui D. and Wallace L.L. 2001. Acclimatization of soil respiration to warming in a tall grass Prairie. Letters to Nature. 413, 622-625.

Luyssaert S., M. Reichstein, E.-D. Schulze, I. A. Janssens, B.E. Law, D. Papale, D. Dragoni, M.L. Goulden, A. Granier, W.L. Kutsch, S. Linder, G. Matteucci, E. Moors, J.W. Munger, K. Pilegaard, M. Saunders, and E.M. Falge. 2009. Toward a consistency cross-check of eddy covariance flux–based and biometric estimates of ecosystem carbon balance. Global Biogeochemical Cycles. 23, GB3009.

Manzoni S. and Porporato A. 2009. Soil carbon and nitrogen mineralization: theory and models across scales. Soil biology and biogeochemistry. 41, 1355-1379.

Manzoni S. and Porporato A. 2007. A theoretical analysis of nonlinearities and feedbacks in soil carbon and nitrogen cycles. Soil biology and biogeochemistry. 39, 1542-1556.

Marconi S., Chiti T., Nolè A., Valentini R., Collalti A. 2017. The role of Respiration in estimation of the net Carbon cycle: coupling soil Carbon dynamics and canopy turnover in a novel version of 3D-CMCC Forest Ecosystem Model. Forests, 8: 220, https://doi.org/10.3390/f8060220.

Marthews TR, Metcalfe D, Malhi Y, Phillips O, Huaraca Huasco W, Riutta T, Ruiz Jaén M, Girardin C, Urrutia R, Butt N, Cain R, Oliveras Menor I and colleagues from the RAINFOR and GEM networks (2012). Measuring Tropical Forest Carbon Allocation and Cycling: A RAINFOR-

GEM Field Manual for Intensive Census Plots (v2.2). Manual, Global Ecosystems Monitoring network, http://gem.tropicalforests.ox.ac.uk/.

Medlyn B.E., Robinson A.P., Clement R. and McMurtrie R.E. 2005. On the validation of models of forest CO2 exchange using eddy covariance data: some perils and pitfalls. Tree Physiology. 25, 839-857.

Migliavacca M., Sonnentag O., Keenan T.F., Cescatti A., O'Keefe J. and Richardson A.D. 2012. On the uncertainty of phenological responses to climate change, and implications for a terrestrial biosphere model. Biogeosciences. 9, 2063-2083.

Monteith, J.L., Szeicz, G. & Yabuki, K. 1964. Crop photosynthesis and the flux of carbon dioxide below the canopy. Journal of Applied Ecology, 1, 321-337.

Moss, R., Edmonds, J., Hibbard, K. et al. 2010. The next generation of scenarios for climate change research and assessment. Nature 463, 747–756.

Morris M.D. 1991. Factorial sampling plans for preliminary computational experiments. Technometrics. 33, 161-174.

Moyano F.E., Manzoni S. and Chenu C. 2013. Responses of soil heterotrophic respiration to moisture availability: an exploration of processes and models. Soil biology and biogeochemistry. 59, 72-85.

Nakane, K., Tsubota, H. & Yamamoto, M.. 1984. Cycling of soil carbon in a Japanese red pine forest I. Before a clear-felling. Botanical Magazine (Tokyo), 97, 39-60.

Nakane, K. 1980. Comparative studies of cycling if soil organic carbon in three primeval moist forests. Japanese Journal of Ecology, 30, 155-172.

Nestorov I. and Rowland M. 1999. Empirical versus mechanistic modelling: comparison of an artificial neural network to a mechanistically based model for quantitative structure pharmacokinetic relationships of a homologous series of barbiturates. AAPS Pharmsci. 1, 5-13.

Noh N.J., Kuribayashi M., Saitoh T.M., Nakaji T., Nakamura M., Hiura T. and Muraoka H. 2015. Responses of soil, heterotrophic, and autotrophic respiration to experimental open-field soil warming in a cool-temperate deciduous forest. Ecosystems. 19, 504-520.

Nolè, A., Collalti, A., Borghetti, M., Chiesi, M., Chirici, G., Magnani, F., Marras, S., Maselli, F., Sirca, C., Spano, D., et al., 2014. The role of managed forest ecosystems: A modeling based approach. Environ. Sci. Eng. 131, 71–8

Oechel W.C., Vourlitis G.L., Hastings S.J., Zulueta R.C., Hinzman L., Kane D. 2000. Acclimaion of ecosystem CO_2 exchange in the Alaskan Arctic in response to decadal climate warming. Nature. 406, 978-981.

Oni S.K., Mieres F., Futter M.N. and Laudon H. 2017. Soil temperature responses to climate change along a gradient of upland-riparian transect in boreal forest.143, 27-41.

Parton W.J., Ojima D.S., Cole C.V. and Schimel D.S. 1994. A general model for soil organic matter dynamics: sensitivity to litter chemistry, texture and management. Soil science society of America.

Parton W.J., Scurlok J.O.M., Ojima D.S., Gilmanov T.G., Scholes R.J., Schimel D.S., Kirchner T., Menaut J-C., Seastedt T., Garcia Moya E., Kamnalrut A. and Kinyamario J.I. 1993. Observations and modeling of biomass and soil organic matter dynamics for the grassland biome worldwide. Global biogeochemical cycles. 7, 785-809.

Parton W.J., Ojima D.S., Schimel D.S., and Kittel T.G.F. 1992. Development of simplified ecosystem models for applications in Earth System studies: the CENTURY experience. Modeling the earth system.

Parton W.J., Stewart J.W.B. and Cole C.V. 1988. Dynamics of C, N, P and S in grassland soils: a model. Biogeochemistry. 5, 109-131.

Parton W.J., Schimel D.S., Cole C.V. and Ojima D.S. 1987. Analysis of factors controlling soil organic matter levels in Great Plains Grasslands. Division S-3 Soil Microbiology and Biogeochemistry.

Parton W.J. and Innis G.S. 1972. Some graphs and their functional forms. Grassland biome. U.S. International Biological Programm.

Peterson, KA.' & Billings, W.D. 1975. Carbon dioxide flux from tundra soils and vegetation as related to temperature at Barrow, Alaska. American Midland Naturalist, 94, 88-98.

Reichstein M. and Beer C. 2008. Soil respiration across scales: the importance of a model-data integration framework for data interpretation. Journal of plant nutrition and soil science. 171, 344-354.

Reinke, D.C., Adriano, D.C. & McLeod, K.W. 1981. Effects of litter alteration on carbon dioxide evolution from a South Carolina Pine forest floor. Soil Science Society ofAmerica Journal, 45, 620-623.

Rey A. and Jarvis P. 2006. Modelling the effect of temperature on carbon mineralization rates across a network of European forest sites (FORCAST). Global Change Biology. 12, 1894-1908.

Richards, B.N. 1981. Forest floor dynamics. Production in Perpetuity, pp. 145-157. Proceedings of the Forest Nutrition Workshop, Canberra, Australia. CSIRO Division of Forest Research, Canberra.

Saltelli A. 2019. A short comment on statistical versus mathematical modelling. Nature communications. 10, 3870.

Schindlbacher A, Zechmeister-Boltenstern S, Jandl R. 2009. Carbon losses due to soil warming: do autotrophic and heterotrophic soil respiration respond equally? Global Change Biology, 15, 901–913.

Schipper L.A., Hobbs J.K., Rutledge S. and Arcus V.L. 2014. Thermodynamic theory explains the temperature optima of soil microbial processes and high Q10 values at low temperatures. Global Change Biology. 20, 3578-3586.

Schmidt W. I., Torn M. S., Abiven S., Dittmar T., Guggenberger G., Janssens I.A., Kleber M., Kögel-Knabner I., Lehmann J., Manning D. A. C., Nannipieri P., Rasse D.P., Weiner S. and Trumbore S.E. 2011. Persistance of soil organic matter as an ecosystem property. Nature. 478, 49-56.

Schulze E.D. 2000. Carbon and nitrogen cycling in European forest ecosystems. Ecological studies 142. Springer, 142.

Shi Z., Crowell S., Luo Y. and Moore B. 2018. Model structures amplify uncertainty in predicted soil carbon responses to climate change. Nature communications. 9, 2171.

Sierra C.A., Mueller M., and Trumbore S.E. 2012. Models of soil organic matter decomposition: the SOILR package, version 1.0. Geoscientific Model Development. 5, 1045-1060.

Silvola, K., Vdlijokki, J. & Aaltonen, H. 1985. Effect of draining and fertilization on soil respiration at three ameliorated peatland sites. Acta Forestalia Fennica, 191, 1-32.

Sitch S., Smith B., Prentice I.C., Arneth A., Bondeau A., Cramer W., Kaplan J.O., Levis S., Lucht W., Sykes M.T., Thonicke K. and Venvsky S. 2003. Evaluation of ecosystem dynamics, plant geography and terrestrial carbon cycling in the LPJ dynamic global vegetation model. Global Change Biology. 9, 161-185.

Snowdon P., Ryan P. and Raison J. 2005. Review of C:N ratios in vegetation, litter and soil under Australian native forests and plantations. Technical report 45.

Steffen A. and Apostolakis J. 2007. On the ease of predicting the thermodynamic properties of beta-cyclodextrin inclusion complexes. 30, 1-29.

Svensson, B.H. 1980. Carbon dioxide and methane fluxes from the ombotrophic parts of a subarctic mire. Ecological Bulletin, 30, 235-350.

Thakur G.C. 1991. Waterflood surveillance techniques – A reservoir management approach. Society of petroleum engineers. 43-10.

Thornton P.E. and Rosenbloom N.A. 2005. Ecosystem model spin-up: estimating steady-state conditions in a coupled terrestrial carbon and nitrogen cycle model. Ecological modelling. 189, 25-48.

Van Ojien M., Rougier J. and Smith R. 2005. Bayesian calibration of process-based forest models: bridging the gap between models and data. Tree physiology. 25, 915-927.

van Vuuren, D.P., Edmonds, J., Kainuma, M. et al. 2011. The representative concentration pathways: an overview. Climatic Change. 109, 5.

Wang X., Liu L., Piao S., Janssens I.A., Tang J., Liu W., Chi Y., Wang J. and Xu S. 2014. Soil respiration under climate warming: differential response of heterotrophic and autotrophic respiration. Global Change Biology. 20, 3229-3237.

Wang Y.P., Law R.M. and Pak B. 2010. A global model of carbon, nitrogen and phosphorous cycles for the terrestrial biosphere. Biogeosciences. 7, 2261-2282.

Wei H., Guenet B., Vicca S., Nunan N., AbdElgawad H., Pouteau V., Shen W. and Janssens I.A. 2014. Thermal acclimation of organic matter decomposition in an artificial forest soil is related to shifts in microbial community structure. Soil Biology & Biogeochemistry. 71, 1-12.

Weil and Brady. 2017. The nature and properties of soils. Pearson Educational Limited.

Wu C., Liang N., Sha L., Xu X., Zhang Y., Lu H., Song L., Song Q. and Xie Y. 2016. Heterotrophic respiration does not acclimate to continuous warming in a subtropical forest. Scientific Report. 6, 21561.

Xu T., White L., Hui D. and Luo Y. 2006. Probabilistic inversion of a terrestrial ecosystem model: analysis of uncertainty in parameter estimation and model prediction. Global biogeochemical cycles.

Yang X., Thornton P.E., Ricciuto D.M. and Post W.M. 2014. The role of phosphorus dynamics in tropical forests – a modeling study using CLM-CNP. Biogeosciences. 11, 1667-1681.

Yoneda, T. & Karita, H. 1978. Soil respiration. Biological Production in a Warm-Temperate Evergreen Oak Forest of Japan (eds T. Kira, Y. Ono & T. Hosokawa), pp. 239-249. University of Tokyo, Tokyo.

Zhang H., Liu B., Zhou D., Wu Z. and Wang T. 2019. Asymmetric soil warming under global climate change. International journal of environmental research and public health. 16, 1504.

Zhang H., Goll D.S., Manzoni S., Ciais P., Guenet B., and Huang Y. 2018. Modeling the effect of litter stoichiometry and soil mineral N availability on soil organic matter formation using CENTURY-CUE (v1.0). Geoscientific Model Development. 11, 4779-4796.

Supplementary material

Table S3.1 *Litter and soil organic matter pools, turnover time (year) in CENTURY (v.4)*

Compartment	Layer	Pool	Description	Turnover time (year)
Fresh Litter	*Aboveground*	*Metabolic*	Readily decomposable compounds (starch, sugar, proteins) from dead leaves	0.17-1
		Structural	Resistant compounds (cellulose, hemicellulose, lignin) from dead leaves	1-5
	Belowground	*Metabolic*	Readily decomposable compounds (starch, sugar, proteins) from dead fine roots	0.17-1
		Structural	Resistant compounds (cellulose, hemicellulose, lignin) from dead fine roots	1-5
Woody Litter	*Aboveground*	*Fine Wood*	Carbon and nitrogen compounds from dead fine branches	0.7-2
	Belowground	*Coarse Wood*	Carbon and nitrogen compounds from dead stems	0.7-2
		Coarse Wood	Carbon and nitrogen compounds from dead coarse roots	0.7-2
Soil Organic Matter	*Aboveground*	*Surface Microbes*	Active fraction of carbon and nitrogen of live soil microbial decomposers	0.14-0.17
	Belowground	*Soil Microbes*	Active fraction of carbon and nitrogen of live soil microbial decomposers	0.14-0.17
		Slow	Physically protected compounds	20-40
		Passive	Chemically recalcitrant compounds	200-1500

Table S3.2 *Fixed fractions of the carbon released to the atmosphere as CO_2 (a) and transferred among litter and SOM pools (b) in CENTURY (v.4)*

(a)

Pool	Fraction
Aboveground Metabolic	0.55
Belowground Metabolic	0.55
Aboveground Structural (to surface microbes)	0.45
Aboveground Structural (to slow SOM)	0.30
Belowground Structural (to surface microbes)	0.55
Belowground Structural (to slow SOM)	0.30
Fine Wood (to surface microbes)	0.45
Fine Wood (to slow SOM)	0.30
Aboveground Coarse Wood (to surface microbes)	0.45
Aboveground Coarse Wood (to slow SOM)	0.30
Belowground Coarse Wood (to surface microbes)	0.55
Belowground Coarse Wood (to slow SOM)	0.30
Slow SOM	0.55
Passive SOM	0.55
Surface Microbes	0.60

(b)

Pool	Fraction
Aboveground Metabolic	0.45
Belowground Metabolic	0.45
Aboveground Structural (to surface microbes)	0.55
Aboveground Structural (to slow SOM)	0.70
Belowground Structural (to surface microbes)	0.45
Belowground Structural (to slow SOM)	0.70
Fine Wood (to surface microbes)	0.55
Fine Wood (to slow SOM)	0.70
Aboveground Coarse Wood (to surface microbes)	0.55
Aboveground Coarse Wood (to slow SOM)	0.70
Belowground Coarse Wood (to surface microbes)	0.45
Belowground Coarse Wood (to slow SOM)	0.70
Slow SOM	0.45
Passive SOM	0.45
Surface Microbes	0.40

Table S3.3 *Functions implemented in CENTURY (v.4)*

Function	Description
fm_frac	Fractionation of carbon input into metabolic and structural litter
candec	Nitrogen limitation on carbon decomposition
agdrat	Computing of C:N ratio of new material from Aboveground Fresh and Woody litter entering the Surface Microbial SOM
bgdrat	Computing of C:N ratio of new material from Belowground Metabolic litter, Slow and Passive SOM entering the Soil Microbial SOM
rnewas	Computing of C:N ratio of new material from Aboveground Structural litter entering the Slow SOM
rneww1_2	Computing of C:N ratio of new material from Fine Woody litter entering the Slow SOM
rneww2_2	Computing of C:N ratio of new material from Aboveground Coarse Woody litter entering the Slow SOM
esched	Schedule organic nitrogen fluxes
mineral_n	Schedule nitrogen mineralization fluxes
immob_n	Schedule nitrogen immobilization fluxes
fT.Century4	Soil Temperature effect on decomposition using an exponential equation
fT.MMRT	Soil Temperature effect on decomposition using the MMRT formulation
fW.CENTURY	Soil Moisture effect on decomposition using the CENTURY4 formulation

Table S3.4 *Optimized parameter set and constants for Hainich and Ankasa*

Parameter	Unit	Description	Hainich	Ankasa
par_lat	degree	Latitude	51°	5°
par_lon	degree	Longitude	10°	-2°
par_clay_frac	-	Soil clay fraction	0.70	0.26
par_silt_frac	-	Soil silt fraction	0.28	0.18
par_sand_frac	-	Soil sand fraction	0.02	0.56
par_a	-	Slope of exponential equation	0.125	0.125
par_b	-	Exponent of exponential equation	0.07	0.07
ΔH0	kJ mol^{-1}	Changes in Enthalpy	45.102	45.102
ΔS0	kJ mol^{-1} K^{-1}	Changes in Entropy	-0.096	-0.096
ΔCp	kJ mol^{-1} K^{-1}	Changes in Heat Capacity	-1	-2
par_Temp_ref	°K	Reference temperature (MMRT)	298.15	298.15
ligfr_as	-	Lignin fraction of aboveground structural litter	0.18	0.19
ligfr_bs	-	Lignin fraction of belowground structural litter	0.18	0.19
ligfr_fw	-	Lignin fraction of fine woody litter	0.22	0.28
ligfr_acw	-	Lignin fraction of aboveground coarse woody litter	0.26	0.28
ligfr_bcw	-	Lignin fraction of belowground coarse woody litter	0.26	0.28
par_pligst	-	lignin effect on structural and woody litter decomposition	3	3
par_animpt	-	Slope of anaerobic effect on decomposition	5	5
par_k_am	$month^{-1}$	Maximum decay rate of aboveground metabolic litter	1.23	1.23
par_k_as	$month^{-1}$	Maximum decay rate of aboveground structural litter	0.33	0.33
par_k_bm	$month^{-1}$	Maximum decay rate of belowground metabolic litter	1.54	1.54
par_k_bs	$month^{-1}$	Maximum decay rate of belowground structural litter	0.41	0.41
par_k_fw	$month^{-1}$	Maximum decay rate of fine woody litter	0.13	0.13
par_k_acw	$month^{-1}$	Maximum decay rate of aboveground coarse woody litter	0.04	0.04
par_k_bcw	$month^{-1}$	Maximum decay rate of belowground coarse woody litter	0.05	0.05
par_k_srfmic	$month^{-1}$	Maximum decay rate of surface microbial SOM	0.50	0.50
par_k_mic	$month^{-1}$	Maximum decay rate of soil microbial SOM	0.61	0.50
par_k_slo	$month^{-1}$	Maximum decay rate of slow SOM	0.02	0.01
par_k_pas	$month^{-1}$	Maximum decay rate of passive SOM	0.0004	0.0001
par_co2am	-	Fraction of C lost as CO_2 from aboveground metabolic litter	0.55	0.55
par_co2bm	-	Fraction of C lost as CO_2 from belowground metabolic litter	0.55	0.55
par_co2as1	-	Fraction of C lost as CO_2 from aboveground structural litter to surface microbial SOM	0.45	0.45
par_co2as2	-	Fraction of C lost as CO_2 from aboveground structural litter to slow SOM	0.30	0.30
par_co2bs1	-	Fraction of C lost as CO_2 from belowground structural litter to soil microbial SOM	0.55	0.55

par_co2bs2	-	Fraction of C lost as CO_2 from belowground structural litter to slow SOM	0.30	0.30
par_co2fw1	-	Fraction of C lost as CO_2 from fine woody litter to surface microbial SOM	0.45	0.45
par_co2fw2	-	Fraction of C lost as CO_2 from fine woody litter to slow SOM	0.30	0.30
par_co2acw1	-	Fraction of C lost as CO_2 from aboveground coarse woody litter to surface microbial SOM	0.45	0.45
par_co2acw2	-	Fraction of C lost as CO_2 from aboveground coarse woody litter to slow SOM	0.30	0.30
par_co2bcw1	-	Fraction of C lost as CO_2 from belowground coarse woody litter to soil microbial SOM	0.55	0.55
par_co2bcw2	-	Fraction of C lost as CO_2 from belowground coarse woody litter to slow SOM	0.30	0.30
par_co2srfmic	-	Fraction of C lost as CO_2 from surface microbial SOM	0.60	0.60
par_co2mic1	-	Intercept CO_2 from Soil Microbial SOM	0.17	0.17
par_co2mic2	-	Slope CO_2 from Soil Microbial SOM	0.68	0.68
par_co2slo	-	Fraction of C lost as CO_2 from slow SOM	0.55	0.55
den_frac	-	Denitrification fraction	0.05	0.05
par_ps1s3a	-	Intercept of C transfer from Soil Microbial to Passive SOM	0.003	0.003
par_ps1s3b	-	Slope of C transfer from Soil Microbial to Passive SOM	0.032	0.032
par_ps2s3a	-	Intercept of C transfer from Slow to Passive SOM	0.003	0.003
par_ps2s3b	-	Slope of C transfer from Slow to Passive SOM	0.009	0.009
par_peftxa	-	Intercept of soil texture effect on microbial decomposition rate	0.25	0.25
par_peftxb	-	Slope of soil texture effect on microbial decomposition rate	0.75	0.75
par_kup	-	Fraction of inorganic nitrogen plant uptake	0.042	0.042
cn_leaf	unitless	C:N ratio of leaf residues	50	70
cn_froo	unitless	C:N ratio of fine root residues	40	60
cn_wood	unitless	C:N ratio of woody residues	200	200
par_ini_cn_rat_abgmet	unitless	Initial C:N ratio of aboveground metabolic litter	88	165
par_ini_cn_rat_abgstr	unitless	Initial C:N ratio of aboveground structural litter	88	165
par_ini_cn_rat_blwmet	unitless	Initial C:N ratio of belowground metabolic litter	66	66
par_ini_cn_rat_blwstr	unitless	Initial C:N ratio of belowground structural litter	66	66
par_ini_cn_rat_fw	unitless	Initial C:N ratio of fine woody litter	100	100
par_ini_cn_rat_acw	unitless	Initial C:N ratio of aboveground coarse woody litter	100	100
par_ini_cn_rat_bcw	unitless	Initial C:N ratio of belowground coarse woody litter	100	100
par_ini_cn_rat_srfmic	unitless	Initial C:N ratio of surface microbial SOM	15	15
par_ini_cn_rat_mic	unitless	Initial C:N ratio of soil microbial SOM	14	15.5
par_ini_cn_rat_slo	unitless	Initial C:N ratio of slow SOM	25	32
par_ini_cn_rat_pas	unitless	Initial C:N ratio of passive SOM	12	18
par_pcemic1	unitless	Maximum C:N ratio of Surface Microbial	16	16

		SOM		
par_pcemic2	unitless	Minimum C:N ratio of Surface Microbial SOM	10	10
par_pcemic3	g N m^{-2}	Minimum nitrogen content of decomposed Aboveground Material by which Srfmic C:N ratio is equal to par_pcemic2	0.02	0.02
biocnv	-	Biomass conversion factor for non-woody material	2.5	2.5
biocnv_wood	-	Biomass conversion factor for woody material	2	2
par_varat1_1	unitless	Maximum C:N ratio of Soil Microbial SOM	15	15
par_varat1_2	unitless	Minimum C:N ratio of Soil Microbial SOM	3	3
par_varat1_3	g N m-^{2}	Amount of inorganic nitrogen when the minimum ratio is applied	2	2
par_varat2_1	unitless	Maximum C:N ratio of Slow SOM	40	20
par_varat2_2	unitless	Minimum C:N ratio of Slow SOM	12	12
par_varat2_3	g N m^{-2}	Amount of inorganic nitrogen when the minimum ratio is applied	2	2
par_varat3_1	unitless	Maximum C:N ratio of Passive SOM	20	12
par_varat3_2	unitless	Minimum C:N ratio of Passive SOM	8	10
par_varat3_3	g N m^{-2}	Amount of inorganic nitrogen when the minimum ratio is applied	2	2
par_rad1p1	-	Intercept for C:N ratio of slow SOM formed from Surface Microbes	12	12
par_rad1p2	-	Slope for C:N ratio of slow SOM formed from Surface Microbes	3	3
par_rad1p3	unitless	Minimum allowable C:N ratio of slow SOM formed from Surface Microbes	5	5
const_kB	J K^{-1}	Boltzmann constant	1.38E-23	
const_h	J sec^{-1}	Planck constant	6.63E-34	
const_R	kJ K^{-1} mol^{-1}	R gas constant	0.00831	